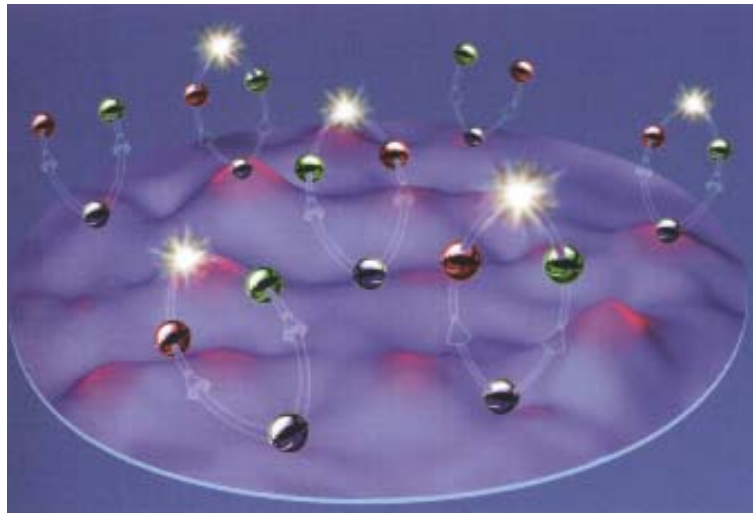


Lectures on nonequilibrium transport dynamics and transport properties of QCD

Dec. 2014

W. Cassing
Institut für Theoretische Physik
Universität Giessen



Contents

1	Nonrelativistic many-body dynamics and transport	4
1.1	Introduction	4
1.2	The two-body problem	4
1.3	The n-body problem in the density–matrix formalism	7
1.3.1	Definition of selfenergies	11
1.3.2	Analyticity	13
1.3.3	Effective parametrizations	13
2	Relativistic dynamics and transport	15
2.1	Relativistic formulations	15
2.1.1	Two-point functions on the CTP	15
2.1.2	The Dyson-Schwinger equation on the CTP	17
2.1.3	Kadanoff-Baym equations	18
2.1.4	Definition of selfenergies	18
2.1.5	Application to the scalar ϕ^4 -theory	19
2.1.6	Homogeneous systems in space	20
2.1.7	The spectral function	23
2.1.8	Results in first order gradient expansion	24
2.1.9	The equilibrium distribution	25
2.2	Full versus approximate dynamics	25
2.2.1	Derivation of the Boltzmann approximation	26
2.2.2	Boltzmann vs. Kadanoff-Baym dynamics	30
3	Derivation of off-shell relativistic transport theory	33
3.1	Kadanoff-Baym transport	36
3.2	Transport in the Botermans-Malfliet scheme	38
3.3	Testparticle representation	39
4	Thermodynamics and transport properties of QCD*	40
4.1	Quasiparticle properties and thermodynamics within the DQPM	40
4.1.1	Spectral functions	42
4.1.2	Thermodynamics of QCD*	44
4.2	Transport coefficients of the QGP	47
4.2.1	Shear viscosity coefficient: the Kubo formalism	47
4.2.2	Shear and bulk viscosities in the RTA	49

4.2.3	Electric conductivity	51
4.2.4	Magnetic response	55
4.2.5	Diamagnetic contribution	57
4.2.6	Paramagnetic contribution	58
4.2.7	Finite quark chemical potential	61
5	Appendix	62
5.1	Kramers-Kronig relation	62
5.2	Cauchy's principal value	64

Chapter 1

Nonrelativistic many-body dynamics and transport

1.1 Introduction

In these notes the many-body problem will be addressed within different scenarios for non-relativistic and relativistic systems in the limit of weak and strong coupling. In order to maintain a common notation the non-relativistic two-body problem is rewritten in operator form and convenient resummation schemes are identified. The many-body problem for N-body Fermi systems is then described in terms of the density-matrix hierarchy and within a suitable (nonperturbative) truncation scheme a generalized (on-shell) transport equation is derived beyond the level of the Boltzmann equation. In Chapter 3 we will address strongly interacting relativistic fields within the theory of Kadanoff and Baym and compare to the corresponding relativistic on-shell Boltzmann limit while Chapter 4 presents the derivation of off-shell transport equations in the Botermans-Malfliet scheme in first order gradients in phase space. As an application for strongly interacting relativistic systems we will address QCD in the partonic phase in Chapter 5 and provide suitable approximations to QCD in thermal equilibrium within the Dynamical QuasiParticle Model (DQPM). The latter will be also employed for the calculation of QCD transport coefficients like shear and bulk viscosities or the electric conductivity and magnetic susceptibility. Some technical aspects and useful relations are shifted to the Appendix¹

1.2 The two-body problem

The stationary (two-body) Schrödinger equation for the energy $E = \hbar\omega = \omega$ ($\hbar = 1$) reads in the cms (after separating the constant center of mass motion):

$$\omega|\Psi\rangle = (H_0 + v)|\Psi\rangle, \tag{1.1}$$

¹Independent of these lecture notes the reader is referred to the book of M. Bonitz [1] for further applications and explicit formulae.

where H_0 is the non-interacting Hamiltonian and the interaction is denoted by v . Alternatively, one has to look for the 'zeros' in ω of the equation

$$(\omega - H_0 - v)|\Psi\rangle =: G^{-1}(\omega)|\Psi\rangle = 0, \quad (1.2)$$

which in the non-relativistic case of two-body interactions v and $H_0 = T = p^2/(2\mu)$ in the cms (with μ denoting the reduced mass) reads in four-momentum space

$$\left(\omega - \frac{\mathbf{p}^2}{2\mu} - v\right)|\Psi\rangle =: G^{-1}(\omega, \mathbf{p})|\Psi\rangle = 0. \quad (1.3)$$

In Hilbert space this defines the retarded operator (in the limit $\epsilon \rightarrow 0^+$)

$$G^+(\omega + i\epsilon, \mathbf{p}) = \frac{1}{\omega - \frac{\mathbf{p}^2}{2\mu} - v + i\epsilon} = \frac{1}{(\omega - \frac{\mathbf{p}^2}{2\mu} + i\epsilon)[1 - v(\omega - \frac{\mathbf{p}^2}{2\mu} + i\epsilon)^{-1}]}, \quad (1.4)$$

which can be rewritten in the geometric expansion (assuming convergence) as

$$\begin{aligned} G^+(\omega + i\epsilon, \mathbf{p}) &= \frac{1}{\omega - \frac{\mathbf{p}^2}{2\mu} + i\epsilon} \sum_{n=0}^{\infty} \left(v \left(\frac{1}{\omega - \frac{\mathbf{p}^2}{2\mu} + i\epsilon} \right) \right)^n \\ &=: G_0^+(\omega + i\epsilon, \mathbf{p}) \sum_{n=0}^{\infty} \left(v G_0^+(\omega + i\epsilon, \mathbf{p}) \right)^n, \end{aligned} \quad (1.5)$$

with the free retarded Green function (in the center-of-mass system)

$$G_0^+(\omega + i\epsilon, \mathbf{p}) = \frac{1}{\omega - \frac{\mathbf{p}^2}{2\mu} + i\epsilon} \quad (1.6)$$

which is analytic in ω in the complex upper half-plane since the poles are in the lower half plane due to the limit $+i\epsilon$ in the denominator. Omitting the arguments we obtain the **Dyson equation**

$$\begin{aligned} G^+ &= G_0^+ \sum_{n=0}^{\infty} \left(v G_0^+ \right)^n = G_0^+ + G_0^+ v G_0^+ + G_0^+ v G_0^+ v G_0^+ + \dots = G_0^+ + G_0^+ v G^+ \\ &= G_0^+ (1 + v G^+) = G_0^+ \frac{1}{(1 - v G_0^+)} = \frac{1}{(1 - G_0^+ v)} G_0^+. \end{aligned} \quad (1.7)$$

In momentum-space representation this Dyson equation reads as

$$\begin{aligned} G^+(\mathbf{p}' - \mathbf{p}) &= \langle \mathbf{p}' | G^+(\omega) | \mathbf{p} \rangle = \langle \mathbf{p}' | G_0^+(\omega) | \mathbf{p} \rangle + \langle \mathbf{p}' | G_0^+(\omega) v G^+(\omega) | \mathbf{p} \rangle \\ &= \frac{\delta^3(\mathbf{p}' - \mathbf{p})}{\omega - \mathbf{p}'^2/2\mu + i\epsilon} + \int d^3 p_1 \frac{1}{\omega - \mathbf{p}'^2/2\mu + i\epsilon} v(\mathbf{p}' - \mathbf{p}_1) G^+(\mathbf{p}_1 - \mathbf{p}). \end{aligned} \quad (1.8)$$

By inversion we obtain alternatively (omitting the (+))

$$G^{-1} = G_0^{-1}(1 - v G_0) = (1 - G_0 v) G_0^{-1} \quad (1.9)$$

or

$$G_0 G^{-1} = 1 - v. \quad (1.10)$$

Note that (1.10) is an equation for the two-body Green function which is of one-body type only after separation of the cms motion!

The (two-body) Green function G^+ in scattering theory - where we have the boundary condition of an incoming undistorted wave $|\Phi_\omega\rangle$ - generates the scattering state of energy ω :

$$|\Psi_\omega^+\rangle = |\Phi_\omega\rangle + G_0^+(\omega)v|\Psi_\omega^+\rangle = \sum_{n=0}^{\infty} (G_0^+(\omega)v)^n |\Phi_\omega\rangle =: \Omega(\omega)|\Phi_\omega\rangle \quad (1.11)$$

with the unitary Moeller operator $\Omega(\omega)$ which follows

$$\Omega(\omega) = \sum_{n=0}^{\infty} (G_0^+(\omega)v)^n = \frac{1}{1 - G_0^+(\omega)v}. \quad (1.12)$$

Explicitly we obtain for the matrix elements

$$\begin{aligned} \langle \mathbf{r} | G_0^{(+)} | \mathbf{r}' \rangle &= \int \int d^3q \, d^3q' \langle \mathbf{r} | \mathbf{q} \rangle \langle \mathbf{q} | G_0^{(+)} | \mathbf{q}' \rangle \langle \mathbf{q}' | \mathbf{r}' \rangle \\ &= \frac{1}{(2\pi)^3} \int d^3q \exp(i\mathbf{q} \cdot \mathbf{r}) \frac{1}{E - \frac{\mathbf{q}^2}{2\mu} + i\epsilon} \exp(-i\mathbf{q} \cdot \mathbf{r}') \\ &= \frac{1}{(2\pi)^3} 2\mu \int d^3q \frac{\exp(i\mathbf{q} \cdot (\mathbf{r} - \mathbf{r}'))}{\mathbf{k}^2 - \mathbf{q}^2 + i\epsilon} = 2\mu G_0^{(+)}(\mathbf{r}, \mathbf{r}'); \end{aligned} \quad (1.13)$$

i.e. the familiar Green function in coordinate-space representation. We have used furthermore

$$\langle \mathbf{r} | \mathbf{q} \rangle = \langle \mathbf{q} | \mathbf{r} \rangle^* = (2\pi)^{-3/2} \exp(i\mathbf{q} \cdot \mathbf{r}). \quad (1.14)$$

These operator equations allow to define a T -matrix via

$$T(\omega)|\Phi_\omega\rangle = v|\Psi_\omega^+\rangle \quad (1.15)$$

which follows the T -matrix (or Born) series

$$T(\omega) = v + vG^+(\omega)T = v \sum_{n=0}^{\infty} (G_0^+(\omega)v)^n = v\Omega(\omega). \quad (1.16)$$

Here we only consider stationary systems without the presence of a third particle in the environment. The two-body density matrix in this case is a pure ensemble build up from the scattering or bound state $|\Psi_\omega^+\rangle$ by

$$\rho_2 = |\Psi_\omega^+\rangle \langle \Psi_\omega^+| \quad \rho_{20} = |\Phi_\omega\rangle \langle \Phi_\omega|, \quad (1.17)$$

i.e.

$$\rho_2 = \Omega(\omega)\rho_{20}\Omega(\omega)^\dagger. \quad (1.18)$$

The matrix elements in momentum space (omitting discrete quantum numbers) can be written as

$$\langle \mathbf{p}_1' \mathbf{p}_2' | \rho_2 | \mathbf{p}_1 \mathbf{p}_1 \rangle = \delta^3(\mathbf{p}_1 + \mathbf{p}_2 - \mathbf{p}_1' - \mathbf{p}_2') \rho_2(\mathbf{q}), \quad (1.19)$$

where $\mathbf{q} = \mathbf{p}_1' - \mathbf{p}_1$ is the momentum transfer in the collision.

In order to address nonequilibrium and medium phenomena one may use a Schrödinger picture (with time-dependent states) or a Heisenberg picture (with time-dependent operators). Also one may start from a formally correct formulation and decrease information (top-down scenario) or start from a perturbative formulation and increase the accuracy (bottom-up scenario). We start with the nonrelativistic top-down scenario.

1.3 The n -body problem in the density–matrix formalism

The starting point is the von-Neumann equation for the density operator ρ_N , that describes an N -particle system in or out-of equilibrium,

$$i \frac{\partial}{\partial t} \rho_N(1, \dots, N; 1' \dots N'; t) = [H_N, \rho_N], \quad (1.20)$$

with H_N denoting the N -particle Hamiltonian for particles $i = 1, \dots, N$. In the approximation of two-body interactions we have

$$H_N = \sum_{i=1}^N h^0(i) + \sum_{i < j}^{N-1} v(ij), \quad (1.21)$$

with

$$h^0(i) = t(i) \quad (1.22)$$

denoting the kinetic energy operator for particle i for convenience. External potentials that act in the same way on all particles may be incorporated here without problems.

The next step is to introduce reduced density matrices $\rho_n(1 \dots n, 1' \dots n'; t)$ by taking the trace over particles $n + 1, \dots, N$:

$$\rho_n = \frac{1}{(N - n)!} \text{Tr}_{n+1, \dots, N} \rho_N = \frac{1}{n + 1} \text{Tr}_{n+1} \{\rho_{n+1}\}. \quad (1.23)$$

One chooses the normalization of ρ_N to $N!$ such that the trace over the single-particle density matrix $\rho_1 = \rho$ becomes,

$$\text{Tr}_{1=1'} \rho(11'; t) = \sum_i \langle a_i^\dagger a_i \rangle = N, \quad (1.24)$$

with a_i^\dagger and a_i denoting Fermi creation and annihilation operators in the single-particle state i . The two-particle density matrix then is normalized as

$$\text{Tr}_{(1,2)} \rho_2 = \sum_{i,j} \langle a_i^\dagger a_j^\dagger a_j a_i \rangle = - \sum_{i,j} \langle a_i^\dagger a_j^\dagger a_i a_j \rangle = \sum_{i,j} \{ \langle a_i^\dagger a_i a_j^\dagger a_j \rangle - \langle a_i^\dagger a_j \rangle \delta_{ij} \} \quad (1.25)$$

$$= (N-1) \sum_j \langle a_j^\dagger a_j \rangle = N(N-1)$$

and so forth.

Taking corresponding traces (i.e. $\text{Tr}_{(n+1, \dots, N)}$) of the von-Neumann equation (1.20) we obtain the **BBGKY**-Hierarchy (**B**ogolyubov, **B**orn, **G**reen, **K**irkwood und **Y**von),

$$i \frac{\partial}{\partial t} \rho_n = \left[\sum_{i=1}^n h^0(i), \rho_n \right] + \left[\sum_{1=i \langle j}^{n-1} v(ij), \rho_n \right] + \sum_{i=1}^n \text{Tr}_{n+1} [v(i, n+1), \rho_{n+1}] \quad (1.26)$$

for $1 \leq n \leq N$ with $\rho_{N+1} = 0$. This set of equations is equivalent to Eq. (1.20); approximations or truncations of this set will reduce the information about the system in a top-down scenario. The explicit equations for $n = 1$, $n = 2$ read:

$$i \frac{\partial}{\partial t} \rho_1 = [h^0(1), \rho_1] + \text{Tr}_2 [v(12), \rho_2], \quad (1.27)$$

$$i \frac{\partial}{\partial t} \rho_2 = \left[\sum_{i=1}^2 h^0(i), \rho_2 \right] + [v(12), \rho_2] + \text{Tr}_3 [v(13) + v(23), \rho_3], \quad (1.28)$$

which are not closed since the equation for ρ_2 requires information from ρ_3 . Its equation reads

$$i \frac{\partial}{\partial t} \rho_3 = \left[\sum_{i=1}^3 h^0(i), \rho_3 \right] + [v(12) + v(13) + v(23), \rho_3] + \text{Tr}_4 [v(14) + v(24) + v(34), \rho_4]. \quad (1.29)$$

We now consider explicitly fermions in this Section. The next step is to introduce a **cluster expansion** as:

$$\rho_1(11') = \rho(11'), \quad (1.30)$$

$$\begin{aligned} \rho_2(12, 1'2') &= \rho(11')\rho(22') - \rho(12')\rho(21') + c_2(12, 1'2') = \rho_{20}(12, 1'2') + c_2(12, 1'2') \\ &= \mathcal{A}_{12}\rho(11')\rho(22') + c_2(12, 1'2'), \end{aligned} \quad (1.31)$$

with the two-body antisymmetrization operator $\mathcal{A}_{ij} = 1 - P_{ij}$. The expansion for the three-body density matrix reads (with the help of the permutation operator P_{ij} or $P_{i'j'}$)

$$\begin{aligned} \rho_3(123, 1'2'3') &= \rho(11')\rho(22')\rho(33') - \rho(12')\rho(21')\rho(33') \\ &\quad - \rho(13')\rho(22')\rho(31') - \rho(11')\rho(32')\rho(23') + \rho(13')\rho(21')\rho(32') + \rho(12')\rho(31')\rho(23') \\ &\quad + \rho(11')c_2(23, 2'3') - \rho(12')c_2(23, 1'3') - \rho(13')c_2(23, 2'1') + \rho(22')c_2(13, 1'3') \\ &\quad - \rho(21')c_2(13, 2'3') - \rho(23')c_2(13, 1'2') + \rho(33')c_2(12, 1'2') - \rho(31')c_2(12, 3'2') \\ &\quad - \rho(32')c_2(12, 1'3') + c_3(123, 1'2'3'). \end{aligned} \quad (1.32)$$

By neglecting c_2 in (1.31) we get the limit of independent particles which is also denoted as Time-Dependent Hartree-Fock (TDHF). This implies that all effects from collisions or correlations are incorporated in c_2 and higher orders in c_3 etc.

For fermions the exchange symmetries of the correlation matrix c_2 read:

$$c_2(12, 1'2') = -c_2(12, 2'1') = -c_2(21, 1'2') = c_2^*(1'2', 12) \quad \text{etc.} \quad (1.33)$$

When discarding explicit three-body correlations c_3 in (1.32) the remaining set of equations is closed and after some tedious analytic work we obtain for the one-body density matrix

$$i\frac{\partial}{\partial t} \rho(11'; t) = [h^0(1) - h^0(1')]\rho(11'; t) \quad (1.34)$$

$$+ \text{Tr}_{(2=2')} [v(12)\mathcal{A}_{12} - v(1'2')\mathcal{A}_{1'2'}]\rho(11'; t)\rho(22'; t) + \text{Tr}_{(2=2')} [v(12) - v(1'2')]c_2(12, 1'2'; t)$$

and for the two-body correlation matrix

$$i\frac{\partial}{\partial t} c_2(12, 1'2'; t) = [h^0(1) + h^0(2) - h^0(1') - h^0(2')]c_2(12, 1'2'; t) \quad (1.35)$$

$$+ \text{Tr}_{(3=3')} [v(13)\mathcal{A}_{13} + v(23)\mathcal{A}_{23} - v(1'3')\mathcal{A}_{1'3'} - v(2'3')\mathcal{A}_{2'3'}]\rho(33'; t)c_2(12, 1'2'; t) \\ + [v(12) - v(1'2')]\rho_{20}(12, 1'2')$$

$$- \text{Tr}_{(3=3')} \{v(13)\rho(23'; t)\rho_{20}(13, 1'2'; t) - v(1'3')\rho(32'; t)\rho_{20}(12, 1'3'; t) \\ + v(23)\rho(13'; t)\rho_{20}(32, 1'2'; t) - v(2'3')\rho(31'; t)\rho_{20}(12, 3'2'; t)\}$$

$$+ [v(12) - v(1'2')]c_2(12, 1'2'; t)$$

$$- \text{Tr}_{(3=3')} \{v(13)\rho(23'; t)c_2(13, 1'2'; t) - v(1'3')\rho(32'; t)c_2(12, 1'3'; t) \\ + v(23)\rho(13'; t)c_2(32, 1'2'; t) - v(2'3')\rho(31'; t)c_2(12, 3'2'; t)\}$$

$$+ \text{Tr}_{(3=3')} \{[v(13)\mathcal{A}_{13}\mathcal{A}_{1'2'} - v(1'3')\mathcal{A}_{1'3'}\mathcal{A}_{12}] \rho(11'; t)c_2(32, 3'2'; t) \\ + [v(23)\mathcal{A}_{23}\mathcal{A}_{1'2'} - v(2'3')\mathcal{A}_{2'3'}\mathcal{A}_{12}] \rho(22'; t)c_2(13, 1'3'; t)\}.$$

To reduce the complexity we introduce a one-body Hamiltonian by

$$h(i) = t(i) + U^s(i) = t(i) + \text{Tr}_{(n=n')} v(in)\mathcal{A}_{in}\rho(nn'; t), \quad (1.36)$$

$$h(i') = t(i') + U^s(i') = t(i') + \text{Tr}_{(n=n')} v(i'n')\mathcal{A}_{i'n'}\rho(nn'; t)$$

that includes the interaction in the self-generated time-dependent mean field. A Pauli-blocking operator is uniquely defined by

$$Q_{ij}^- = 1 - \text{Tr}_{(n=n')} (P_{in} + P_{jn})\rho(nn'; t); \quad Q_{i'j'}^- = 1 - \text{Tr}_{(n=n')} (P_{i'n'} + P_{j'n'})\rho(nn'; t), \quad (1.37)$$

and the effective interaction in the medium by

$$V^-(ij) = Q_{ij}^- v(ij); \quad V^-(i'j') = Q_{i'j'}^- v(i'j'), \quad (1.38)$$

with all exchange operators acting to the right.

The equations for ρ and c_2 achieve the compact form:

$$i\frac{\partial}{\partial t} \rho(11'; t) = [h(1) - h(1')]\rho(11'; t) + \text{Tr}_{(2=2')} [v(12) - v(1'2')]c_2(12, 1'2'; t), \quad (1.39)$$

and

$$\begin{aligned}
i\frac{\partial}{\partial t} c_2(12, 1'2'; t) &= \left[\sum_{i=1}^2 h(i) - \sum_{i'=1'}^{2'} h(i') \right] c_2(12, 1'2'; t) \\
&+ [V^=(12) - V^=(1'2')] \rho_{20}(12, 1'2'; t) \\
&+ [V^=(12) - V^=(1'2')] c_2(12, 1'2'; t) \\
&+ \text{Tr}_{(3=3')} \{ [v(13) \mathcal{A}_{13} \mathcal{A}_{1'2'} - v(1'3') \mathcal{A}_{1'3'} \mathcal{A}_{12}] \rho(11'; t) c_2(32, 3'2'; t) \\
&+ [v(23) \mathcal{A}_{23} \mathcal{A}_{1'2'} - v(2'3') \mathcal{A}_{2'3'} \mathcal{A}_{12}] \rho(22'; t) c_2(13, 1'3'; t) \}.
\end{aligned} \tag{1.40}$$

Equation (1.39) describes the propagation of a particle in the self-generated mean field $U^s(i)$ with additional two-body correlations that are further specified in (1.40). In Eq. (1.40) the first line describes the propagation of two particles in the mean field U^s , the second line incorporates off-shell collisions in the Born approximation while the third line incorporates a resummation of the in-medium interaction in the sense of a \mathcal{G} -matrix ladder resummation

$$v(ij) \rightarrow \mathcal{G}(ij) = v + v g_{20}^+(\omega) Q^- \mathcal{G} = v \sum_{n=0}^{\infty} (g_{20}^+(\omega) Q^- v)^n = v \frac{1}{1 - g_{20}^+(\omega) Q^- v} \tag{1.41}$$

in analogy to the T -matrix in (1.16) but with an intermediate Pauli-blocking operator Q^- (1.37). Since there is no longer a common center-of-mass system for all particle pairs the bare retarded propagator now includes the mean-fields U^s and reads (more generally)

$$G_0^+(\omega) \rightarrow g_{20}^+(\omega) = \frac{1}{\omega - h(1) - h(2) + i\epsilon} \tag{1.42}$$

instead of G_0^+ (1.6). These relations are readily derived in the limit $i\partial/\partial t \rightarrow \tilde{\omega} \equiv \omega - \omega'$ (see below). The last two lines in (1.40) describe additional particle - hole interactions that are important for groundstate correlations (vacuum correlations) and the damping of low energy modes but might be neglected for configurations at high temperatures where also the Pauli-blocking operator plays a minor role.

We mention that for the special limit considered here one can alternatively rewrite the cluster expansion for the three-body density matrix as

$$\begin{aligned}
\rho_3(123, 1'2'3') &= \rho(11') \rho_2(23, 2'3') - \rho(12') \rho_2(23, 1'3') \\
&- \rho(13') \rho_2(23, 2'1') + \rho(22') \rho_2(13, 1'3') \\
&- \rho(21') \rho_2(13, 2'3') - \rho(23') \rho_2(13, 1'2') + \rho(33') \rho_2(12, 1'2') - \rho(31') \rho_2(12, 3'2') \\
&- \rho(32') \rho_2(12, 1'3') + c_3(123, 1'2'3') \\
&= (1 - P_{1'2'} - P_{1'3'}) [\rho(11') \rho_2(23, 2'3') + \rho(22') \rho_2(13, 1'3') + \rho(33') \rho_2(12, 1'2')] + c_3(123, 1'2'3')
\end{aligned} \tag{1.43}$$

and neglect the 3-body correlations c_3 . This expansion also closes the equations (1.27) and (1.28). By insertion of (1.43) in (1.28) we get

$$i\frac{\partial}{\partial t} \rho_2(12, 1'2'; t) - \left[\sum_{i=1}^2 h(i) - \sum_{i'=1'}^{2'} h(i') \right] \rho_2(12, 1'2'; t) \tag{1.44}$$

$$\begin{aligned}
&= [V^=(12) - V^=(1'2')] \rho_2(12, 1'2'; t) \\
&+ \text{Tr}_{(3=3')} \{ [v(13) \mathcal{A}_{13} \mathcal{A}_{1'2'} - v(1'3') \mathcal{A}_{1'3'} \mathcal{A}_{12}] \rho(11'; t) \rho_2(32, 3'2'; t) \\
&\quad + [v(23) \mathcal{A}_{23} \mathcal{A}_{1'2'} - v(2'3') \mathcal{A}_{2'3'} \mathcal{A}_{12}] \rho(22'; t) \rho_2(13, 1'3'; t) \}.
\end{aligned}$$

The last lines describe particle-hole interactions. When discarding again the particle-hole interaction terms we end up with the compact form

$$\begin{aligned}
&i \frac{\partial}{\partial t} \rho_2(12, 1'2'; t) - \left[\sum_{i=1}^2 h(i) - \sum_{i'=1'}^{2'} h(i') \right] \rho_2(12, 1'2'; t) \\
&= [V^=(12) - V^=(1'2')] \rho_2(12, 1'2'; t).
\end{aligned} \tag{1.45}$$

Performing a Fourier transformation in time to the variable $\tilde{\omega}$ and rewriting $\tilde{\omega} = \omega - \omega'$ Eq. (1.45) is rewritten as:

$$\begin{aligned}
&(\omega - h(1) - h(2) - V^=(12) + i\epsilon) \rho_2(12, 1'2'; \omega) \\
&= \rho_2(12, 1'2'; \omega') (\omega' - h(1') - h(2') - V^=(1'2') - i\epsilon)
\end{aligned} \tag{1.46}$$

where we have tacitly added/subtracted a $\pm i\epsilon$ term. In this form Eq. (1.41) becomes immediately transparent using $V^= = Q^=v$.

1.3.1 Definition of selfenergies

Coming back to the identity (1.18) in the free case and in view of Eq. (1.46) we may define an interacting two-body density operator ρ_2 in ladder resummation by

$$\rho_2 = \tilde{\Omega}(\omega) \rho_{20} \tilde{\Omega}(\omega)^\dagger \tag{1.47}$$

with

$$\tilde{\Omega}(\omega) = \sum_{n=0}^{\infty} (g_{20}^+(\omega) Q^=v)^n = \frac{1}{1 - g_{20}^+(\omega) Q^=v}, \tag{1.48}$$

i.e. the resummed complex interaction reads

$$\mathcal{G}(\omega) = v \tilde{\Omega}(\omega). \tag{1.49}$$

This leads to the identities ($Q^{=\dagger} = Q^=$)

$$\begin{aligned}
\tilde{\Omega}(\omega) &= 1 + g_{20}^+(\omega) Q^=v \tilde{\Omega}(\omega) = 1 + g_{20}^+(\omega) Q^=\mathcal{G}(\omega) \\
\tilde{\Omega}(\omega)^\dagger &= 1 + \mathcal{G}(\omega)^\dagger Q^=g_{20}^-(\omega)
\end{aligned} \tag{1.50}$$

which will be exploited in different versions (using e.g. $\Im(\mathcal{G}\mathcal{G}^\dagger) = 0$). Having established this specific (nonperturbative) limit of the many-body problem we may rewrite the matrix elements

$$\begin{aligned}
&\text{Tr}_{2=2'} \langle 1'2' | [v, \rho_2] | 12 \rangle = \text{Tr}_{2=2'} \langle 1'2' | (v \rho_2 - \rho_2 v) | 12 \rangle \\
&= \text{Tr}_{2=2'} \langle 1'2' | (\mathcal{G}(\omega) \rho_{20} \tilde{\Omega}(\omega)^\dagger - \tilde{\Omega}(\omega) \rho_{20} \mathcal{G}(\omega)^\dagger) | 12 \rangle
\end{aligned} \tag{1.51}$$

and (using (1.50))

$$\begin{aligned} \text{Tr}_{2=2'} \langle 1'2' | [v, \rho_2] | 12 \rangle &= \text{Tr}_{2=2'} \langle 1'2' | (\mathcal{G}(\omega) \rho_{20} - \rho_{20} \mathcal{G}(\omega)^\dagger) | 12 \rangle \\ &+ \text{Tr}_{2=2'} \langle 1'2' | (\mathcal{G}(\omega) \rho_{20} \mathcal{G}(\omega)^\dagger Q^\dagger g_{20}^-(\omega) - g_{20}^+(\omega) Q^\dagger \mathcal{G}(\omega) \rho_{20} \mathcal{G}(\omega)^\dagger) | 12 \rangle. \end{aligned} \quad (1.52)$$

This allows to define the real part of the selfenergy $\Re(\Sigma)$ as:

$$\langle 1' | [\Re(\Sigma), \rho] | 1 \rangle = \text{Tr}_{2=2'} \langle 1'2' | [\Re(\mathcal{G}), \rho_{20}] | 12 \rangle \quad (1.53)$$

or

$$\langle 1' | \Re(\Sigma) | 1 \rangle = \text{Tr}_{2=2'} \langle 1'2' | \Re(\mathcal{G}) \mathcal{A} \rho | 12 \rangle. \quad (1.54)$$

The imaginary part of the selfenergy follows accordingly from the imaginary part of \mathcal{G} as:

$$\langle 1' | [\Im(\Sigma), \rho] | 1 \rangle = \text{Tr}_{2=2'} \langle 1'2' | [\Im(\mathcal{G}), \rho_{20}] | 12 \rangle \quad (1.55)$$

or

$$\langle 1' | \Im(\Sigma) | 1 \rangle = \text{Tr}_{2=2'} \langle 1'2' | \Im(\mathcal{G}) \mathcal{A} \rho | 12 \rangle \quad (1.56)$$

which will turn out to give the loss part in the collision term (see below). In lowest order in the interaction v we regain the selfconsistent Hartree-Fock potential U^s in (1.36) while the series in (1.41) provides a controlled higher order expansion for $\Re(\Sigma)$.

We now separate the real and imaginary parts of the commutator (1.51) employing additionally the identity

$$\Im(\mathcal{G}) = \mathcal{G}^\dagger Q^\dagger \mathcal{G} \Im(g_{20}^+) \quad (1.57)$$

since $\mathcal{G}^\dagger Q^\dagger \mathcal{G}$, Q^\dagger and v are hermitian operators.

For the remaining parts of the commutator we have

$$\begin{aligned} \text{Tr}_{2=2'} \langle 1'2' | (\Im(\mathcal{G}(\omega)) \rho_{20} - \rho_{20} \Im(\mathcal{G}(\omega)^\dagger)) | 12 \rangle \\ + \text{Tr}_{2=2'} \langle 1'2' | (\mathcal{G}(\omega) \rho_{20} \mathcal{G}(\omega)^\dagger Q^\dagger g_{20}^-(\omega) - g_{20}^+(\omega) Q^\dagger \mathcal{G}(\omega) \rho_{20} \mathcal{G}(\omega)^\dagger) | 12 \rangle \end{aligned} \quad (1.58)$$

since ρ_{20} is hermitian. One can now show that (1.58) is identical to an Uehling-Uhlenbeck on-shell collision term for fermions where the imaginary part of g_{20}^+ gives an energy conserving δ -function, the matrix-element squared is given by $\mathcal{G} \mathcal{G}^\dagger \mathcal{A}$ and Q^\dagger introduces the Pauli-blocking factors. This is most easily seen in the infinite nuclear matter limit where the one-body density matrix in momentum space and Q^\dagger become diagonal, i.e.

$$\begin{aligned} \langle \mathbf{p}' | \rho | \mathbf{p} \rangle &= (2\pi)^3 \delta^3(\mathbf{p}' - \mathbf{p}) f(\mathbf{p}) \\ \langle \mathbf{p}'_1 \mathbf{p}'_2 | Q^\dagger | \mathbf{p}_1 \mathbf{p}_2 \rangle &= (2\pi)^6 \delta^3(\mathbf{p}'_1 - \mathbf{p}_1) \delta^3(\mathbf{p}'_2 - \mathbf{p}_2) (1 - f(\mathbf{p}'_1) - f(\mathbf{p}'_2)) \\ \langle \mathbf{p}'_1 \mathbf{p}'_2 | \mathcal{G} | \mathbf{p}_1 \mathbf{p}_2 \rangle &= (2\pi)^3 \delta^3(\mathbf{p}_1 + \mathbf{p}_2 - \mathbf{p}'_1 - \mathbf{p}'_2) \mathcal{G}(\mathbf{p}_2 - \mathbf{p}'_2). \end{aligned} \quad (1.59)$$

Here we have dropped the discrete quantum numbers in the matrix elements (spin, isospin etc.). Note that

$$\langle \mathbf{p}'_1 \mathbf{p}'_2 | \Im(g_{20}^+(\omega)) | \mathbf{p}_1 \mathbf{p}_2 \rangle = (2\pi)^6 \delta^3(\mathbf{p}'_1 - \mathbf{p}_1) \delta^3(\mathbf{p}'_2 - \mathbf{p}_2) \frac{-i\epsilon}{(\omega - h(\mathbf{p}_1) - h(\mathbf{p}_2))^2 + \epsilon^2} \quad (1.60)$$

$$= -\pi(2\pi)^6 \delta^3(\mathbf{p}'_1 - \mathbf{p}_1) \delta^3(\mathbf{p}'_1 - \mathbf{p}_1) \delta(\omega - h(\mathbf{p}_1) - h(\mathbf{p}_2))$$

In lowest order we regain the Born transition matrix element squared $vv^\dagger \mathcal{A}$ in the collision term where the antisymmetrization \mathcal{A} only works for the interaction of fermions with the same spin and isospin. The relation to the differential cross section $d\sigma/d\Omega$ for nonidentical particles is given by

$$\frac{d\sigma}{d\Omega} = \frac{\mu^2}{4\pi^2} \mathcal{G}(\mathbf{q}) \mathcal{G}^\dagger(\mathbf{q}) \quad (1.61)$$

where \mathbf{q} is the momentum transfer in the elastic scattering event. The nonrelativistic (and nonperturbative) transport equation for Fermions finally reads with the single-particle hamiltonian

$$h_{eff}(\mathbf{r}, \mathbf{p}; t) = \frac{\mathbf{p}^2}{2M} + \Re(\Sigma)(\mathbf{r}, \mathbf{p}; t) \quad (1.62)$$

$$\left(\frac{\partial}{\partial t} + \nabla_p h_{eff}(\mathbf{r}, \mathbf{p}; t) \cdot \nabla_r - \nabla_r h_{eff}(\mathbf{r}, \mathbf{p}; t) \cdot \nabla_p \right) f(\mathbf{r}, \mathbf{p}; t) = \quad (1.63)$$

$$\begin{aligned} & \int \frac{d^3 p_2}{(2\pi)^3} \int \frac{d^3 p'_1}{(2\pi)^3} \int \frac{d^3 p'_2}{(2\pi)^3} |\mathcal{G} \mathcal{G}^\dagger \mathcal{A}|^2((\mathbf{p}_1 + \mathbf{p}_2), \mathbf{p}'_2 - \mathbf{p}_2) \\ & \quad \times \delta(h(\mathbf{p}_1) + h(\mathbf{p}_2) - h(\mathbf{p}'_1) - h(\mathbf{p}'_2)) \\ & \quad \times (f(\mathbf{r}, \mathbf{p}'_1; t) f(\mathbf{r}, \mathbf{p}'_2; t) (1 - f(\mathbf{r}, \mathbf{p}; t)) (1 - f(\mathbf{r}, \mathbf{p}_2; t)) \\ & \quad - f(\mathbf{r}, \mathbf{p}; t) f(\mathbf{r}, \mathbf{p}_2; t) (1 - f(\mathbf{r}, \mathbf{p}'_1; t)) (1 - f(\mathbf{r}, \mathbf{p}'_2; t))) \end{aligned} \quad (1.64)$$

Where (1.63) represents the selfconsistent Vlasov term while (1.64) describes the on-shell collision term with a non-perturbative transition probability.

1.3.2 Analyticity

Since the propagator $g_{20}(\omega)$ in (1.42) is analytic in the complex upper half plane (by virtue of the $i\epsilon$ in the denominator) the real and imaginary part of \mathcal{G} and also the selfenergy Σ follow the Kramers–Kronig relation (see Appendix)

$$\Re(\Sigma(\omega)) = \frac{2}{\pi} \mathcal{P} \int_0^\infty \frac{\omega' \Im(\Sigma(\omega'))}{\omega'^2 - \omega^2} d\omega' \quad (1.65)$$

if $\Im(\Sigma(\omega'))$ is vanishing rapidly enough for $\omega' \rightarrow \infty$. A similar relation also holds for the retarded propagator $G^+(\omega)$ in (1.4).

1.3.3 Effective parametrizations

In practice the real part of the \mathcal{G} -matrix in the nuclear physics context is parametrized by some functional in the nuclear density ρ which – in the infinite nuclear matter limit – is taken as a constant, e.g.

$$\Re(\mathcal{G}(\mathbf{r}_1 - \mathbf{r}_2)) \approx -A\delta(\mathbf{r}_1 - \mathbf{r}_2) + B\delta(\mathbf{r}_1 - \mathbf{r}_2)\rho((\mathbf{r}_1 + \mathbf{r}_2)/2)^\gamma \quad (1.66)$$

where A and B denote the strength of the attractive and repulsive interaction and $0.3 \leq \gamma \leq 1$ some density dependence of the repulsive interaction. Spin- and isospin dependencies have been discarded as well as finite range (Yukawa) interactions. A non-relativistic mean field (or selfenergy) is obtained by

$$\Sigma_{HF}(\rho) = U_{HF}(\rho) = \frac{3}{4} \left(-A\rho + \frac{B}{1+\gamma} \rho^{1+\gamma} \right), \quad (1.67)$$

where the prefactor $3/4$ stems from subtracting the Fock part of the interaction from the direct Hartree part in case of two spin and isospin degrees-of-freedom. The potential energy density \mathcal{V} is obtained by integration over ρ :

$$\mathcal{V}(\rho) = \frac{3}{4} \left(-\frac{A}{2} \rho^2 + \frac{B}{(1+\gamma)(2+\gamma)} \rho^{2+\gamma} \right). \quad (1.68)$$

Alternatively, having fixed the potential energy density \mathcal{V} e.g. by some effective Lagrangian or method, the selfenergy is obtained by a (functional) derivative with respect to the density and the 'local' effective interaction by another (functional) derivative. In the 'top-down' scenario one first defines a specific truncation scheme of the many-body hierarchy, defines some non-perturbative (or perturbative) interaction like \mathcal{G} and obtains a selfenergy by functional integration. Note that in non-relativistic formulations the selfenergy has the dimension [energy] whereas in relativistic formulations the selfenergy has dimension [energy²].

Chapter 2

Relativistic dynamics and transport

2.1 Relativistic formulations

Relativistic formulations of the many-body problem are essentially described within covariant field theory. Since the fields themselves are distributions in space-time $x = (t, \mathbf{x})$ one changes from the Schrödinger picture discussed before to the Heisenberg picture. Furthermore, the field theoretical problem in principle encounters infinitely many particles in a wavefunction such that a 'top-down' scenario is no longer appropriate. Nevertheless, we will encounter very similar structures to the BBGKY hierarchy in the Martin-Schwinger hierarchy. In the Heisenberg picture the time evolutions of the system is described by time-dependent operators that are evolved with the help of the time-evolution operator $\hat{U}(t, t')$ which follows

$$i \frac{\partial \hat{U}(t, t')}{\partial t} = \hat{H}(t) \hat{U}(t, t') \quad , \quad (2.1)$$

with \hat{H} denoting the Hamilton operator of the system. Eq. (2.1) is formally solved by

$$\hat{U}(t, t') = T(\exp[-i \int_{t'}^t dz \hat{H}(z)]) = \sum_{n=0}^{\infty} \frac{T[-i \int_{t'}^t dz \hat{H}(z)]^n}{n!} \quad , \quad (2.2)$$

where T denotes the time-ordering operator, which is also denoted as Dyson series. Let's assume that the initial state is given by some density matrix $\hat{\rho}$, which may be a pure or mixed state, then the time evolution of any operator \hat{O} in the Heisenberg picture from time $t_0=0$ to t is given by

$$O(t) = \langle \hat{O}_H(t) \rangle = \text{Tr}(\hat{\rho} \hat{O}_H(t)) = \text{Tr}(\hat{\rho} \hat{U}(0, t) \hat{O} \hat{U}(t, 0)) = \text{Tr}(\hat{\rho} \hat{U}^\dagger(t, 0) \hat{O} \hat{U}(t, 0)) \quad . \quad (2.3)$$

This implies that first the system is evolved from $t_0 = 0$ to t and then backward from t to $t_0 = 0$. This may be expressed as a time integral along the (Keldysh-)Contour shown in Fig. 2.1.

2.1.1 Two-point functions on the CTP

Now Green functions on the contour may have time arguments on the same branch of the contour or on opposite branches. This gives four possibilities for the Green functions defined –

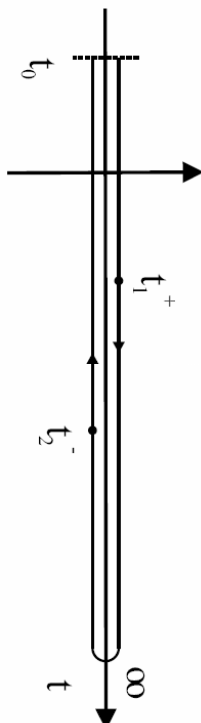


Figure 2.1: The Keldysh contour for the time integration in the Heisenberg picture.

in case of a field theory with only scalar fields $\phi(x)$ – by

$$iG^c(x, y) = iG^{++}(x, y) = \langle \hat{T}^c(\phi(x)\phi(y)) \rangle \quad (2.4)$$

$$iG^<(x, y) = iG^{+-}(x, y) = \langle \phi(y)\phi(x) \rangle \quad (2.5)$$

$$iG^>(x, y) = iG^{-+}(x, y) = \langle \phi(x)\phi(y) \rangle \quad (2.6)$$

$$iG^a(x, y) = iG^{--}(x, y) = \langle \hat{T}^a(\phi(x)\phi(y)) \rangle, \quad (2.7)$$

which are not independent! Here $x = (x^0, \mathbf{x})$ and $y = (y^0, \mathbf{y})$. Time-ordering has to be fulfilled if both time arguments are on the same axis. The causal time-ordering operator \mathcal{T}^c places fields at later times to the left while the anticausal operator \mathcal{T}^a places fields at later times to the right. The Green functions $G^>$ and $G^<$ are denoted as **Wightman functions** and will play the essential role in the dynamical description of the system. One may also write the Green function on the Keldysh contour in terms of a 2×2 matrix

$$G(x, y) = \begin{pmatrix} + & - \\ - & + \end{pmatrix} \begin{pmatrix} G^c(x, y) & G^<(x, y) \\ G^>(x, y) & G^a(x, y) \end{pmatrix}. \quad (2.8)$$

Note that the Green functions defined in (2.4) to (2.7) are two-point functions, i.e. they correspond to a single-particle species!

The further derivation again starts with a Dyson equation (cf. (1.7))

$$G(x, y) = G_0(x, y) + G_0(x, y)\Sigma(x, y)G(x, y) \quad (2.9)$$

which is of one-body type and instead of $G(x, y)$ we might write in shorthand notation $G(11)$. The selfenergy $\Sigma(x, y) = \Sigma(1, 1')$ has the meaning of a one-body mean-field potential and in lowest order for fermions is given by the Hartree-Fock potential ($\times 2M$) since in the relativistic case Σ has the dimension [energy]².

The relation to the one-body density matrix ρ in the previous Section is given by

$$\rho(\mathbf{x}, \mathbf{x}'; t) = -iG^<(\mathbf{x}, \mathbf{x}'; t, t) \quad (2.10)$$

since the time diagonal Green function can be identified with an integral over the time difference $\tau - \tau'$ (for $t = (\tau + \tau')/2$)

$$G^<(\mathbf{x}, \mathbf{x}'; t) = \int_{-\infty}^{\infty} d(\tau - \tau') G^<(\mathbf{x}, \mathbf{x}'; \tau, \tau'). \quad (2.11)$$

Two-point functions F on the closed-time-path (CTP) generally can be expressed by retarded and advanced components as

$$F^R(x, y) = F^c(x, y) - F^<(x, y) = F^>(x, y) - F^a(x, y) \quad , \quad (2.12)$$

$$F^A(x, y) = F^c(x, y) - F^>(x, y) = F^<(x, y) - F^a(x, y) \quad (2.13)$$

giving in particular

$$F^R(x, y) - F^A(x, y) = F^>(x, y) - F^<(x, y). \quad (2.14)$$

Note that the advanced and retarded components of the Green functions only contain spectral and no statistical information,

$$F^{R/A}(x, y) = F_0 \delta(t_1 - t_2) \pm \Theta(\pm(t_1 - t_2)) [F^>(x, y) - F^<(x, y)]. \quad (2.15)$$

2.1.2 The Dyson-Schwinger equation on the CTP

The Dyson-Schwinger equation (2.9) on the closed-time-path reads in matrix form:

$$\begin{pmatrix} G^c(x, y) & G^<(x, y) \\ G^>(x, y) & G^a(x, y) \end{pmatrix} = \begin{pmatrix} G_0^c(x, y) & G_0^<(x, y) \\ G_0^>(x, y) & G_0^a(x, y) \end{pmatrix} + \quad (2.16)$$

$$\begin{pmatrix} G_0^c(x, x') & G_0^<(x, x') \\ G_0^>(x, x') & G_0^a(x, x') \end{pmatrix} \odot \begin{pmatrix} \Sigma^c(x', y') & -\Sigma^<(x', y') \\ -\Sigma^>(x', y') & \Sigma^a(x', y') \end{pmatrix} \odot \begin{pmatrix} G^c(y', y) & G^<(y', y) \\ G^>(y', y) & G^a(y', y) \end{pmatrix}, \quad (2.17)$$

where the symbol \odot stands for an intermediate integration over space-time, i.e. x' or y' . The selfenergy Σ on the CPT is defined along (2.13) and incorporates interactions of higher order. In lowest order $\Sigma/2M$ is given by the Hartree or Hartree-Fock mean field but it follows a nonperturbative expansion in analogy to (1.53).

An example for this formal procedure may be given by the scalar ϕ^4 -theory which is a laboratory for testing theoretical approximations. Its Lagrangian reads

$$\mathcal{L}(x) = \frac{1}{2} \partial_\mu^x \phi(x) \partial_x^\mu \phi(x) - \frac{1}{2} m^2 \phi(x)^2 - \frac{\lambda}{4!} \phi^4(x) \quad (2.18)$$

In this (Bose) case the free propagator is defined via the negative inverse Klein-Gordon operator in space-time representation

$$\hat{G}_{0x}^{-1} = -(\partial_\mu^x \partial_x^\mu + m^2), \quad (2.19)$$

which is a solution of the Klein-Gordon equation in the following sense:

$$\hat{G}_{0x}^{-1} \begin{pmatrix} G_0^c(x, y) & G_0^<(x, y) \\ G_0^>(x, y) & G_0^a(x, y) \end{pmatrix} = \delta(\mathbf{x} - \mathbf{y}) \begin{pmatrix} \delta(x_0 - y_0) & 0 \\ 0 & -\delta(x_0 - y_0) \end{pmatrix} = \delta(\mathbf{x} - \mathbf{y}) \delta_p(x_0 - y_0) \quad , \quad (2.20)$$

$$\hat{G}_{0x}^{-1} G_0^{R/A}(x, y) = \delta(x - y) \quad ,$$

with δ_p is the δ -function on the CTP.

2.1.3 Kadanoff-Baym equations

To derive the **Kadanoff-Baym equations** one multiplies (2.17) with G_{0x}^{-1} (2.19). This gives four equations which can be cast into the form:

$$-(\partial_\mu^x \partial_x^\mu + m^2)G^{R/A}(x, y) = \delta(x - y) + \Sigma^{R/A}(x, x') \odot G^{A/R}(x', y) \quad , \quad (2.21)$$

$$-(\partial_\mu^x \partial_x^\mu + m^2)G^<(x, y) = \Sigma^R(x, x') \odot G^<(x', y) + \Sigma^<(x, x') \odot G^A(x', y) \quad , \quad (2.22)$$

$$-(\partial_\mu^x \partial_x^\mu + m^2)G^>(x, y) = \Sigma^R(x, x') \odot G^>(x', y) + \Sigma^>(x, x') \odot G^A(x', y) \quad , \quad (2.23)$$

The propagation of the Green functions in the variable y is defined by the adjoint equations:

$$-(\partial_\mu^y \partial_y^\mu + m^2)G^{R/A}(x, y) = \delta(x - y) + G^{R/A}(x, x') \odot \Sigma^{R/A}(x', y) \quad , \quad (2.24)$$

$$-(\partial_\mu^y \partial_y^\mu + m^2)G^<(x, y) = G^R(x, x') \odot \Sigma^<(x', y) + G^<(x, x') \odot \Sigma^A(x', y) \quad , \quad (2.25)$$

$$-(\partial_\mu^y \partial_y^\mu + m^2)G^>(x, y) = G^R(x, x') \odot \Sigma^>(x', y) + G^>(x, x') \odot \Sigma^A(x', y) \quad . \quad (2.26)$$

Note again that the evolution of the retarded/advanced Green functions only depends on retarded/advanced quantities.

2.1.4 Definition of selfenergies

For the solution of the KB equations the computation /fixing of the selfenergies Σ is mandatory. In the context of field theory the latter is extracted from the effective action

$$\Gamma[G] = \Gamma^0[G_0] + \frac{i}{2}[\ln(1 - \odot_p G_0 \odot_p \Sigma) + \odot_p G \odot_p \Sigma] + \Phi[G] \quad (2.27)$$

assuming a vanishing vacuum expectation value $\langle 0|\phi(x)|0\rangle$. Here $\Gamma^0[G_0]$ only depends on the free Green function and can be considered as constant in the following. In $\Phi[G]$ all closed two-particle irreducible (2PI) diagrams are included in lowest (nontrivial) order. 2PI diagrams are those that cannot be separated in two disjunct diagrams by cutting two propagator lines; formally this implies that after second order differentiation with respect to G no separate diagrams survive. The functional $\Phi[G]$ plays a similar role as the potential energy density $\mathcal{V}(\rho)$ (1.68) in the non-relativistic case where the (non-relativistic) selfenergy results from functional derivation of \mathcal{V} with respect to ρ , i.e. $\Sigma = \delta\mathcal{V}/\delta\rho$.

For the derivation of selfenergies one now considers the variation of the action $\Gamma[G]$ with respect to G requiring $\delta\Gamma = 0$,

$$\delta\Gamma = 0 = \frac{i}{2}\Sigma \delta G - \frac{i}{2} \frac{G_0}{1 - G_0 \Sigma} \delta\Sigma + \frac{i}{2}G \delta\Sigma + \delta\Phi \quad (2.28)$$

$$= \frac{i}{2}\Sigma \delta G - \frac{i}{2} \underbrace{\frac{1}{G_0^{-1} - \Sigma}}_{=G} \delta\Sigma + \frac{i}{2}G \delta\Sigma + \delta\Phi = \frac{i}{2}\Sigma \delta G + \delta\Phi \quad .$$

$$\Rightarrow \Sigma = 2i \frac{\delta\Phi}{\delta G} = 2 \frac{\delta\Phi}{\delta(-iG)} \quad . \quad (2.29)$$

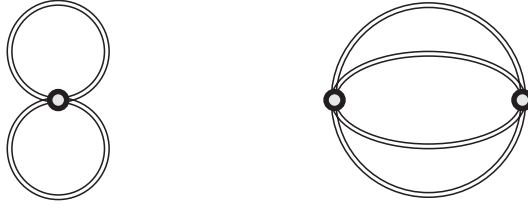


Figure 2.2: Contributions to the Φ -functional for the Kadanoff-Baym equation: two-loop contribution (l.h.s.) giving the tadpole self-energy and three-loop contribution (r.h.s.) generating the sunset self-energy. The Φ -functional is built-up by full Green functions (double lines) while open dots symbolize the integration over the inner coordinates.

Note that $-iG^<$ plays the role of the one-body density matrix in non-relativistic formulations. The selfenergies thus are obtained by opening of a propagator-line in the irreducible diagrams Φ . Note that this definition of the selfenergy preserves all conservation laws of the theory (as well as causality) and does not introduce further conserved currents. In principle the Φ -functional includes irreducible diagrams up to infinite order, but here we will consider only the contributions up to second order in the coupling (2PI). For our present purpose this approximation is sufficient since we include the leading mean-field effects as well as the leading order scattering processes that pave the way to thermalization.

2.1.5 Application to the scalar ϕ^4 -theory

The contributions up to the 3-loop order for the Φ -functional (cf. Fig. 2.2) read explicitly for the ϕ^4 -theory

$$i\Phi = \frac{i\lambda}{8} \int_{\mathcal{C}} d^{d+1}x G(x, x)^2 - \frac{\lambda^2}{48} \int_{\mathcal{C}} d^{d+1}x \int_{\mathcal{C}} d^{d+1}y G(x, y)^4, \quad (2.30)$$

where d denotes the spatial dimension of the problem.

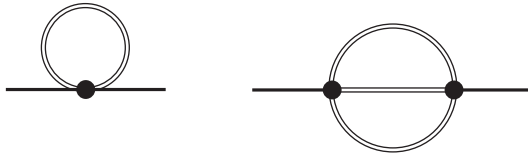


Figure 2.3: Self-energies of the Kadanoff-Baym equation: tadpole self-energy (l.h.s.) and sunset self-energy (r.h.s.) for the ϕ^4 -theory. Since the lines represent full Green functions the self-energies are self-consistent (see text) with the external coordinates indicated by full dots.

$$\begin{aligned}
\Sigma(x, y) &= 2i \frac{\delta\Phi}{\delta G(y, x)} = -\frac{i\lambda}{2} G(x, x) - \frac{\lambda^2}{6} G(x, y) G(x, y) G(y, x) \\
&= -\frac{\lambda}{2} i G(x, x) - \frac{\lambda^2}{6} [G(x, y)]^3 \\
&= \Sigma_p^\delta(x_0 - y_0) + \theta_p(x_0 - y_0) \Sigma^>(x, y) + \theta_p(y_0 - x_0) \Sigma^<(x, y),
\end{aligned} \tag{2.31}$$

with δ_p defined in (2.20) while θ_p is the Heavyside function on the CTP (taking care about the sign on the upper (+) or lower (-) branch).

Within the 3-loop approximation for the 2PI effective action (i.e. the Φ -functional (2.30)) we get two different self-energies: In leading order of the coupling constant only the tadpole diagram (l.h.s. of Fig. 2.3) contributes and leads to the generation of an effective mass (squared) for the field quanta. This self-energy (in coordinate space) is given by

$$\Sigma^\delta(x) = \frac{\lambda}{2} i G^<(x, x), \tag{2.32}$$

and is local in space and time. In next order in the coupling constant (i.e. λ^2) the non-local sunset self-energy (r.h.s. of Fig. 2.3) enters the time evolution as

$$\Sigma^{\lessgtr}(x, y) = -\frac{\lambda^2}{6} G^{\lessgtr}(x, y) G^{\lessgtr}(x, y) G^{\gtrless}(y, x) \tag{2.33}$$

$$\longrightarrow \Sigma^{\lessgtr}(x, y) = -\frac{\lambda^2}{6} \left[G^{\lessgtr}(x, y) \right]^3. \tag{2.34}$$

Thus the Kadanoff-Baym equation (2.22) in our case includes the influence of a mean-field on the particle propagation – generated by the tadpole diagram – as well as scattering processes as inherent in the sunset diagram.

The Kadanoff-Baym equation describes the full quantum nonequilibrium time evolution on the two-point level for a system prepared at an initial time t_0 , i.e. when higher order correlations are discarded. The causal structure of this initial value problem is obvious since the time integrations are performed over the past up to the actual time x_0 (or y_0 , respectively) and do not extend to the future.

2.1.6 Homogeneous systems in space

In the following we will consider homogeneous systems in space. To obtain a numerical solution the Kadanoff-Baym equation (2.22) is transformed to momentum space in case of the ϕ^4 -theory:

$$\begin{aligned}
\partial_{t_1}^2 G^<(\mathbf{p}, t_1, t_2) &= -[\mathbf{p}^2 + m^2 + \bar{\Sigma}^\delta(t_1)] G^<(\mathbf{p}, t_1, t_2) \\
&- \int_{t_0}^{t_1} dt' [\Sigma^>(\mathbf{p}, t_1, t') - \Sigma^<(\mathbf{p}, t_1, t')] G^<(\mathbf{p}, t', t_2)
\end{aligned} \tag{2.35}$$

$$\begin{aligned}
& + \int_{t_0}^{t_2} dt' \Sigma^<(\mathbf{p}, t_1, t') [G^>(\mathbf{p}, t', t_2) - G^<(\mathbf{p}, t', t_2)] \\
& = -[\mathbf{p}^2 + m^2 + \bar{\Sigma}^\delta(t_1)] G^<(\mathbf{p}, t_1, t_2) + I_1^<(\mathbf{p}, t_1, t_2)
\end{aligned}$$

where both memory integrals are summarized in the function $I_1^<$. The equation of motion in the second time direction t_2 is given analogously. In two-time, momentum space (\mathbf{p}, t, t') representation the selfenergies read

$$\bar{\Sigma}^\delta(t) = \frac{\lambda}{2} \int \frac{d^d p}{(2\pi)^d} i G^<(\mathbf{p}, t, t), \quad (2.36)$$

$$\begin{aligned}
\Sigma^{\lessgtr}(\mathbf{p}, t, t') & = -\frac{\lambda^2}{6} \int \frac{d^d q}{(2\pi)^d} \int \frac{d^d r}{(2\pi)^d} G^{\lessgtr}(\mathbf{q}, t, t') G^{\lessgtr}(\mathbf{r}, t, t') G^{\gtrless}(\mathbf{q}+\mathbf{r}-\mathbf{p}, t', t). \\
& = -\frac{\lambda^2}{6} \int \frac{d^d q}{(2\pi)^d} \int \frac{d^d r}{(2\pi)^d} G^{\lessgtr}(\mathbf{q}, t, t') G^{\lessgtr}(\mathbf{r}, t, t') G^{\lessgtr}(\mathbf{p}-\mathbf{q}-\mathbf{r}, t', t).
\end{aligned}$$

By insertion of (2.36) in Eq. (2.35) we get for the collision term:

$$\begin{aligned}
I_1^<(\mathbf{p}, t_1, t_2) & = \\
& + \int_{t_0}^{t_1} dt' \frac{\lambda^2}{6} \int \frac{d^d q}{(2\pi)^d} \int \frac{d^d r}{(2\pi)^d} G^>(\mathbf{q}, t_1, t') G^>(\mathbf{r}, t_1, t') G^<(\mathbf{q}+\mathbf{r}-\mathbf{p}, t', t_1) G^<(\mathbf{p}, t', t_2) \\
& - \int_{t_0}^{t_2} dt' \frac{\lambda^2}{6} \int \frac{d^d q}{(2\pi)^d} \int \frac{d^d r}{(2\pi)^d} G^<(\mathbf{q}, t_1, t') G^<(\mathbf{r}, t_1, t') G^>(\mathbf{q}+\mathbf{r}-\mathbf{p}, t', t_1) G^>(\mathbf{p}, t', t_2) \\
& + \int_{t_0}^{t_2} dt' \frac{\lambda^2}{6} \int \frac{d^d q}{(2\pi)^d} \int \frac{d^d r}{(2\pi)^d} G^<(\mathbf{q}, t_1, t') G^<(\mathbf{r}, t_1, t') G^>(\mathbf{q}+\mathbf{r}-\mathbf{p}, t', t_1) G^<(\mathbf{p}, t', t_2) \\
& - \int_{t_0}^{t_1} dt' \frac{\lambda^2}{6} \int \frac{d^d q}{(2\pi)^d} \int \frac{d^d r}{(2\pi)^d} G^<(\mathbf{q}, t_1, t') G^<(\mathbf{r}, t_1, t') G^>(\mathbf{q}+\mathbf{r}-\mathbf{p}, t', t_1) G^<(\mathbf{p}, t', t_2)
\end{aligned} \quad (2.37)$$

which apart from '2 \leftrightarrow 2' processes also involves '1 \leftrightarrow 3' processes which are not allowed by energy conservation in an on-shell collision term for massive particles!

For the solution of the Kadanoff-Baym equations (2.35) a flexible and accurate algorithm has been developed: Instead of solving the second order differential equation (2.35) one can generate a set of first order differential equations for the Green functions in the Heisenberg picture,

$$\begin{aligned}
i G_{\phi\phi}^<(x_1, x_2) & = \langle \phi(x_2) \phi(x_1) \rangle = i G^<(x_1, x_2), \\
i G_{\pi\phi}^<(x_1, x_2) & = \langle \phi(x_2) \pi(x_1) \rangle = \partial_{t_1} i G_{\phi\phi}^<(x_1, x_2), \\
i G_{\phi\pi}^<(x_1, x_2) & = \langle \pi(x_2) \phi(x_1) \rangle = \partial_{t_2} i G_{\phi\phi}^<(x_1, x_2), \\
i G_{\pi\pi}^<(x_1, x_2) & = \langle \pi(x_2) \pi(x_1) \rangle = \partial_{t_1} \partial_{t_2} i G_{\phi\phi}^<(x_1, x_2),
\end{aligned} \quad (2.38)$$

with the canonical field momentum $\pi(x) = \partial_{x_0} \phi(x)$. The first index π or ϕ is always related to the first space-time argument. Exploiting the time-reflection symmetry of the Green functions

some of the differential equations are redundant. The required equations of motion are given as

$$\begin{aligned}
\partial_{t_1} G_{\phi\phi}^<(\mathbf{p}, t_1, t_2) &= G_{\pi\phi}^<(\mathbf{p}, t_1, t_2), \tag{2.39} \\
\partial_{\bar{t}} G_{\phi\phi}^<(\mathbf{p}, \bar{t}, \bar{t}) &= 2i \Im \{ G_{\pi\phi}^<(\mathbf{p}, \bar{t}, \bar{t}) \}, \\
\partial_{t_1} G_{\pi\phi}^<(\mathbf{p}, t_1, t_2) &= -\Omega^2(t_1) G_{\phi\phi}^<(\mathbf{p}, t_1, t_2) + I_1^<(\mathbf{p}, t_1, t_2), \\
\partial_{t_2} G_{\pi\phi}^<(\mathbf{p}, t_1, t_2) &= G_{\pi\pi}^<(\mathbf{p}, t_1, t_2), \\
\partial_{\bar{t}} G_{\pi\phi}^<(\mathbf{p}, \bar{t}, \bar{t}) &= -\Omega^2(\bar{t}) G_{\phi\phi}^<(\mathbf{p}, \bar{t}, \bar{t}) + G_{\pi\pi}^<(\mathbf{p}, \bar{t}, \bar{t}) + I_1^<(\mathbf{p}, \bar{t}, \bar{t}), \\
\partial_{t_1} G_{\pi\pi}^<(\mathbf{p}, t_1, t_2) &= -\Omega^2(t_1) G_{\phi\pi}^<(\mathbf{p}, t_1, t_2) + I_{1,2}^<(\mathbf{p}, t_1, t_2), \\
\partial_{\bar{t}} G_{\pi\pi}^<(\mathbf{p}, \bar{t}, \bar{t}) &= -\Omega^2(\bar{t}) 2i \Im \{ G_{\pi\phi}^<(\mathbf{p}, \bar{t}, \bar{t}) \} + 2i \Im \{ I_{1,2}^<(\mathbf{p}, \bar{t}, \bar{t}) \},
\end{aligned}$$

where $\bar{t} = (t_1 + t_2)/2$ is the mean time variable. Thus one explicitly considers the propagation in the time diagonal. In the equations of motion (2.39) the current (renormalized) effective energy including the time dependent tadpole contribution enters,

$$\Omega^2(t) = \mathbf{p}^2 + m^2 + \delta m_{tad}^2 + \delta m_{sun}^2 + \bar{\Sigma}^\delta(t), \tag{2.40}$$

with δm_{tad}^2 and δm_{sun}^2 specified in Ref. [2]. The evolution in the t_2 direction has not to be taken into account for $G_{\phi\phi}^<$ and $G_{\pi\pi}^<$ since the Green functions beyond the time diagonal ($t_2 > t_1$) are determined via the time reflection symmetry $G_{\phi\phi}^<(\mathbf{p}, t_1, t_2) = -[G_{\phi\phi}^<(\mathbf{p}, t_2, t_1)]^*$ from the known values for the lower time triangle in both cases. Since there is no time reflection symmetry for the $G_{\pi\phi}$ functions, they have to be calculated (and stored) in the whole t_1, t_2 range. However, we can ignore the evolution of $G_{\phi\pi}$ since it is obtained by the relation $G_{\phi\pi}^<(\mathbf{p}, t_1, t_2) = -[G_{\pi\phi}^<(\mathbf{p}, t_2, t_1)]^*$. The correlation integrals in (2.39) are given by

$$\begin{aligned}
I_1^<(\mathbf{p}, t_1, t_2) &= -\int_0^{t_1} dt' [\Sigma^>(\mathbf{p}, t_1, t') - \Sigma^<(\mathbf{p}, t_1, t')] G_{\phi\phi}^<(\mathbf{p}, t', t_2) \tag{2.41} \\
&+ \int_0^{t_2} dt' \Sigma^<(\mathbf{p}, t_1, t') [G_{\phi\phi}^<(-\mathbf{p}, t_2, t') - G_{\phi\phi}^<(\mathbf{p}, t', t_2)],
\end{aligned}$$

$$\begin{aligned}
I_{1,2}^<(\mathbf{p}, t_1, t_2) &\equiv \partial_{t_2} I_1^<(\mathbf{p}, t_1, t_2) \tag{2.42} \\
&= -\int_0^{t_1} dt' [\Sigma^>(\mathbf{p}, t_1, t') - \Sigma^<(\mathbf{p}, t_1, t')] G_{\phi\pi}^<(\mathbf{p}, t', t_2) \\
&+ \int_0^{t_2} dt' \Sigma^<(\mathbf{p}, t_1, t') [G_{\pi\phi}^<(-\mathbf{p}, t_2, t') - G_{\phi\pi}^<(\mathbf{p}, t', t_2)].
\end{aligned}$$

In (2.39) and (2.42) one can replace $G_{\phi\pi}^<(\mathbf{p}, t_1, t_2) = -[G_{\pi\phi}^<(\mathbf{p}, t_2, t_1)]^*$ such that the set of equations is closed in the Green functions $G_{\phi\phi}^<$, $G_{\pi\phi}^<$ and $G_{\pi\pi}^<$.

The disadvantage, to integrate more Green functions in time in this first-order scheme, is compensated by its good accuracy. As mentioned before, we especially take into account the

propagation along the time diagonal which leads to an improved numerical precision. The set of differential equations (2.39) is solved by means of a 4th order Runge-Kutta algorithm. For the calculation of the self energies a Fast Fourier transformation method is applied. The self energies (2.36), furthermore, are calculated in coordinate space – where they are products of coordinate-space Green functions (that are available by Fourier transformation) – and finally transformed to momentum space.

In order to obtain a solution of the KB equations some initial conditions for $iG^<(\mathbf{p}, t = 0, t = 0)$ have to be specified. The corresponding initial distribution functions in the occupation density $n(\mathbf{p}, t = 0)$, related to $iG^<(\mathbf{p}, t = 0, t = 0)$ by

$$2\omega_{\mathbf{p}}iG^<(\mathbf{p}, t = 0, t = 0) = 2n(\mathbf{p}, t = 0) + 1 \quad (2.43)$$

follow immediately. For explicit examples and results of calculations the reader is referred to Ref. [2].

2.1.7 The spectral function

The spectral function of the fields ϕ is of particular interest since it follows from the field commutator at unequal times and reflects the quantization of the theory. For scalar, symmetric fields ϕ it is given by

$$A(x, y) = \langle [\phi(x), \phi(y)]_- \rangle = i[G^>(x, y) - G^<(x, y)] = i[G^R(x, y) - G^A(x, y)] \quad (2.44)$$

or in momentum-time representation as

$$\begin{aligned} A(\mathbf{p}, t_1, t_2) &= i[G^<(\mathbf{p}, t_2, t_1) - G^<(\mathbf{p}, t_1, t_2)] = i[-[G^<(\mathbf{p}, t_1, t_2)]^* - G^<(\mathbf{p}, t_1, t_2)] \\ &= -2i \Re(G^<(\mathbf{p}, \mathbf{t}_1, \mathbf{t}_2)) \quad . \end{aligned} \quad (2.45)$$

The quantity (2.45) is displayed in Fig. 2.4 as a function of $\Delta t = t_1 - t_2$ and $t = (t_1 + t_2)/2$ for low lying momentum modes in case of the ϕ^4 -theory for strong coupling λ . We observe a damped oscillation in Δt in all cases with characteristic time scale $1/\gamma$ which practically does not depend on the average time t .

The spectral function in energy-momentum representation is obtained by Fourier transformation with respect to the time difference $\Delta t = (t_1 - t_2)$ for each average time t :

$$\bar{A}(\mathbf{p}, p_0, t) = \int_{-\infty}^{\infty} d\Delta t \exp(i\Delta t p_0) A(\mathbf{p}, t_1 = t + \Delta t/2, t_2 = t - \Delta t/2) \quad , \quad (2.46)$$

where \bar{A} stands for the full spectral function. Since the spectral function essentially shows a damped oscillation (cf. Fig. 2.4) this implies that the Fourier transform (2.46) is of relativistic Breit-Wigner shape with a width γ (see below).

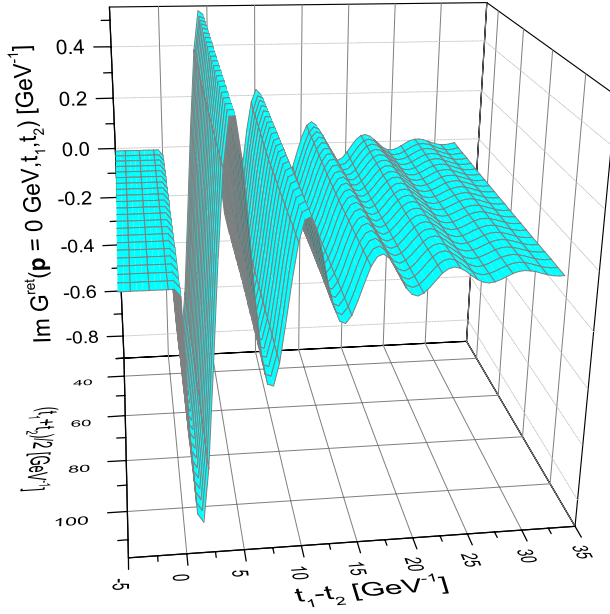


Figure 2.4: The imaginary part of the retarded Green function as a function of $t_1 - t_2$ and the average time $(t_1 + t_2)/2$, for ϕ^4 -theory in strong coupling as emerging from the Kadanoff-Baym approach.

2.1.8 Results in first order gradient expansion

In first order in the gradient expansion the retarded and advanced Green functions can be written as

$$\bar{G}^{R/A} = \Re(\bar{G}^R) \pm i \Im(\bar{G}^R) = \Re(\bar{G}^R) \mp i \bar{A}/2 \quad , \quad (2.47)$$

$$\bar{\Sigma}^{R/A} = \Re(\bar{\Sigma}^R) \pm i \Im(\bar{\Sigma}^R) = \Re(\bar{\Sigma}^R) \mp i \bar{\Gamma}/2 \quad .$$

Rewriting the imaginary part of the selfenergy we get

$$\bar{A}(\mathbf{p}, p_0, t) = \frac{\bar{\Gamma}}{(p_0^2 - \omega_0^2)^2 + \bar{\Gamma}^2/4} \quad , \quad (2.48)$$

$$\bar{\Gamma} = -2 \operatorname{Im}(\bar{\Sigma}^R) = 4p_0\gamma \quad ,$$

$$\omega_0^2 = \mathbf{p}^2 + m^2 - \bar{\Sigma}^\delta + \operatorname{Re}(\bar{\Sigma}^R) \quad ,$$

which is of relativistic Breit-Wigner form. Its normalization is given by

$$\int_{-\infty}^{\infty} \frac{dp_0}{2\pi} p_0 \bar{A}(\mathbf{p}, p_0, t) = 1 \quad (2.49)$$

and reflects the quantization condition for the interacting field ϕ .

2.1.9 The equilibrium distribution

Now we introduce the energy and momentum dependent distribution function $N(\mathbf{p}, p_0, \bar{t})$ at any system time \bar{t} by the definition

$$\begin{aligned} i G^<(\mathbf{p}, p_0, \bar{t}) &= A(\mathbf{p}, p_0, \bar{t}) N(\mathbf{p}, p_0, \bar{t}), \\ i G^>(\mathbf{p}, p_0, \bar{t}) &= A(\mathbf{p}, p_0, \bar{t}) [N(\mathbf{p}, p_0, \bar{t}) + 1], \end{aligned} \quad (2.50)$$

since $G^<(\mathbf{p}, p_0, \bar{t})$ and $G^>(\mathbf{p}, p_0, \bar{t})$ are known from the integration of the Kadanoff-Baym equations as well as $A(\mathbf{p}, p_0, \bar{t})$. In equilibrium (at temperature T) the Green functions obey the Kubo-Martin-Schwinger relation (KMS) for all momenta \mathbf{p} ,

$$G_{eq}^>(\mathbf{p}, p_0) = e^{p_0/T} G_{eq}^<(\mathbf{p}, p_0) \quad \forall \mathbf{p}. \quad (2.51)$$

If there exists a conserved quantum number in the theory we have, furthermore, a contribution of the corresponding chemical potential in the exponential function which leads to a shift of arguments: $p_0/T \rightarrow (p_0 - \mu)/T$. In the present case, however, there is no conserved quantum number and thus the equilibrium state has $\mu = 0$.

From the KMS condition of the Green functions (2.51) we obtain the equilibrium form of the distribution function (2.50) at temperature T as

$$N_{eq}(\mathbf{p}, p_0) = N_{eq}(p_0) = \frac{1}{e^{p_0/T} - 1} = N_{bose}(p_0/T), \quad (2.52)$$

from

$$\frac{G^<}{G^>} = e^{-p_0/T} = \frac{N_{eq}}{N_{eq} + 1}$$

which is the well-known Bose distribution. As is obvious from (2.52) the equilibrium distribution can only be a function of energy and not of the momentum variable \mathbf{p} in addition.

2.2 Full versus approximate dynamics

The Kadanoff-Baym equations studied in the previous Sections represent the full quantum-field theoretical equations on the single-particle level. However, its numerical solution is quite involved and it is of strong interest to investigate, in how far approximate schemes deviate from the full calculation. Nowadays, transport models are widely used in the description of quantum systems out of equilibrium. Most of these models work in the 'quasi-particle' picture, where all particles obey a fixed energy-momentum relation and the energy is no independent degree of freedom anymore; it is determined by the momentum and the (effective) mass of the particle (cf. Chapter 1). Accordingly, these particles are treated with their δ -function spectral shape as infinitely long living, i.e. stable objects. This assumption is very questionable e.g. for high-energy heavy-ion reactions, where the particles achieve a large width due to the frequent collisions with other particles in the high-density and/or high-energy regime. Furthermore, this is doubtful for particles that are unstable even in the vacuum. The question, in how far the quasiparticle approximation influences the dynamics in comparison to the full Kadanoff-Baym calculation, is of widespread interest.

2.2.1 Derivation of the Boltzmann approximation

In the following we will present a short derivation of the Boltzmann equation starting directly from the Kadanoff-Baym dynamics in the two-time and momentum-space representation. This derivation is briefly reviewed since we want i) to emphasize the link of the full Kadanoff-Baym equation with its approximated version and ii) to clarify the assumptions that enter the Boltzmann equation.

Since the Boltzmann equation describes the time evolution of distribution functions for quasi-particles we first consider the quasi-particle Green functions in two-time representation for homogeneous systems

$$\begin{aligned}
G_{\phi\phi,qp}^{\lesssim}(\mathbf{p}, t, t') &= \frac{-i}{2\omega_{\mathbf{p}}} \{ N_{qp}(\mp\mathbf{p}) e^{\pm i\omega_{\mathbf{p}}(t-t')} + [N_{qp}(\pm\mathbf{p})+1] e^{\mp i\omega_{\mathbf{p}}(t-t')} \} \quad (2.53) \\
G_{\phi\pi,qp}^{\lesssim}(\mathbf{p}, t, t') &= \frac{1}{2} \{ \mp N_{qp}(\mp\mathbf{p}) e^{\pm i\omega_{\mathbf{p}}(t-t')} \pm [N_{qp}(\pm\mathbf{p})+1] e^{\mp i\omega_{\mathbf{p}}(t-t')} \} \\
G_{\pi\phi,qp}^{\lesssim}(\mathbf{p}, t, t') &= \frac{1}{2} \{ \pm N_{qp}(\mp\mathbf{p}) e^{\pm i\omega_{\mathbf{p}}(t-t')} \mp [N_{qp}(\pm\mathbf{p})+1] e^{\mp i\omega_{\mathbf{p}}(t-t')} \} \\
G_{\pi\pi,qp}^{\lesssim}(\mathbf{p}, t, t') &= \frac{-i\omega_{\mathbf{p}}}{2} \{ N_{qp}(\mp\mathbf{p}) e^{\pm i\omega_{\mathbf{p}}(t-t')} + [N_{qp}(\pm\mathbf{p})+1] e^{\mp i\omega_{\mathbf{p}}(t-t')} \},
\end{aligned}$$

where for each momentum \mathbf{p} the Green functions are freely oscillating in relative time $t - t'$ with the on-shell energy $\omega_{\mathbf{p}}$. The time-dependent quasi-particle distribution functions are given with the energy variable fixed to the on-shell energy as $N_{qp}(\mathbf{p}, \bar{t}) \equiv N(\mathbf{p}, p_0 = \omega_{\mathbf{p}}, \bar{t})$, where the on-shell energies $\omega_{\mathbf{p}}$ might depend on time as well. Such a time variation e.g. might be due to an effective mass as generated by the time-dependent tadpole self-energy. In this case the on-shell energy reads

$$\omega_{\mathbf{p}}(\bar{t}) = \sqrt{\mathbf{p}^2 + m^2 + \bar{\Sigma}_{ren}^{\delta}(\bar{t})}. \quad (2.54)$$

Vice versa we can define the quasi-particle distribution function by means of the quasi-particle Green functions at equal times \bar{t} as

$$\begin{aligned}
N_{qp}(\mathbf{p}, \bar{t}) &= \left[\frac{\omega_{\mathbf{p}}(\bar{t})}{2} i G_{\phi\phi,qp}^{\lessdot}(\mathbf{p}, \bar{t}, \bar{t}) + \frac{1}{2\omega_{\mathbf{p}}(\bar{t})} i G_{\pi\pi,qp}^{\lessdot}(\mathbf{p}, \bar{t}, \bar{t}) \right] \quad (2.55) \\
&\quad - \frac{1}{2} \left[G_{\pi\phi,qp}^{\lessdot}(\mathbf{p}, \bar{t}, \bar{t}) - G_{\phi\pi,qp}^{\lessdot}(\mathbf{p}, \bar{t}, \bar{t}) \right].
\end{aligned}$$

Using the equations of motions for the Green functions in diagonal time direction (2.39) (exploiting $G_{\phi\pi}^{\lessdot}(\mathbf{p}, \bar{t}, \bar{t}) = -[G_{\pi\phi}^{\lessdot}(\mathbf{p}, \bar{t}, \bar{t})]^*$) the time evolution of the distribution function is given by

$$\partial_{\bar{t}} N_{qp}(\mathbf{p}, \bar{t}) = -Re \left\{ I_{1;qp}^{\lessdot}(\mathbf{p}, \bar{t}, \bar{t}) \right\} - \frac{1}{\omega_{\mathbf{p}}(\bar{t})} Im \left\{ I_{1,2;qp}^{\lessdot}(\mathbf{p}, \bar{t}, \bar{t}) \right\}. \quad (2.56)$$

The time derivatives of the on-shell energies cancel out since the quasiparticle Green functions obey

$$G_{\pi\pi}^{\lessdot}(\mathbf{p}, \bar{t}, \bar{t}) = \omega_{\mathbf{p}}^2(\bar{t}) G_{\phi\phi}^{\lessdot}(\mathbf{p}, \bar{t}, \bar{t}) \quad (2.57)$$

as seen from (2.53). Furthermore, it is remarkable that contributions containing the energy $\omega_{\mathbf{p}}^2$ - as present in the equation of motion for the Green functions (2.39) - no longer show up. The time evolution of the distribution function is entirely determined by (equal-time) collision integrals containing (time derivatives of the) Green functions and self-energies.

$$I_{1;qp}^<(\mathbf{p}, \bar{t}, \bar{t}) = \int_{t_0}^{\bar{t}} dt' \left(\Sigma_{qp}^<(\mathbf{p}, \bar{t}, t') G_{\phi\phi,qp}^>(\mathbf{p}, t', \bar{t}) - \Sigma_{qp}^>(\mathbf{p}, \bar{t}, t') G_{\phi\phi,qp}^<(\mathbf{p}, t', \bar{t}) \right), \quad (2.58)$$

$$I_{1,2;qp}^<(\mathbf{p}, \bar{t}, \bar{t}) = \int_{t_0}^{\bar{t}} dt' \left(\Sigma_{qp}^<(\mathbf{p}, \bar{t}, t') G_{\phi\pi,qp}^>(\mathbf{p}, t', \bar{t}) - \Sigma_{qp}^>(\mathbf{p}, \bar{t}, t') G_{\phi\pi,qp}^<(\mathbf{p}, t', \bar{t}) \right).$$

Since we are dealing with a system of on-shell quasi-particles within the Boltzmann approximation, the Green functions in the collision integrals (2.58) are given by the respective quasi-particle quantities of (2.53). Moreover, the collisional self-energies (2.36) are obtained in accordance with the quasi-particle approximation as

$$\begin{aligned} \Sigma_{qp}^{\lessgtr}(\mathbf{p}, t, t') &= -i \frac{\lambda^2}{6} \int \frac{d^d q}{(2\pi)^d} \int \frac{d^d r}{(2\pi)^d} \int \frac{d^d s}{(2\pi)^d} (2\pi)^d \delta^{(d)}(\mathbf{p} - \mathbf{q} - \mathbf{r} - \mathbf{s}) \frac{1}{2\omega_{\mathbf{q}} 2\omega_{\mathbf{r}} 2\omega_{\mathbf{s}}} \quad (2.59) \\ &\left\{ \begin{array}{llll} N_{qp}(\mp \mathbf{q}) & N_{qp}(\mp \mathbf{r}) & N_{qp}(\mp \mathbf{s}) & e^{+i[t-t'][\pm\omega_{\mathbf{q}} \pm \omega_{\mathbf{r}} \pm \omega_{\mathbf{s}}]} \\ +3 & N_{qp}(\mp \mathbf{q}) & N_{qp}(\mp \mathbf{r}) & [N_{qp}(\pm \mathbf{s}) + 1] e^{+i[t-t'][\pm\omega_{\mathbf{q}} \pm \omega_{\mathbf{r}} \mp \omega_{\mathbf{s}}]} \\ +3 & N_{qp}(\mp \mathbf{q}) & [N_{qp}(\pm \mathbf{r}) + 1] & [N_{qp}(\pm \mathbf{s}) + 1] e^{+i[t-t'][\pm\omega_{\mathbf{q}} \mp \omega_{\mathbf{r}} \mp \omega_{\mathbf{s}}]} \\ & + [N_{qp}(\pm \mathbf{q}) + 1] & [N_{qp}(\pm \mathbf{r}) + 1] & [N_{qp}(\pm \mathbf{s}) + 1] e^{+i[t-t'][\mp \omega_{\mathbf{q}} \mp \omega_{\mathbf{r}} \mp \omega_{\mathbf{s}}]} \end{array} \right\}. \end{aligned}$$

For a free theory the distribution functions $N_{qp}(\mathbf{p})$ are obviously constant in time which, of course, is no longer valid for an interacting system out of equilibrium. Thus one has to specify the above expressions for the quasi-particle Green functions (2.53) to account for the time dependence of the distribution functions.

The actual Boltzmann approximation is defined in the limit, that the distribution functions have to be taken always at *the latest time argument* of the two-time Green function. Accordingly, for the general non-equilibrium case, we introduce the ansatz for the Green functions in the collision term

$$\begin{aligned} G_{\phi\phi,qp}^{\lessgtr}(\mathbf{p}, t, t') &= \frac{-i}{2\omega_{\mathbf{p}}} \left\{ N_{qp}(\mp \mathbf{p}, t_{max}) e^{\pm i\omega_{\mathbf{p}}(t-t')} + [N_{qp}(\pm \mathbf{p}, t_{max}) + 1] e^{\mp i\omega_{\mathbf{p}}(t-t')} \right\} \quad (2.60) \\ G_{\phi\pi,qp}^{\lessgtr}(\mathbf{p}, t, t') &= \frac{1}{2} \left\{ \mp N_{qp}(\mp \mathbf{p}, t_{max}) e^{\pm i\omega_{\mathbf{p}}(t-t')} \pm [N_{qp}(\pm \mathbf{p}, t_{max}) + 1] e^{\mp i\omega_{\mathbf{p}}(t-t')} \right\}, \end{aligned}$$

with the maximum time $t_{max} = \max(t, t')$. The same ansatz is employed for the time dependent on-shell energies which enter the representation of the quasi-particle two-time Green functions (2.60) with their value at t_{max} , i.e. $\omega_{\mathbf{p}} = \omega_{\mathbf{p}}(t_{max} = \max(t, t'))$.

The collision term contains a time integration which extends from an initial time t_0 to the current time \bar{t} . All two-time Green functions and self-energies depend on the current time \bar{t} as well as on the integration time $t' \leq \bar{t}$. Thus only distribution functions at the current time, i.e. the maximum time of all appearing two-time functions, enter the collision integrals and the evolution equation for the distribution function becomes local in time. Since the distribution functions are given at fixed time \bar{t} , they can be taken out of the time integral. When inserting the expressions for the self-energies and the Green functions in the collision integrals the evolution equation for the quasi-particle distribution function reads

$$\begin{aligned} \partial_{\bar{t}} N_{qp}(\mathbf{p}, \bar{t}) &= \frac{\lambda^2}{3} \int \frac{d^d q}{(2\pi)^d} \int \frac{d^d r}{(2\pi)^d} \int \frac{d^d s}{(2\pi)^d} (2\pi)^d \delta^{(d)}(\mathbf{p} - \mathbf{q} - \mathbf{r} - \mathbf{s}) \frac{1}{2\omega_{\mathbf{p}} 2\omega_{\mathbf{q}} 2\omega_{\mathbf{r}} 2\omega_{\mathbf{s}}} \quad (2.61) \\ &\left\{ \left[\bar{N}_{\mathbf{p}, \bar{t}} \bar{N}_{-\mathbf{q}, \bar{t}} \bar{N}_{-\mathbf{r}, \bar{t}} \bar{N}_{-\mathbf{s}, \bar{t}} - N_{\mathbf{p}, \bar{t}} N_{-\mathbf{q}, \bar{t}} N_{-\mathbf{r}, \bar{t}} N_{-\mathbf{s}, \bar{t}} \right] \int_{t_0}^{\bar{t}} dt' \cos([\bar{t} - t']) [\omega_{\mathbf{p}} + \omega_{\mathbf{q}} + \omega_{\mathbf{r}} + \omega_{\mathbf{s}}] \right. \\ &+ 3 \left[\bar{N}_{\mathbf{p}, \bar{t}} \bar{N}_{-\mathbf{q}, \bar{t}} \bar{N}_{-\mathbf{r}, \bar{t}} N_{\mathbf{s}, \bar{t}} - N_{\mathbf{p}, \bar{t}} N_{-\mathbf{q}, \bar{t}} N_{-\mathbf{r}, \bar{t}} \bar{N}_{\mathbf{s}, \bar{t}} \right] \int_{t_0}^{\bar{t}} dt' \cos([\bar{t} - t']) [\omega_{\mathbf{p}} + \omega_{\mathbf{q}} + \omega_{\mathbf{r}} - \omega_{\mathbf{s}}] \\ &+ 3 \left[\bar{N}_{\mathbf{p}, \bar{t}} \bar{N}_{-\mathbf{q}, \bar{t}} N_{\mathbf{r}, \bar{t}} N_{\mathbf{s}, \bar{t}} - N_{\mathbf{p}, \bar{t}} N_{-\mathbf{q}, \bar{t}} \bar{N}_{\mathbf{r}, \bar{t}} \bar{N}_{\mathbf{s}, \bar{t}} \right] \int_{t_0}^{\bar{t}} dt' \cos([\bar{t} - t']) [\omega_{\mathbf{p}} + \omega_{\mathbf{q}} - \omega_{\mathbf{r}} - \omega_{\mathbf{s}}] \\ &\left. + \left[\bar{N}_{\mathbf{p}, \bar{t}} N_{\mathbf{q}, \bar{t}} N_{\mathbf{r}, \bar{t}} N_{\mathbf{s}, \bar{t}} - N_{\mathbf{p}, \bar{t}} \bar{N}_{\mathbf{q}, \bar{t}} \bar{N}_{\mathbf{r}, \bar{t}} \bar{N}_{\mathbf{s}, \bar{t}} \right] \int_{t_0}^{\bar{t}} dt' \cos([\bar{t} - t']) [\omega_{\mathbf{p}} - \omega_{\mathbf{q}} - \omega_{\mathbf{r}} - \omega_{\mathbf{s}}] \right\}, \end{aligned}$$

where we have introduced the abbreviation $N_{\mathbf{p}, \bar{t}} = N_{qp}(\mathbf{p}, \bar{t})$ for the distribution function at current time \bar{t} and $\bar{N}_{\mathbf{p}, \bar{t}} = N_{qp}(\mathbf{p}, \bar{t}) + 1$ for the according Bose factor. Furthermore, a possible time dependence of the on-shell energies is suppressed in the above notation.

The contributions in the collision term (2.61) for particles of momentum \mathbf{p} are ordered as they describe different types of scattering processes where, however, we always find the typical gain and loss structure. The first line in (2.61) corresponds to the production and annihilation of four on-shell particles ($0 \rightarrow 4, 4 \rightarrow 0$), where a particle of momentum \mathbf{p} is produced or destroyed simultaneous with three other particles with momenta $\mathbf{q}, \mathbf{r}, \mathbf{s}$. The second line and the fourth line describe ($1 \rightarrow 3$) and ($3 \rightarrow 1$) processes where the quasi-particle with momentum \mathbf{p} is the single one or appears with two other particles. The relevant contribution in the Boltzmann limit is the third line which represents ($2 \rightarrow 2$) scattering processes; quasi-particles with momentum \mathbf{p} can be scattered out of their momentum cell by collisions with particles of momenta \mathbf{q} (second term) or can be produced within a reaction of on-shell particles with momenta \mathbf{r}, \mathbf{s} (first term).

The time evolution of the quasi-particle distribution is given as an initial value problem for the function $N_{qp}(\mathbf{p})$ prepared at initial time t_0 . For large system times \bar{t} (compared to the initial time) the time integration over the trigonometric function results in an energy conserving δ -function:

$$\lim_{\bar{t} - t_0 \rightarrow \infty} \int_{t_0}^{\bar{t}} dt' \cos((\bar{t} - t') \hat{\omega}) = \lim_{\bar{t} - t_0 \rightarrow \infty} \frac{1}{\hat{\omega}} \sin((\bar{t} - t_0) \hat{\omega}) = \pi \delta(\hat{\omega}). \quad (2.62)$$

Here $\hat{\omega} = \omega_{\mathbf{p}} \pm \omega_{\mathbf{q}} \pm \omega_{\mathbf{r}} \pm \omega_{\mathbf{s}}$ represents the energy sum which is conserved in the limit $\bar{t} - t_0 \rightarrow \infty$

where the initial time t_0 is considered as fixed. In this limit the time evolution of the distribution function amounts to

$$\begin{aligned} \partial_{\bar{t}} N_{qp}(\mathbf{p}, \bar{t}) &= \frac{\lambda^2}{6} \int \frac{d^d q}{(2\pi)^d} \int \frac{d^d r}{(2\pi)^d} \int \frac{d^d s}{(2\pi)^d} (2\pi)^{d+1} \frac{1}{2\omega_{\mathbf{p}} 2\omega_{\mathbf{q}} 2\omega_{\mathbf{r}} 2\omega_{\mathbf{s}}} \quad (2.63) \\ &\left\{ [\bar{N}_{\mathbf{p},\bar{t}} \bar{N}_{\mathbf{q},\bar{t}} \bar{N}_{\mathbf{r},\bar{t}} \bar{N}_{\mathbf{s},\bar{t}} - N_{\mathbf{p},\bar{t}} N_{\mathbf{q},\bar{t}} N_{\mathbf{r},\bar{t}} N_{\mathbf{s},\bar{t}}] \delta^{(d)}(\mathbf{p}+\mathbf{q}+\mathbf{r}+\mathbf{s}) \delta(\omega_{\mathbf{p}}+\omega_{\mathbf{q}}+\omega_{\mathbf{r}}+\omega_{\mathbf{s}}) \right. \\ &+3 [\bar{N}_{\mathbf{p},\bar{t}} \bar{N}_{\mathbf{q},\bar{t}} \bar{N}_{\mathbf{r},\bar{t}} N_{\mathbf{s},\bar{t}} - N_{\mathbf{p},\bar{t}} N_{\mathbf{q},\bar{t}} N_{\mathbf{r},\bar{t}} \bar{N}_{\mathbf{s},\bar{t}}] \delta^{(d)}(\mathbf{p}+\mathbf{q}+\mathbf{r}-\mathbf{s}) \delta(\omega_{\mathbf{p}}+\omega_{\mathbf{q}}+\omega_{\mathbf{r}}-\omega_{\mathbf{s}}) \\ &+3 [\bar{N}_{\mathbf{p},\bar{t}} \bar{N}_{\mathbf{q},\bar{t}} N_{\mathbf{r},\bar{t}} N_{\mathbf{s},\bar{t}} - N_{\mathbf{p},\bar{t}} N_{\mathbf{q},\bar{t}} \bar{N}_{\mathbf{r},\bar{t}} \bar{N}_{\mathbf{s},\bar{t}}] \delta^{(d)}(\mathbf{p}+\mathbf{q}-\mathbf{r}-\mathbf{s}) \delta(\omega_{\mathbf{p}}+\omega_{\mathbf{q}}-\omega_{\mathbf{r}}-\omega_{\mathbf{s}}) \\ &\left. + [\bar{N}_{\mathbf{p},\bar{t}} \bar{N}_{\mathbf{q},\bar{t}} N_{\mathbf{r},\bar{t}} N_{\mathbf{s},\bar{t}} - N_{\mathbf{p},\bar{t}} \bar{N}_{\mathbf{q},\bar{t}} \bar{N}_{\mathbf{r},\bar{t}} \bar{N}_{\mathbf{s},\bar{t}}] \delta^{(d)}(\mathbf{p}-\mathbf{q}-\mathbf{r}-\mathbf{s}) \delta(\omega_{\mathbf{p}}-\omega_{\mathbf{q}}-\omega_{\mathbf{r}}-\omega_{\mathbf{s}}) \right\}. \end{aligned}$$

In the energy conserving long-time limit (2.62) only the $2 \rightarrow 2$ scattering processes are non-vanishing, because all other terms do not contribute since the energy δ -functions can not be fulfilled for massive on-shell quasi-particles. Furthermore, the system evolution is explicitly local in time because it depends only on the current configuration; there are no memory effects from the integration over past times as present in the full Kadanoff-Baym equation.

In the following we will solve the energy conserving Boltzmann equation for on-shell particles:

$$\begin{aligned} \partial_{\bar{t}} N_{qp}(\mathbf{p}, \bar{t}) &= \frac{\lambda^2}{2} \int \frac{d^d q}{(2\pi)^d} \int \frac{d^d r}{(2\pi)^d} \int \frac{d^d s}{(2\pi)^d} (2\pi)^{d+1} \frac{1}{2\omega_{\mathbf{p}} 2\omega_{\mathbf{q}} 2\omega_{\mathbf{r}} 2\omega_{\mathbf{s}}} \quad (2.64) \\ &[\bar{N}_{\mathbf{p},\bar{t}} \bar{N}_{\mathbf{q},\bar{t}} N_{\mathbf{r},\bar{t}} N_{\mathbf{s},\bar{t}} - N_{\mathbf{p},\bar{t}} N_{\mathbf{q},\bar{t}} \bar{N}_{\mathbf{r},\bar{t}} \bar{N}_{\mathbf{s},\bar{t}}] \delta^{(d)}(\mathbf{p}+\mathbf{q}-\mathbf{r}-\mathbf{s}) \delta(\omega_{\mathbf{p}}+\omega_{\mathbf{q}}-\omega_{\mathbf{r}}-\omega_{\mathbf{s}}). \end{aligned}$$

The numerical algorithm employed for the solution of (2.64) is basically the same as for the solution of the Kadanoff-Baym equation (cf. Section 2.1.6). We explicitly calculate the time integral in (2.61). Energy conservation can be assured by a precalculation including a shift of the lower boundary t_0 to earlier times. We note, that in contrast to the Kadanoff-Baym equation no correlation energy is generated in the Boltzmann limit!

In addition to the procedure presented above we calculate the actual momentum-dependent on-shell energy for every momentum mode by a solution of the dispersion relation including contributions from the tadpole and the real part of the (retarded) sunset self energy. In this way one can guarantee that at every time t the particles are treated as quasi-particles with the correct energy-momentum relation.

Before presenting the actual numerical results we comment on the derivation of the Boltzmann equation within the conventional scheme that is different from the one presented above. Here, at first the Kadanoff-Baym equation (in coordinate space) is transformed to the Wigner representation by Fourier transformation with respect to the relative coordinates in space and time. The problem then is formulated in terms of energy and momentum variables together with a single system time. For non-homogeneous systems a mean spatial coordinate is necessary as well. As a next step the 'semiclassical approximation' is introduced, which consists

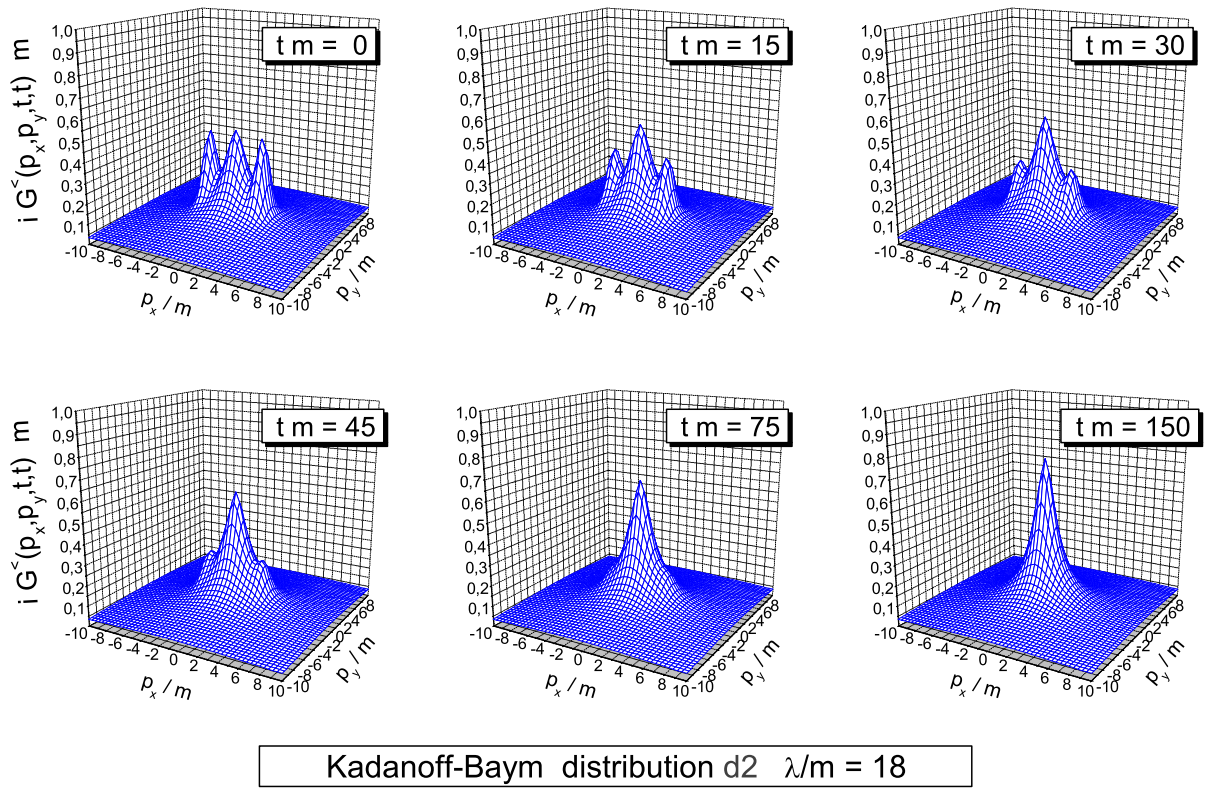


Figure 2.5: Evolution of the Green function in momentum space. The equal time Green function is displayed for various times $t \cdot m = 0, 15, 30, 45, 75, 150$. Starting from an initially non-isotropic shape it develops towards a rotational symmetric distribution in momentum space. This figure is taken from Ref. [2].

of a gradient expansion of the convolution integrals in coordinate space within the Wigner transformation. For the time evolution only contributions up to first order in the gradients are kept. Finally, the quasi-particle assumption is introduced as follows: The Green functions appearing in the transport equation – explicitly or implicitly via the self-energies – are written in Wigner representation as a product of a distribution function N and the spectral function A . The quasi-particle assumption is then realized by employing a δ -like form for the spectral function which connects the energy variable to the momentum. By integrating the first order transport equation over all (positive) energies, furthermore, the Boltzmann equation for the time evolution of the on-shell distribution function (2.64) is obtained.

Inspite of the fact, that the Boltzmann equation (2.64) can be obtained in different subsequent approximation schemes, it is of basic interest, how its actual solutions compare to those from the full Kadanoff-Baym dynamics.

2.2.2 Boltzmann vs. Kadanoff-Baym dynamics

In the following we will compare the solutions of the Boltzmann equation with the solution of the Kadanoff-Baym theory in two spatial dimensions. We start with a presentation of the non-equilibrium time evolution of two colliding particle accumulations (tsunamis) within the

full Kadanoff-Baym calculation (see Figure 2.5 taken from Ref. [2]).

During the time evolution the bumps at finite momenta (in p_x direction) slowly disappear, while the one close to zero momentum – which initially stems from the vacuum contribution to the Green function – is decreased as seen for different snapshots at times $t \cdot m = 0, 15, 30, 45, 75, 150$ in Fig. 2.5. The system with initially apparent collision axis slowly merges – as expected – into an isotropic final distribution in momentum space.

For the comparison between the full Kadanoff-Baym dynamics and the Boltzmann approximation we concentrate on equilibration times. To this aim we define a 'quadrupole' moment for a given momentum distribution $n(\mathbf{p})$ at time \bar{t} as

$$Q(\bar{t}) = \frac{\int \frac{d^d p}{(2\pi)^d} (p_x^2 - p_y^2) N(\mathbf{p}, \bar{t})}{\int \frac{d^d p}{(2\pi)^d} N(\mathbf{p}, \bar{t})}, \quad (2.65)$$

which vanishes for the equilibrium state. For the Kadanoff-Baym case we employ the actual distribution function by the relation

$$n(\mathbf{p}, \bar{t}) = \sqrt{G_{\phi\phi}^<(\mathbf{p}, \bar{t}, \bar{t}) G_{\pi\pi}^<(\mathbf{p}, \bar{t}, \bar{t})} - \frac{1}{2}. \quad (2.66)$$

Note that when constructing the distribution function by means of equal-time Green functions the energy variable has been effectively integrated out. This has the advantage that the distribution function is given independently of the actual on-shell energies.

The relaxation of the quadrupole moment (2.66) has been studied for two different initial distributions (cf. Ref. [2] for details): The evolution of distribution d2 is displayed in Fig. 2.5 while for distribution d1 the position and the width of the two particle bumps have been modified. The calculated quadrupole moment (2.66) shows a nearly exponential decrease with time (cf. Fig. 2.6) and one can extract a relaxation rate Γ_Q via the relation

$$Q(\bar{t}) \sim \exp(-\Gamma_Q \bar{t}). \quad (2.67)$$

Fig. ?? shows for both initializations that the relaxation in the full quantum calculation occurs faster for large coupling constants than in the quasi-classical approximation, whereas for small couplings the equilibration times of the full and the approximate evolutions are comparable. We find that the scaled relaxation rate Γ_Q/λ^2 is nearly constant in the Boltzmann case, but increases with the coupling strength in the Kadanoff-Baym calculation (especially for initial distribution d2).

These findings are readily explained: Since the free Green function – as used in the Boltzmann calculation – has only support on the mass shell, only ($2 \leftrightarrow 2$) scattering processes are described in the Boltzmann limit. All other processes with a different number of incoming and outgoing particles vanish (as noted before). Within the full Kadanoff-Baym calculation this is different, since here the spectral function – determined from the self-consistent Green function – acquires a finite width. Thus the Green function has support at all energies although it drops fast far off the mass shell. Especially for large coupling constants, where the spectral function is sufficiently broad, the three particle production process gives a significant contribution to

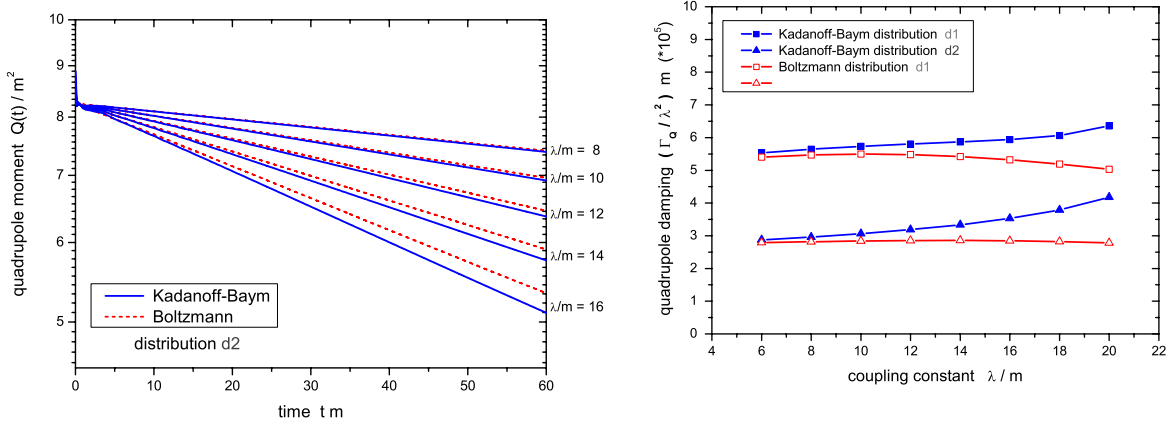


Figure 2.6: (l.h.s.) Decrease of the quadrupole moment in time for different coupling constants $\lambda/m = 8$ (2) 16 for the full Kadanoff-Baym calculation and the Boltzmann approximation. This figure is taken from Ref. [2]. (r.h.s.) Relaxation rate (divided by the coupling λ squared) for Kadanoff-Baym and Boltzmann calculations as a function of the interaction strength. For the two different initial configurations the full Kadanoff-Baym evolution leads to a faster equilibration. This figure is taken from Ref. [2].

the collision integral. Since the width of the spectral function increases with the interaction strength, such processes become more important in the high coupling regime. As a consequence the difference between both approaches is larger for stronger interactions as observed in Fig. ???. For small couplings λ/m in both approaches basically the usual $2 \leftrightarrow 2$ scattering contributes and the results for the thermalization rate Γ_Q are quite similar.

In summarizing this Section we point out that the full solution of the Kadanoff-Baym equations does include $1 \leftrightarrow 3$ and $2 \leftrightarrow 2$ off-shell collision processes which – in comparison to the Boltzmann on-shell $2 \leftrightarrow 2$ collision limit – become important when the spectral width of the particles reaches $\sim 1/3$ of the particle mass. On the other hand, the simple Boltzmann limit works surprisingly well for smaller couplings and those cases, where the spectral function is sufficiently narrow.

Chapter 3

Derivation of off-shell relativistic transport theory

Formal derivations of off-shell transport equations have been presented about 40 years ago by Kadanoff and Baym [3] but actual solutions have barely been addressed. This Chapter is devoted to a transparent derivation of generalized transport equations in first order gradient expansion including a generalized testparticle-ansatz for the solution of the off-shell transport equation.

The derivation of generalized transport equations starts by rewriting the Kadanoff-Baym equation for the Wightman functions in coordinate space $(x_1 = (t_1, \mathbf{x}_1), x_2 = (t_2, \mathbf{x}_2))$ (2.35) as

$$[\partial_{x_1}^\mu \partial_\mu^{x_1} + m^2 + \Sigma^\delta(x_1)] iG^{\lessgtr}(x_1, x_2) = iI_1^{\lessgtr}(x_1, x_2). \quad (3.1)$$

The collision terms on the r.h.s. of (3.1) are given in $D = d + 1$ space-time dimensions by convolution integrals over coordinate space self-energies and Green functions:

$$\begin{aligned} I_1^{\lessgtr}(x_1, x_2) = & - \int_{t_0}^{t_1} d^D z [\Sigma^>(x_1, z) - \Sigma^<(x_1, z)] G^{\lessgtr}(z, x_2) \\ & + \int_{t_0}^{t_2} d^D z \Sigma^{\lessgtr}(x_1, z) [G^>(z, x_2) - G^<(z, x_2)]. \end{aligned} \quad (3.2)$$

In the general case of an arbitrary (scalar) quantum field theory Σ^δ is the local (non-dissipative) part of the path self-energy while Σ^{\lessgtr} resemble the non-local collisional self-energy contributions. In the representation (3.2) the integration boundaries are exclusively given for the time coordinates, while the integration over the spatial coordinates extends over the whole spatial volume from $-\infty$ to $+\infty$ in d dimensions.

Since transport theories are formulated in phase-space one changes to the Wigner representation via Fourier transformation with respect to the rapidly varying ('intrinsic') relative coordinate $\Delta x = x_1 - x_2$ and treats the system evolution in terms of the ('macroscopic') mean space-time coordinate $x = (x_1 + x_2)/2$ and the four-momentum $p = (p_0, \mathbf{p})$. The functions in Wigner space are obtained as

$$\bar{F}(p, x) = \int_{-\infty}^{\infty} d^D \Delta x e^{+i \Delta x_\mu p^\mu} F(x_1 = x + \Delta x/2, x_2 = x - \Delta x/2). \quad (3.3)$$

For the formulation of transport theory in the Wigner representation we have to focus not only on the transformation properties of ordinary two-point functions as given in (3.3), but also of convolution integrals as appearing in Eq. (3.2). A convolution integral in D dimensions (for arbitrary functions F, G),

$$H(x_1, x_2) = \int_{-\infty}^{\infty} d^D z F(x_1, z) G(z, x_2) \quad (3.4)$$

transforms as

$$\begin{aligned} \bar{H}(p, x) &= \int_{-\infty}^{\infty} d^D \Delta x e^{+i \Delta x_\mu p^\mu} H(x_1, x_2) \\ &= \int_{-\infty}^{\infty} d^D \Delta x e^{+i \Delta x_\mu p^\mu} \int_{-\infty}^{\infty} d^D z F(x_1, z) G(z, x_2) \\ &= e^{+i \frac{1}{2} (\partial_p^\mu \cdot \partial_{x'}^\mu - \partial_x^\mu \cdot \partial_{p'}^\mu)} \left[\bar{F}(p, x) \bar{G}(p', x') \right] \Big|_{x'=x, p'=p}. \end{aligned} \quad (3.5)$$

In accordance with the standard assumption of transport theory we assume that all functions only smoothly evolve in the mean space-time coordinates and thus restrict to first order derivatives. All terms proportional to second or higher order derivatives in the mean space-time coordinates (also mixed ones) will be dropped. Thus the Wigner transformed convolution integrals (3.4) are given in *first order gradient approximation* by,

$$\bar{H}(p, x) = \bar{F}(p, x) \bar{G}(p, x) + i \frac{1}{2} \{ \bar{F}(p, x), \bar{G}(p, x) \} + \mathcal{O}(\partial_x^2), \quad (3.6)$$

using the relativistic generalization of the Poisson bracket

$$\{ \bar{F}(p, x), \bar{G}(p, x) \} = \partial_\mu^p \bar{F}(p, x) \cdot \partial_x^\mu \bar{G}(p, x) - \partial_x^\mu \bar{F}(p, x) \cdot \partial_\mu^p \bar{G}(p, x). \quad (3.7)$$

In order to obtain the dynamics for the spectral functions within the approximate scheme we start with the Dyson-Schwinger equations for the retarded and advanced Green functions in coordinate space (2.21). – Note that the convolution integrals in (2.21) extend over the whole space and time range in contrast to the equations of motion for the Wightman functions given in (2.22) and (2.23)! – The further procedure consists in the following steps: First we

i) transform the above equations into the Wigner representation and apply the first order gradient approximation. In this limit the convolution integrals yield the product terms and the general Poisson bracket of the self-energies and the Green functions $\{ \Sigma^{R/A}, G^{R/A} \}$. We, further on, represent both equations in terms of real quantities by the decomposition of the retarded and advanced Green functions and self-energies as

$$\begin{aligned} \bar{G}^{R/A} &= Re \bar{G}^R \pm i Im \bar{G}^R = Re \bar{G}^R \mp i \bar{A}/2, & \bar{A} &= \mp 2 Im \bar{G}^{R/A}, \\ \bar{\Sigma}^{R/A} &= Re \bar{\Sigma}^R \pm i Im \bar{\Sigma}^R = Re \bar{\Sigma}^R \mp i \bar{\Gamma}/2, & \bar{\Gamma} &= \mp 2 Im \bar{\Sigma}^{R/A}. \end{aligned} \quad (3.8)$$

We find that in Wigner space the real parts of the retarded and advanced Green functions and self-energies are equal, while the imaginary parts have opposite sign and are proportional to

the spectral function \bar{A} and the width $\bar{\Gamma}$, respectively. The next step consists in

ii) the separation of the real part and the imaginary part of the two equations for the retarded and advanced Green functions, that have to be fulfilled independently. Thus we obtain four real-valued equations for the self-consistent retarded and advanced Green functions. In the last step

iii) we get simple relations by linear combination of these equations, i.e. by adding/subtracting the relevant equations.

This finally leads to two algebraic relations for the spectral function \bar{A} and the real part of the retarded Green function $Re \bar{G}^R$ in terms of the width $\bar{\Gamma}$ and the real part of the retarded self-energy $Re \bar{\Sigma}^R$ as [2, 4]:

$$[p_0^2 - \mathbf{p}^2 - m^2 - \bar{\Sigma}^\delta + Re \bar{\Sigma}^R] Re \bar{G}^R = 1 + \frac{1}{4} \bar{\Gamma} \bar{A}, \quad (3.9)$$

$$[p_0^2 - \mathbf{p}^2 - m^2 - \bar{\Sigma}^\delta + Re \bar{\Sigma}^R] \bar{A} = \bar{\Gamma} Re \bar{G}^R. \quad (3.10)$$

Note that all terms with first order gradients have disappeared in (3.9) and (3.10). A first consequence of (3.10) is a direct relation between the real and the imaginary parts of the retarded/advanced Green function, which reads (for $\bar{\Gamma} \neq 0$):

$$Re \bar{G}^R = \frac{p_0^2 - \mathbf{p}^2 - m^2 - \bar{\Sigma}^\delta - Re \bar{\Sigma}^R}{\bar{\Gamma}} \bar{A}. \quad (3.11)$$

Inserting (3.11) in (3.9) we end up with the following result for the spectral function and the real part of the retarded Green function

$$\bar{A} = \frac{\bar{\Gamma}}{[p_0^2 - \mathbf{p}^2 - m^2 - \bar{\Sigma}^\delta - Re \bar{\Sigma}^R]^2 + \bar{\Gamma}^2/4} = \frac{\bar{\Gamma}}{\bar{M}^2 + \bar{\Gamma}^2/4}, \quad (3.12)$$

$$Re \bar{G}^R = \frac{[p_0^2 - \mathbf{p}^2 - m^2 - \bar{\Sigma}^\delta - Re \bar{\Sigma}^R]}{[p_0^2 - \mathbf{p}^2 - m^2 - \bar{\Sigma}^\delta - Re \bar{\Sigma}^R]^2 + \bar{\Gamma}^2/4} = \frac{\bar{M}}{\bar{M}^2 + \bar{\Gamma}^2/4}, \quad (3.13)$$

where we have introduced the mass-function $\bar{M}(p, x)$ in Wigner space:

$$\bar{M}(p, x) = p_0^2 - \mathbf{p}^2 - m^2 - \bar{\Sigma}^\delta(x) - Re \bar{\Sigma}^R(p, x). \quad (3.14)$$

The spectral function (3.12) shows a typical Breit-Wigner shape with energy- and momentum-dependent self-energy terms. Although the above equations are purely algebraic solutions and contain no derivative terms, they are valid up to the first order in the gradients!

In addition, subtraction of the real parts and adding up the imaginary parts lead to the time evolution equations

$$p^\mu \partial_\mu^x \bar{A} = \frac{1}{2} \{ \bar{\Sigma}^\delta + Re \bar{\Sigma}^R, \bar{A} \} + \frac{1}{2} \{ \bar{\Gamma}, Re \bar{G}^R \}, \quad (3.15)$$

$$p^\mu \partial_\mu^x Re \bar{G}^R = \frac{1}{2} \{ \bar{\Sigma}^\delta + Re \bar{\Sigma}^R, Re \bar{G}^R \} - \frac{1}{8} \{ \bar{\Gamma}, \bar{A} \}. \quad (3.16)$$

The Poisson bracket containing the mass-function \bar{M} leads to the well-known drift operator $p^\mu \partial_\mu^x \bar{F}$ (for an arbitrary function \bar{F}), i.e.

$$\{\bar{M}, \bar{F}\} = \{p_0^2 - \mathbf{p}^2 - m^2 - \bar{\Sigma}^\delta - Re \bar{\Sigma}^R, \bar{F}\} \quad (3.17)$$

$$= 2p^\mu \partial_\mu^x \bar{F} - \{\bar{\Sigma}^\delta + Re \bar{\Sigma}^R, \bar{F}\}, \quad (3.18)$$

such that the first order equations (3.15) and (3.16) can be written in a more comprehensive form as

$$\{\bar{M}, \bar{A}\} = \{\bar{\Gamma}, Re \bar{G}^R\}, \quad (3.19)$$

$$\{\bar{M}, Re \bar{G}^R\} = -\frac{1}{4} \{\bar{\Gamma}, \bar{A}\}. \quad (3.20)$$

When inserting (3.12) and (3.13) we find that these first order time evolution equations are *solved* by the algebraic expressions. In this case the following relations hold:

$$\{\bar{M}, \bar{A}\} = \{\bar{\Gamma}, Re \bar{G}^R\} = \{\bar{M}, \bar{\Gamma}\} \frac{\bar{M}^2 - \bar{\Gamma}^2/4}{[\bar{M}^2 + \bar{\Gamma}^2/4]^2}, \quad (3.21)$$

$$\{\bar{M}, Re \bar{G}^R\} = -\frac{1}{4} \{\bar{\Gamma}, \bar{A}\} = \{\bar{M}, \bar{\Gamma}\} \frac{\bar{M} \bar{\Gamma}/2}{[\bar{M}^2 + \bar{\Gamma}^2/4]^2}. \quad (3.22)$$

Thus we have derived the proper structure of the spectral function (3.12) within the first-order gradient (or semiclassical) approximation. Together with the explicit form for the real part of the retarded Green function (3.13) we now have fixed the dynamics of the spectral properties, which is consistent up to first order in the gradients.

3.1 Kadanoff-Baym transport

As a next step we rewrite the memory terms in the collision integrals such that the time integrations extend from $-\infty$ to $+\infty$. In this respect we consider the initial time $t_0 = -\infty$ whereas the upper time boundaries t_1, t_2 are taken into account by Θ -functions, i.e.

$$\begin{aligned} I_1^{\lesseqgtr}(x_1, x_2) &= - \int_{-\infty}^{\infty} d^D x' \Theta(t_1 - t') [\Sigma^>(x_1, x') - \Sigma^<(x_1, x')] G^{\lesseqgtr}(x', x_2) \\ &\quad + \int_{-\infty}^{\infty} d^D x' \Sigma^{\lesseqgtr}(x_1, x') \Theta(t_2 - t') [G^>(x', x_2) - G^<(x', x_2)] \\ &= - \int_{-\infty}^{\infty} d^D x' \Sigma^R(x_1, x') G^{\lesseqgtr}(x', x_2) + \Sigma^{\lesseqgtr}(x_1, x') G^A(x', x_2). \end{aligned} \quad (3.23)$$

We now perform the analogous steps as invoked before for the retarded and advanced Dyson-Schwinger equations. We start with a first order gradient expansion of the Wigner transformed

Kadanoff-Baym equation using (3.23) for the memory integrals. Again we separate the real and the imaginary parts in the resulting equation, which have to be satisfied independently. At the end of this procedure we obtain a generalized transport equation:

$$\underbrace{2p^\mu \partial_\mu^x i\bar{G}^{\lessgtr} - \{\bar{\Sigma}^\delta + Re \bar{\Sigma}^R, i\bar{G}^{\lessgtr}\}}_{\{\bar{M}, i\bar{G}^{\lessgtr}\}} - \{i\bar{\Sigma}^{\lessgtr}, Re \bar{G}^R\} = i\bar{\Sigma}^< i\bar{G}^> - i\bar{\Sigma}^> i\bar{G}^< \quad (3.24)$$

as well as a generalized mass-shell equation

$$\underbrace{[p^2 - m^2 - \bar{\Sigma}^\delta - Re \bar{\Sigma}^R]}_{\bar{M}} i\bar{G}^{\lessgtr} = i\bar{\Sigma}^{\lessgtr} Re \bar{G}^R + \frac{1}{4} \{i\bar{\Sigma}^>, i\bar{G}^<\} - \frac{1}{4} \{i\bar{\Sigma}^<, i\bar{G}^>\} \quad (3.25)$$

with the mass-function \bar{M} specified in (3.14). Since the Green function $G^{\lessgtr}(x_1, x_2)$ consists of an antisymmetric real part and a symmetric imaginary part with respect to the relative coordinate $x_1 - x_2$, the Wigner transform of this function is purely imaginary. It is thus convenient to represent the Wightman functions in Wigner space by the real-valued quantities $i\bar{G}^{\lessgtr}(p, x)$. Since the collisional self-energies obey the same symmetry relations in coordinate space and in phase-space, they will be kept also as $i\bar{\Sigma}^{\lessgtr}(p, x)$ further on.

In the transport equation (3.24) one recognizes on the l.h.s. the drift term $p^\mu \partial_\mu^x i\bar{G}^{\lessgtr}$, as well as the Vlasov term with the local self-energy $\bar{\Sigma}^\delta$ and the real part of the retarded self-energy $Re \bar{\Sigma}^R$. On the other hand the r.h.s. represents the collision term with its typical ‘gain and loss’ structure. The loss term $i\bar{\Sigma}^> i\bar{G}^<$ (proportional to the Green function itself) describes the scattering out of a respective phase-space cell whereas the gain term $i\bar{\Sigma}^< i\bar{G}^>$ takes into account scatterings into the actual cell. The last term on the l.h.s. $\{i\bar{\Sigma}^{\lessgtr}, Re \bar{G}^R\}$ is very *peculiar* since it does not contain directly the distribution function $i\bar{G}^<$. This second Poisson bracket vanishes in the quasiparticle approximation and thus does not appear in the on-shell Boltzmann limit.

As demonstrated in detail in Refs. [2, 3] the second Poisson bracket $\{i\bar{\Sigma}^{\lessgtr}, Re \bar{G}^R\}$ governs the evolution of the off-shell dynamics for nonequilibrium systems.

Although the generalized transport equation (3.24) and the generalized mass-shell equation (3.25) have been derived from the same Kadanoff-Baym equation in a first order gradient expansion, both equations are not exactly equivalent [5, 2]. Instead, they deviate from each other by contributions of second gradient order, which are hidden in the term $\{i\bar{\Sigma}^{\lessgtr}, Re \bar{G}^R\}$. This raises the question: *which one of these two equations has to be considered of higher priority?* The question is answered in practical applications by the prescription of solving the generalized transport equation (3.24) for $i\bar{G}^<$ in order to study the dynamics of the nonequilibrium system in phase-space. Since the dynamical evolution of the spectral properties is taken into account by the equations derived in first order gradient expansion from the retarded and advanced Dyson-Schwinger equations, one can neglect the generalized mass-shell equation (3.25). Thus

for our actual numerical studies in Section 2.2 we will use the generalized transport equation (3.24) supported by the algebraic relations (3.12) and (3.13).

3.2 Transport in the Botermans-Malfliet scheme

Furthermore, one recognizes by subtraction of the $i\bar{G}^>$ and $i\bar{G}^<$ mass-shell and transport equations, that the dynamics of the spectral function $\bar{A} = i\bar{G}^> - i\bar{G}^<$ is determined in the same way as derived from the retarded and advanced Dyson-Schwinger equations (3.12) and (3.19). The inconsistency between the two equations (3.24) and (3.25) vanishes since the differences are contained in the collisional contributions on the r.h.s. of (3.24).

In order to evaluate the $\{i\bar{\Sigma}^<, Re \bar{G}^R\}$ -term on the l.h.s. of (3.24) and to explore the differences between the KB- and BM-form of the transport equations (see below) it is useful to introduce distribution functions for the Green functions and self-energies as

$$i\bar{G}^<(p, x) = \bar{N}(p, x) \bar{A}(p, x), \quad i\bar{G}^>(p, x) = [1 + \bar{N}(p, x)] \bar{A}(p, x), \quad (3.26)$$

$$i\bar{\Sigma}^<(p, x) = \bar{N}^\Sigma(p, x) \bar{\Gamma}(p, x), \quad i\bar{\Sigma}^>(p, x) = [1 + \bar{N}^\Sigma(p, x)] \bar{\Gamma}(p, x). \quad (3.27)$$

In equilibrium the distribution function with respect to the Green functions \bar{N} and the self-energies \bar{N}^Σ are given as Bose functions in the energy p_0 at given temperature; they thus are equal in equilibrium but in general might differ out-of-equilibrium. Following the argumentation of Botermans and Malfliet [5] the distribution functions \bar{N} and \bar{N}^Σ in (3.26) should be identical within the second term of the l.h.s. of (3.24) in order to obtain a consistent first order gradient expansion (without hidden higher order gradient terms). In order to demonstrate their argument we write

$$i\bar{\Sigma}^< = \bar{\Gamma} \bar{N}^\Sigma = \bar{\Gamma} \bar{N} + \bar{K}. \quad (3.28)$$

The ‘correction’ term

$$\bar{K} = \bar{\Gamma} (\bar{N}^\Sigma - \bar{N}) = (i\bar{\Sigma}^< i\bar{G}^> - i\bar{\Sigma}^> i\bar{G}^<) \bar{A}^{-1}, \quad (3.29)$$

is proportional to the collision term of the generalized transport equation (3.24), which itself is already of first order in the gradients. Thus, whenever a distribution function \bar{N}^Σ appears within a Poisson bracket, the difference term $(\bar{N}^\Sigma - \bar{N})$ becomes of second order in the gradients and should be omitted for consistency. As a consequence \bar{N}^Σ can be replaced by \bar{N} and thus the self-energy $\bar{\Sigma}^<$ by $\bar{G}^< \cdot \bar{\Gamma} / \bar{A}$ in the Poisson bracket term $\{\bar{\Sigma}^<, Re \bar{G}^R\}$. The generalized transport equation (3.24) then can be written in short-hand notation

$$\frac{1}{2} \bar{A} \bar{\Gamma} \left[\{\bar{M}, i\bar{G}^<\} - \frac{1}{\bar{\Gamma}} \{\bar{\Gamma}, \bar{M} \cdot i\bar{G}^<\} \right] = i\bar{\Sigma}^< i\bar{G}^> - i\bar{\Sigma}^> i\bar{G}^< \quad (3.30)$$

with the mass-function \bar{M} (3.14). The transport equation (3.30) within the Botermans-Malfliet (BM) form resolves the discrepancy between the generalized mass-shell equation (3.25) and the generalized transport equation in its original Kadanoff-Baym (KB) form (3.24).

3.3 Testparticle representation

The generalized transport equation (3.30) allows to extend the traditional on-shell transport approaches for which efficient numerical recipes have been set up. In order to obtain a practical solution to the transport equation (3.30) we use a testparticle ansatz for the Green function $G^<$, more specifically for the real and positive semi-definite quantity

$$F_{XP} = i G^<(X, P) \sim \sum_{i=1}^N \delta^{(3)}(\mathbf{X} - \mathbf{X}_i(t)) \delta^{(3)}(\mathbf{P} - \mathbf{P}_i(t)) \delta(P_0 - \epsilon_i(t)). \quad (3.31)$$

In the most general case (where the self energies depend on four-momentum P , time t and the spatial coordinates \mathbf{X}) the equations of motion for the testparticles read

$$\frac{d\vec{X}_i}{dt} = \frac{1}{1 - C_{(i)}} \frac{1}{2\epsilon_i} \left[2\vec{P}_i + \vec{\nabla}_{P_i} \text{Re}\Sigma_{(i)}^{ret} + \frac{\epsilon_i^2 - \vec{P}_i^2 - M_0^2 - \text{Re}\Sigma_{(i)}^{ret}}{\Gamma_{(i)}} \vec{\nabla}_{P_i} \Gamma_{(i)} \right], \quad (3.32)$$

$$\frac{d\vec{P}_i}{dt} = -\frac{1}{1 - C_{(i)}} \frac{1}{2\epsilon_i} \left[\vec{\nabla}_{X_i} \text{Re}\Sigma_{(i)}^{ret} + \frac{\epsilon_i^2 - \vec{P}_i^2 - M_0^2 - \text{Re}\Sigma_{(i)}^{ret}}{\Gamma_{(i)}} \vec{\nabla}_{X_i} \Gamma_{(i)} \right], \quad (3.33)$$

$$\frac{d\epsilon_i}{dt} = \frac{1}{1 - C_{(i)}} \frac{1}{2\epsilon_i} \left[\frac{\partial \text{Re}\Sigma_{(i)}^{ret}}{\partial t} + \frac{\epsilon_i^2 - \vec{P}_i^2 - M_0^2 - \text{Re}\Sigma_{(i)}^{ret}}{\Gamma_{(i)}} \frac{\partial \Gamma_{(i)}}{\partial t} \right], \quad (3.34)$$

where the notation $F_{(i)}$ implies that the function is taken at the coordinates of the testparticle, i.e. $F_{(i)} \equiv F(t, \mathbf{X}_i(t), \mathbf{P}_i(t), \epsilon_i(t))$.

In (3.32-3.34) a common multiplication factor $(1 - C_{(i)})^{-1}$ appears, which contains the energy derivatives of the retarded self energy

$$C_{(i)} = \frac{1}{2\epsilon_i} \left[\frac{\partial}{\partial \epsilon_i} \text{Re}\Sigma_{(i)}^{ret} + \frac{\epsilon_i^2 - \vec{P}_i^2 - M_0^2 - \text{Re}\Sigma_{(i)}^{ret}}{\Gamma_{(i)}} \frac{\partial}{\partial \epsilon_i} \Gamma_{(i)} \right]. \quad (3.35)$$

It yields a shift of the system time t to the 'eigntime' of particle i defined by $\tilde{t}_i = t/(1 - C_{(i)})$. As the reader immediately verifies, the derivatives with respect to the 'eigntime', i.e. $d\mathbf{X}_i/d\tilde{t}_i$, $d\mathbf{P}_i/d\tilde{t}_i$ and $d\epsilon_i/d\tilde{t}_i$ then emerge without this renormalization factor for each testparticle i when neglecting higher order time derivatives in line with the semiclassical approximation scheme.

Some limiting cases should be mentioned explicitly: In case of a momentum-independent 'width' $\Gamma(X)$ we take $M^2 = P^2 - \text{Re}\Sigma^{ret}$ as an independent variable instead of P_0 , which then fixes the energy (for given \mathbf{P} and M^2) to

$$P_0^2 = \mathbf{P}^2 + M^2 + \text{Re}\Sigma_{X\mathbf{P}M^2}^{ret}. \quad (3.36)$$

Eq. (3.34) then turns to $(\Delta M_i^2 = M_i^2 - M_0^2)$

$$\frac{d\Delta M_i^2}{dt} = \frac{\Delta M_i^2}{\Gamma_{(i)}} \frac{d\Gamma_{(i)}}{dt} \leftrightarrow \frac{d}{dt} \ln \left(\frac{\Delta M_i^2}{\Gamma_{(i)}} \right) = 0 \quad (3.37)$$

for the time evolution of the test-particle i in the invariant mass squared. In case of $\Gamma = \text{const.}$ the familiar equations of motion for testparticles in on-shell transport approaches are regained. We mention in passing that in the Parton-Hadron-String Dynamics (PHSD) transport approach the width of partonic degrees of freedom is taken as momentum independent such that the simple limit (3.37) applies.

Chapter 4

Thermodynamics and transport properties of QCD*

Early concepts of the Quark-Gluon-Plasma (QGP) were guided by the idea of a weakly interacting system of massless partons which might be described by perturbative QCD (pQCD). However, experimental observations at RHIC indicated that the new medium created in ultra-relativistic Au+Au collisions is interacting more strongly than hadronic matter. It is presently widely accepted that this medium is an almost perfect liquid of partons as extracted experimentally from the strong radial expansion and the scaling of the elliptic flow $v_2(p_T)$ of mesons and baryons with the number of constituent quarks and antiquarks. At vanishing quark chemical potential the QCD problem can be addressed at zero and finite temperature by lattice QCD calculations on a 3+1 dimensional torus with a suitable discretization of the QCD action on the lattice. These calculations so far have provided valuable information on the QCD equation of state, chiral symmetry restoration and various correlators that can be attributed to transport coefficients. Due to the Fermion 'sign'-problem lQCD calculations at finite μ_q are presently not robust and one has to rely on nonperturbative - but effective - models to obtain information in the (T, μ_q) plane or for systems out-of equilibrium.

4.1 Quasiparticle properties and thermodynamics within the DQPM

A consistent dynamical approach for the description of strongly interacting systems - also out-of equilibrium - can be formulated on the basis of Kadanoff-Baym (KB) equations (cf. Chapter 2) or off-shell transport equations in phase-space representation (cf. Chapter 3), respectively. In the KB theory the field quanta are described in terms of dressed propagators with complex selfenergies. Whereas the real part of the selfenergies can be related to mean-field potentials (of Lorentz scalar, vector or tensor type), the imaginary parts provide information about the lifetime and/or reaction rates of time-like 'particles'. Once the proper (complex) selfenergies of the degrees of freedom are known, the time evolution of the system is fully governed by off-shell transport equations (cf. Chapter 3). The determination/extraction of complex selfenergies for the partonic degrees of freedom can be performed within the Dynamical QuasiParticle Model (DQPM) by fitting lattice QCD (lQCD) 'data' in thermal equilibrium. In fact, the DQPM

allows for a simple and transparent interpretation of lattice QCD results for thermodynamic quantities as well as correlators and leads to effective strongly interacting partonic quasiparticles with broad spectral functions. We stress that mean-field potentials for the 'quarks' and 'gluons' as well as effective interactions can be extracted from lQCD within the DQPM as well (see below). Furthermore, the DQPM can be extended to finite quark chemical potential μ_q . In the scope of the DQPM the running coupling constant (squared) is approximated by

$$g^2(T/T_c) = \frac{48\pi^2}{(11N_c - 2N_f) \ln[\lambda^2(T/T_c - T_s/T_c)^2]}, \quad (4.1)$$

where the parameters $\lambda \approx 2.42$ and $T_s/T_c \approx 0.56$ have to be extracted from a fit to the lattice data. In (4.1), $N_c = 3$ stands for the number of colors, T_c is the critical temperature (≈ 158 MeV), while $N_f (= 3)$ denotes the number of flavors. The parameter T_s is essentially important for the infrared enhancement of the coupling at low temperature T . As demonstrated in Fig. 4.1 this functional form for the strong coupling $\alpha_s = g^2/(4\pi)$ is in accordance with the lQCD calculations of the Bielefeld group for the long range part of the $q - \bar{q}$ potential. Furthermore, it matches the hard-thermal-loop (HTL) limit for high temperatures T .

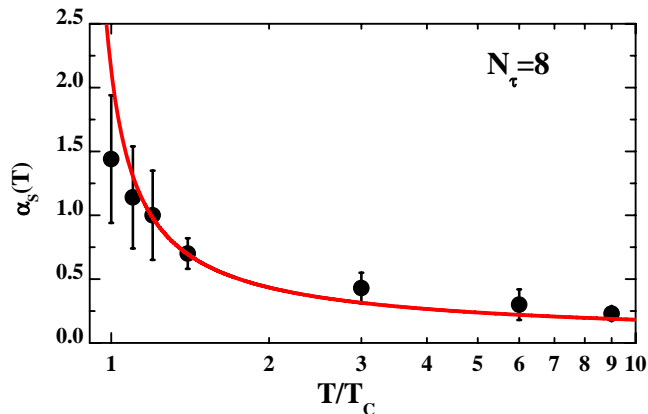


Figure 4.1: The coupling $\alpha_s(T) = g^2(T)/(4\pi)$ (solid red line) as a function of T/T_c in comparison to the long range part of the strong coupling as extracted from the Bielefeld group from the free energy of a quark-antiquark pair in quenched lQCD (for $N_\tau = 8$).

The dynamical quasiparticle mass (for gluons and quarks) is assumed to be given by the (HTL) thermal mass in the asymptotic high-momentum regime, i.e. for gluons

$$M_g^2(T) = \frac{g^2}{6} \left(\left(N_c + \frac{1}{2} N_f \right) T^2 + \frac{N_c}{2} \sum_q \frac{\mu_q^2}{\pi^2} \right), \quad (4.2)$$

and for quarks (antiquarks)

$$M_{q(\bar{q})}^2(T) = \frac{N_c^2 - 1}{8N_c} g^2 \left(T^2 + \frac{\mu_q^2}{\pi^2} \right), \quad (4.3)$$

but with the coupling given in (4.1). The effective quarks, antiquarks and gluons in the DQPM have finite widths, which for $\mu_q = 0$ are adopted in the form

$$\Gamma_g(T) = \frac{1}{3} N_c \frac{g^2 T}{8\pi} \ln \left(\frac{2c}{g^2} + 1 \right), \quad (4.4)$$

$$\Gamma_{q(\bar{q})}(T) = \frac{1}{3} \frac{N_c^2 - 1}{2N_c} \frac{g^2 T}{8\pi} \ln \left(\frac{2c}{g^2} + 1 \right), \quad (4.5)$$

where $c = 14.4$ is related to a magnetic cut-off, which is one of the few parameters of the DQPM.

The physical processes contributing to the width Γ_g are both $gg \leftrightarrow gg$, $gq \leftrightarrow gq$ scattering as well as splitting and fusion reactions $gg \leftrightarrow g$, $gg \leftrightarrow ggg$, $ggg \leftrightarrow gggg$ or $g \leftrightarrow q\bar{q}$ etc. On the fermion side elastic fermion-fermion scattering $pp \leftrightarrow pp$, where p stands for a quark q or antiquark \bar{q} , fermion-gluon scattering $pg \leftrightarrow pg$, gluon bremsstrahlung $pp \leftrightarrow pp + g$ or quark-antiquark fusion $q\bar{q} \leftrightarrow g$ etc. emerge. Note, however, that the explicit form of (4.4) is derived for hard two-body scatterings only. It is worth to point out that the ratio of the masses to their widths $\sim g \ln(2c/g^2 + 1)$ approaches zero only asymptotically for $T \rightarrow \infty$ such that the width of the quasiparticles is comparable to the pole mass slightly above T_c up to all terrestrial energy scales.

4.1.1 Spectral functions

The parton spectral functions are no longer δ -functions in the invariant mass squared but taken as (cf. Chapter 3)

$$\rho_j(\omega, \mathbf{p}) = \frac{\Gamma_j}{E_j} \left(\frac{1}{(\omega - E_j)^2 + \Gamma_j^2} - \frac{1}{(\omega + E_j)^2 + \Gamma_j^2} \right) \quad (4.6)$$

separately for quarks, antiquarks and gluons ($j = q, \bar{q}, g$). Here $E_j^2(\mathbf{p}^2) = \mathbf{p}^2 + M_j^2 - \Gamma_j^2$, where the parameters Γ_j, M_j from the DQPM have been described above. The spectral function (4.6) is antisymmetric in ω and normalized as

$$\int_{-\infty}^{\infty} \frac{d\omega}{2\pi} \omega \rho_j(\omega, \mathbf{p}) = \int_0^{\infty} \frac{d\omega}{2\pi} 2\omega \rho_j(\omega, \mathbf{p}) = 1 \quad (4.7)$$

as mandatory for quantum-field theory.

The actual gluon mass M_g and width Γ_g – employed as input in the further calculations – as well as the quark mass M_q and width Γ_q are depicted in Fig. 4.2 (l.h.s.) as a function of T/T_c . Note that for $\mu_q = 0$ the DQPM gives

$$M_q = \frac{2}{3} M_g, \quad \Gamma_q = \frac{4}{9} \Gamma_g. \quad (4.8)$$

These variations of the masses with the temperature T – that appear drastic in Fig. 4.2 (l.h.s.) – become, however, rather smooth if viewed as a function of the scalar parton density ρ_s defined

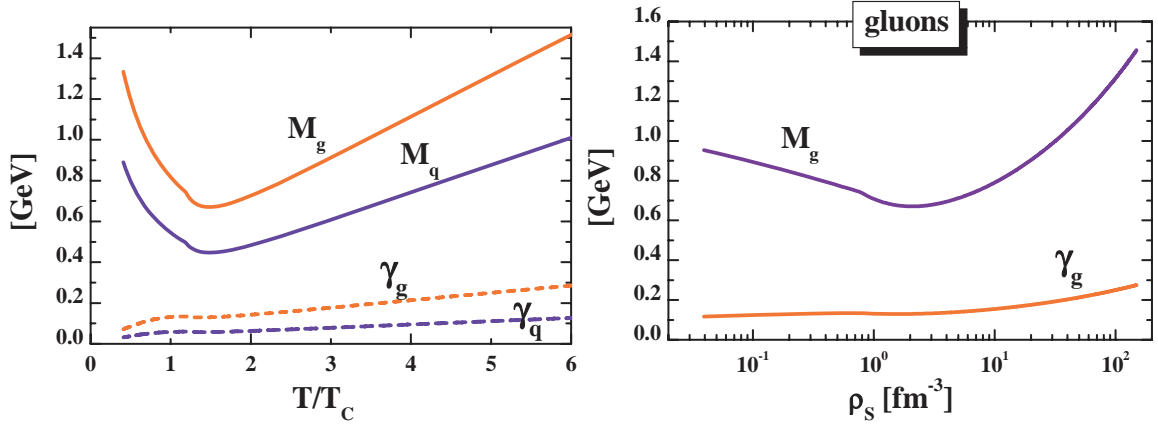


Figure 4.2: (l.h.s.) The effective gluon mass M_g and width Γ_g as function of the scaled temperature T/T_c (red lines). The blue lines show the corresponding quantities for quarks. (r.h.s.) The effective gluon mass M_g and width Γ_g as function of the scalar density ρ_s within the DQPM. The corresponding mass and width for quarks (for $\mu_q = 0$) is obtained from Eq. (4.8). Note the logarithmic scale in ρ_s .

(in thermal equilibrium) by

$$\begin{aligned}
\rho_s \left(\frac{T}{T_c} \right) = & d_g \int_0^\infty \frac{d\omega}{2\pi} \int \frac{d^3p}{(2\pi)^3} 2\sqrt{p^2} \rho_g(\omega, \mathbf{p}) n_B(\omega/T) \Theta(p^2) \\
& + d_q \int_0^\infty \frac{d\omega}{2\pi} \int \frac{d^3p}{(2\pi)^3} 2\sqrt{p^2} \rho_q(\omega, \mathbf{p}) n_F((\omega - \mu_q)/T) \Theta(p^2) \\
& + d_{\bar{q}} \int_0^\infty \frac{d\omega}{2\pi} \int \frac{d^3p}{(2\pi)^3} 2\sqrt{p^2} \rho_{\bar{q}}(\omega, \mathbf{p}) n_F((\omega + \mu_q)/T) \Theta(p^2) ,
\end{aligned} \tag{4.9}$$

where n_B and n_F denote the Bose and Fermi functions, respectively, while μ_q stands for the quark chemical potential. The number of transverse gluonic degrees of freedom is $d_g = 16$ while the fermion degrees of freedom amount to $d_q = d_{\bar{q}} = 2N_c N_f = 18$ in case of three flavors ($N_f=3$). The function $\Theta(p^2)$ (with $p^2 = \omega^2 - \mathbf{p}^2$) projects on **time-like** four-momenta since only this fraction of the four-momentum distribution can be propagated within the light cone. The dependence of the gluon mass M_g and width Γ_g as a function of ρ_s (within the DQPM) is displayed in Fig. 4.2(r.h.s.) and demonstrates that the explicit variation with ρ_s is rather moderate in view of the logarithmic scale in ρ_s . Note that in transport theory the scalar forces on a 'particle' are given by the ratio of the particle mass over its energy times the gradient of the scalar mean-field $U_s(x)$. The latter gradient is conventionally written as $\nabla U_s(x) = dU_s/d\rho_s \nabla \rho_s(x)$ which demonstrates the separation of geometry - expressed by $\nabla \rho_s(x)$ - from the strength of the force determined by $dU_s/d\rho_s$ (see below).

4.1.2 Thermodynamics of QCD*

With the quasiparticle properties (or propagators) fixed (cf. Fig. 4.2) one can evaluate the entropy density $s(T)$, the pressure $P(T)$ and energy density $\epsilon(T)$ in a straight forward manner (for $\mu_q=0$) by starting with the entropy density in the quasiparticle limit from Baym,

$$\begin{aligned}
s^{dqp} &= -d_g \int \frac{d\omega}{2\pi} \frac{d^3p}{(2\pi)^3} \frac{\partial n_B}{\partial T} \left(\Im \ln(-\Delta^{-1}) + \Im \Pi \Re \Delta \right) \\
&- d_q \int \frac{d\omega}{2\pi} \frac{d^3p}{(2\pi)^3} \frac{\partial n_F((\omega - \mu_q)/T)}{\partial T} \left(\Im \ln(-S_q^{-1}) + \Im \Sigma_q \Re S_q \right), \\
&- d_{\bar{q}} \int \frac{d\omega}{2\pi} \frac{d^3p}{(2\pi)^3} \frac{\partial n_F((\omega + \mu_q)/T)}{\partial T} \left(\Im \ln(-S_{\bar{q}}^{-1}) + \Im \Sigma_{\bar{q}} \Re S_{\bar{q}} \right),
\end{aligned} \tag{4.10}$$

where $n_B(\omega/T) = (\exp(\omega/T) - 1)^{-1}$ and $n_F((\omega - \mu_q)/T) = (\exp((\omega - \mu_q)/T) + 1)^{-1}$ denote the Bose and Fermi distribution functions, respectively, while $\Delta = (P^2 - \Pi)^{-1}$, $S_q = (P^2 - \Sigma_q)^{-1}$ and $S_{\bar{q}} = (P^2 - \Sigma_{\bar{q}})^{-1}$ stand for the full (scalar) quasiparticle propagators of gluons g , quarks q and antiquarks \bar{q} . In Eq. (4.10) Π and $\Sigma = \Sigma_q \approx \Sigma_{\bar{q}}$ denote the (retarded) quasiparticle selfenergies. In principle, Π as well as Δ are Lorentz tensors and should be evaluated in a nonperturbative framework. The DQPM treats these degrees of freedom as independent scalar fields with scalar selfenergies which are assumed to be identical for quarks and antiquarks. Note that one has to treat quarks and antiquarks separately in (4.10) as their abundance differs at finite quark chemical potential μ_q .

Since the nonperturbative evaluation of the propagators and selfenergies in QCD is a formidable task [and addressed in Dyson-Schwinger (DS) Bethe-Salpeter (BS) approaches] an alternative and practical procedure is to use physically motivated *Ansätze* with Lorentzian spectral functions for quarks¹ and gluons as in (4.6). With this choice the complex selfenergies read $\Pi = M_g^2 - 2i\omega\Gamma_g$ and $\Sigma_{q(\mathbf{q})} = M_{q(\mathbf{q})}^2 - 2i\Gamma_{q(\mathbf{q})}$ are fully defined via (4.2), (4.3), (4.4), (4.5). Note that the retarded propagator defined by

$$G^{-1} = \omega^2 - \mathbf{p}^2 - M^2 + 2i\Gamma\omega \tag{4.11}$$

corresponds to the propagator of a damped harmonic oscillator (with an additional \mathbf{p}^2) and preserves microcausality. Although the 'Ansatz' for the parton propagators is not QCD we will demonstrate that a variety of QCD observables on the lattice are compatible with this choice. Since within the DQPM the real and imaginary parts of the propagators Δ and S now are fixed analytically the entropy density (4.10) can be evaluated numerically. As we deal with a grandcanonical ensemble the Maxwell relations give (at $\mu_q = 0$),

$$s = \frac{\partial P}{\partial T}, \tag{4.12}$$

such that the pressure can be obtained by integration of the entropy density s over T , where one tacitly identifies the 'full' entropy density s with the quasiparticle entropy density s^{dqp} (4.10). The starting point for the integration in T is chosen between $100 \text{ MeV} < T < 120 \text{ MeV}$ where

¹In the following the abbreviation is used that 'quarks' denote quarks and antiquarks if not specified explicitly.

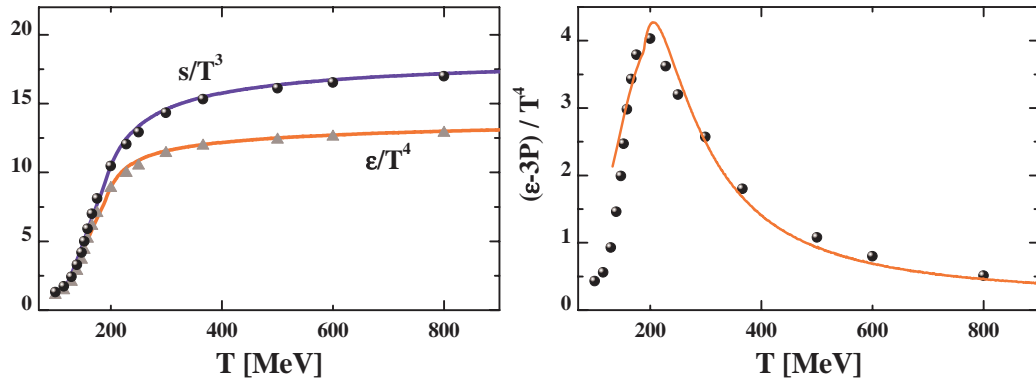


Figure 4.3: (l.h.s.) The scaled entropy density $s(T)/T^3$ (blue line) and scaled energy density $\epsilon(T)/T^4$ (red line) from the DQPM in comparison to the IQCD results from the BMW group (full dots and triangles). (r.h.s.) The dimensionless 'interaction measure' $(\epsilon - 3P)/T^4$ within the DQPM in comparison to the IQCD results from the BMW group.

the entropy density is approximated by that of a noninteracting pion, η and kaon gas.

The energy density ϵ then follows from the thermodynamical relation

$$\epsilon = Ts - P \quad (4.13)$$

(for $\mu_q = 0$) and thus is also fixed by the entropy $s(T)$ as well as the interaction measure

$$W(T) := \epsilon(T) - 3P(T) = Ts - 4P \quad (4.14)$$

that vanishes for massless and noninteracting degrees of freedom.

A direct comparison of the resulting entropy density $s(T)$ and energy density $\epsilon(T)$ from the DQPM with IQCD results from the BMW group is presented in Fig. 4.3 (l.h.s.). Both results have been divided by T^3 and T^4 , respectively, to demonstrate the scaling with temperature. We briefly note that the agreement is sufficiently good. This also holds for the dimensionless 'interaction measure', i.e. $(\epsilon - 3P)/T^4$ as demonstrated in Fig. 4.3 (r.h.s.).

The DQPM uniquely defines a potential energy density

$$V_p(T, \mu_q) = T_{g^-}^{00}(T, \mu_q) + T_{q^-}^{00}(T, \mu_q) + T_{\bar{q}^-}^{00}(T, \mu_q) \quad (4.15)$$

where the different contributions $T_{j^-}^{00}$ correspond to the space-like part of the energy-momentum tensor component T_j^{00} of parton $j = g, q, \bar{q}$. It is found that this quantity is practically independent on the quark chemical potential (for moderate μ_q) when displayed as a function of the scalar density ρ_s instead of T and μ_q separately. Note that the field quanta involved in (4.15) are virtual and thus correspond to partons exchanged in interaction diagrams.

A scalar mean-field $U_s(\rho_s)$ for quarks and antiquarks can be defined by the derivative /cf. (1.68),

$$U_s(\rho_s) = \frac{dV_p(\rho_s)}{d\rho_s}, \quad (4.16)$$

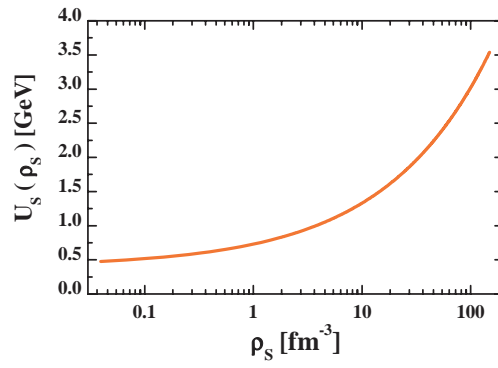


Figure 4.4: The scalar mean field (4.16) for quarks and antiquarks from the DQPM as a function of the scalar parton density ρ_s for $\mu_q = 0$.

which is evaluated numerically within the DQPM. The result is displayed in Fig. 4.4 as a function of the parton scalar density ρ_s ([?]) and shows that the scalar mean field is in the order of a few GeV for $\rho_s > 10 \text{ fm}^{-3}$. This mean-field (4.16) is employed in the Parton-Hadron-String Dynamics (PHSD) transport calculations and determines the force on a quasiparticle j , i.e. $\sim M_j/E_j \nabla U_s(x) = M_j/E_j dU_s/d\rho_s \nabla \rho_s(x)$ where the scalar density $\rho_s(x)$ is determined numerically on a space-time grid (see below).

Since the coupling (squared) in DQPM is a function of T/T_c and in HTL approximation depends on

$$T * (T, \mu_q) = \sqrt{T^2 \mu_q^2 / \pi^2}, \quad (4.17)$$

a straight forward extension of the DQPM to finite μ_q is to consider the coupling as a function of $T^*/T_c(\mu_q)$ with a μ_q -dependent critical temperature,

$$\frac{T_c(\mu_q)}{T_c(\mu_q = 0)} = \sqrt{1 - \alpha \mu_q^2} \approx 1 - \alpha/2 \mu_q^2 + \dots \quad (4.18)$$

with $\alpha \approx 8.79 \text{ GeV}^{-2}$. The expression of $T_c(\mu_q)$ in (4.18) is obtained by requiring a constant energy density ϵ for the system at $T = T_c(\mu_q)$ where ϵ at $T_c(\mu_q = 0) \approx 0.158 \text{ GeV}$ is fixed by a lattice QCD calculation at $\mu_q = 0$. The coefficient in front of the μ_q^2 -dependent part can be compared to recent lQCD calculations at finite (but small) μ_B which gives (arXiv:1410.5758)

$$\frac{T_c(\mu_B)}{T_c} = 1 - \kappa \left(\frac{\mu_B}{T_c} \right)^2 + \dots \quad (4.19)$$

with $\kappa = 0.013(2)$. Rewriting (4.18) in the form (4.19) and using $\mu_B \approx 3\mu_q$ we get $\kappa_{DQPM} \approx 0.0122$ which compares very well with the lQCD result. Consequently one has to expect an approximate scaling of the DQPM results if the partonic width is assumed to have the form,

$$\begin{aligned} \Gamma_g(T, \mu_q) &= \frac{1}{3} N_c \frac{g^2(T^*/T_c(\mu_q))}{8\pi} T \ln \left(\frac{2c}{g^2(T^*/T_c(\mu_q))} + 1 \right), \\ \Gamma_q(T, \mu_q) &= \frac{1}{3} \frac{N_c^2 - 1}{2N_c} \frac{g^2(T^*/T_c(\mu_q))}{8\pi} T \ln \left(\frac{2c}{g^2(T^*/T_c(\mu_q))} + 1 \right), \end{aligned} \quad (4.20)$$

This choice leads to an approximate independence of the potential energies per degree of freedom as a function of μ_q . Nevertheless, the conjecture (4.20) should be explicitly controlled by

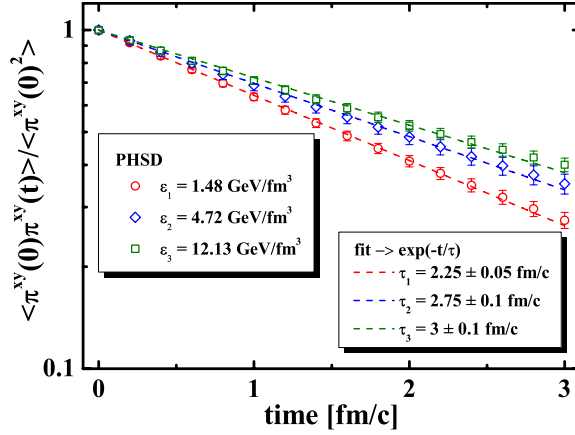


Figure 4.5: (color online) The correlation functions $\langle \pi^{xy}(0)\pi^{xy}(t) \rangle$, which are normalized by $\langle \pi^{xy}(0)^2 \rangle$, as a function of time obtained by the PHSD simulations in the box (open symbols) for systems at different energy densities and corresponding exponential fits (dashed lines) with extracted relaxation times.

future lQCD studies for $N_f=3$ at finite quark chemical potential. Unfortunately, this task is presently out of reach and one has to live with the uncertainty in (4.20) which is assumed in the following investigations.

We point out, furthermore, that in general the quasiparticle masses M_j as well as the widths Γ_j should depend also on the four-momentum q relative to the medium at rest and approach the perturbative values at high q^2 . So far, the momentum-dependence of the complex selfenergy cannot reliably be extracted from the lQCD results in thermodynamic equilibrium which are essentially sensitive to momenta in the order of a few times the temperature. This is presently an open issue and will have to be re-addressed in future.

On the basis of the DQPM for the partonic phase a relativistic off-shell transport approach has been developed in the past decade that gives approximately the same dynamics as the DQPM for partonic systems in equilibrium but also contains interacting hadrons and a dynamical transition between hadronic and partonic degrees of freedom. This approach that can also be employed for systems out-of equilibrium – such as heavy-ion collisions – is denoted by Parton-Hadron-String Dynamics (PHSD). The detailed set up of PHSD as well as its comparison to heavy-ion data from low SPS to LHC energies is described elsewhere.

4.2 Transport coefficients of the QGP

4.2.1 Shear viscosity coefficient: the Kubo formalism

In this Section we concentrate on the extraction of the shear viscosity from the ‘infinite’ parton-hadron matter employing the Kubo formalism. Using the PHSD model we simulate the ‘infinite’

matter within a cubic box with periodic boundary conditions at various values for the quark density (or chemical potential) and energy density. The size of the box is fixed to 9^3 fm^3 . The initialization is done by populating the box with light (u, d) and strange (s) quarks, antiquarks and gluons for temperatures above T_c and by a hadron gas for temperatures below T_c . The system is initialized slightly out of equilibrium and approaches kinetic and chemical equilibrium during its evolution by PHSD.

The Kubo formalism relates linear transport coefficients such as heat conductivity, shear and bulk viscosities to non-equilibrium correlations of the corresponding dissipative fluxes, and treats dissipative fluxes as perturbations to local thermal equilibrium. The Green-Kubo formula for the shear viscosity η is as follows:

$$\eta = \frac{1}{T} \int d^3r \int_0^\infty dt \langle \pi^{xy}(\mathbf{0}, 0) \pi^{xy}(\mathbf{r}, t) \rangle, \quad (4.21)$$

where T is the temperature of the system, t refers to a time after the system equilibrates, which is set at $t = 0$; $\langle \dots \rangle$ denotes the ensemble average in thermal equilibrium, and π^{xy} is the shear component (traceless part) of the energy momentum tensor $\pi^{\mu\nu}$:

$$\pi^{xy}(\mathbf{x}, t) \equiv T^{xy}(\mathbf{x}, t) = \int \frac{d^3p}{(2\pi)^3} \frac{p^x p^y}{E} f(\mathbf{x}, \mathbf{p}; t), \quad (4.22)$$

where the mean-field U_s enters in the energy $E = \sqrt{\mathbf{p}^2 + U_s + M_0^2}$.

In our numerical simulation the volume averaged shear component of the energy momentum tensor can be written as

$$\pi^{xy}(t) = \frac{1}{V} \sum_{i=1}^N \frac{p_i^x p_i^y}{E_i}, \quad (4.23)$$

where V is the volume of the system and the sum runs over all particles in the box at time t . Taking into account that point particles are uniformly distributed in our box (implying $\pi^{xy}(\mathbf{r}, t) = \pi^{xy}(t)$), we can simplify the Kubo formula for the shear viscosity to

$$\eta = \frac{V}{T} \int_0^\infty dt \langle \pi^{xy}(0) \pi^{xy}(t) \rangle. \quad (4.24)$$

The correlation functions $\langle \pi^{xy}(0) \pi^{xy}(t) \rangle$ are empirically found to decay exponentially in time

$$\langle \pi^{xy}(0) \pi^{xy}(t) \rangle = \langle \pi^{xy}(0) \pi^{xy}(0) \rangle e^{-t/\tau} \quad (4.25)$$

as shown in Fig. 4.5, where τ is the so-called *relaxation time*. Finally, we end up with the Green-Kubo formula for the shear viscosity

$$\eta = \frac{V}{T} \langle \pi^{xy}(0)^2 \rangle \tau, \quad (4.26)$$

which we use to extract the shear viscosity from the PHSD simulations in the box.

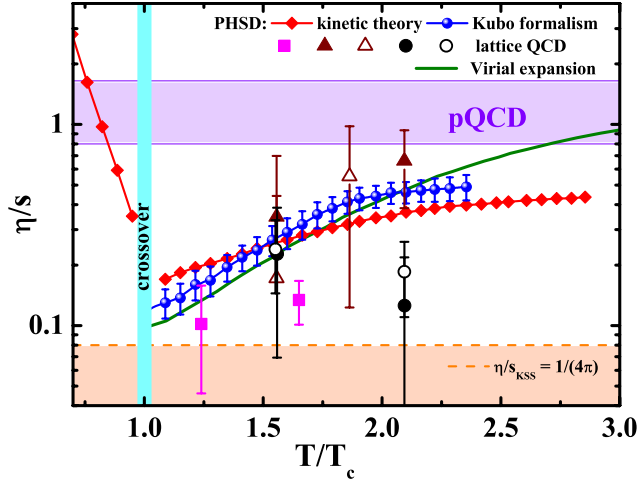


Figure 4.6: The shear viscosity to entropy density ratio η/s as a function of temperature of the system obtained by the PHSD simulations using different methods: the relaxation time approximation (red line+diamonds) and the Kubo formalism (blue line+dots). The others symbols denote lattice QCD data for pure $SU_c(3)$ gauge theory from different sources. The orange dashed line demonstrates the Kovtun-Son-Starinets bound $(\eta/s)_{KSS} = 1/(4\pi)$. For comparison, the results in the virial expansion approach (green line) are shown as a function of temperature, too.

4.2.2 Shear and bulk viscosities in the RTA

The starting hypothesis of the relaxation time approximation (RTA) is that the collision integral can be approximated (linearized) by

$$C[f] = -\frac{f - f^{eq}}{\tau} = - : \Gamma(f - f^{eq}) \quad (4.27)$$

where τ is the relaxation time and f^{eq} the equilibrium distribution. In this approach it has been shown that the shear and bulk viscosities (without mean-field or potential effects) can be written as (e.g. by J. Kapusta):

$$\eta = \frac{1}{15T} \sum_a \int \frac{d^3p}{(2\pi)^3} \frac{|\mathbf{p}|^4}{E_a^2} \tau_a(E_a) f_a^{eq}(E_a/T), \quad (4.28)$$

$$\zeta = \frac{1}{9T} \sum_a \int \frac{d^3p}{(2\pi)^3} \frac{\tau_a(E_a)}{E_a^2} [(1 - 3v_s^2)E_a^2 - M_a^2] f_a^{eq}(E_a/T), \quad (4.29)$$

where the sum is over particles of different type a (in our case, $a = q, \bar{q}, g$). In the PHSD transport approach the relaxation time can be expressed in the following way:

$$\tau_a = \Gamma_a^{-1}, \quad (4.30)$$

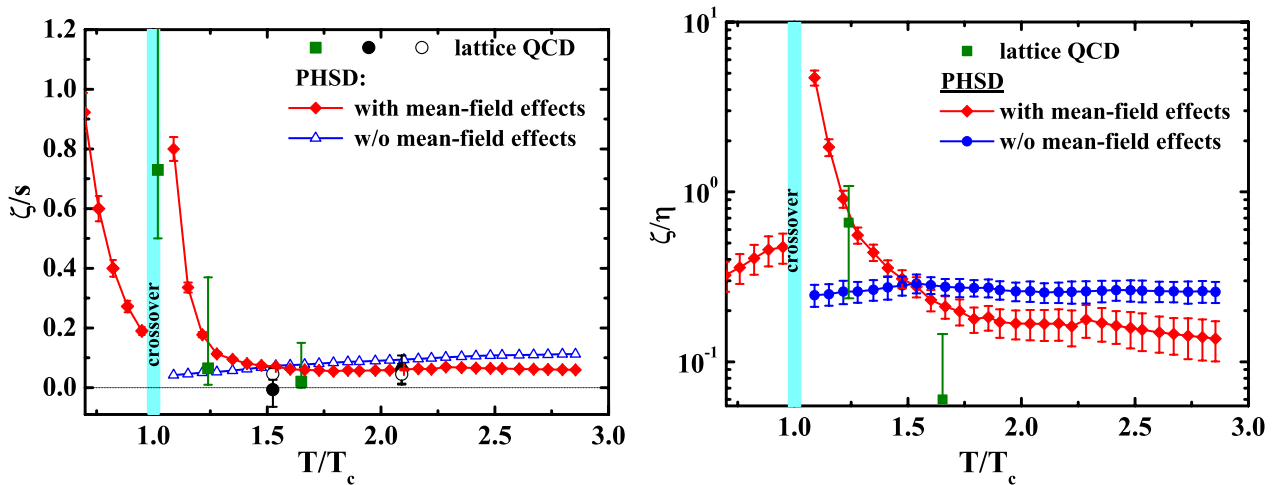


Figure 4.7: (l.h.s.) The bulk viscosity to entropy density ratio ζ/s as a function of temperature of the system extracted from the PHSD simulations in the box using the relaxation time approximation including mean-field effects (red line+diamonds) and without potential effects (blue line+open triangles). The other symbols show the available lattice QCD data from different sources (r.h.s.). The bulk to shear viscosity ratio as a function of temperature of the system obtained by the PHSD simulations in the box employing the relaxation time approximation including mean-field effects (red line+diamonds) and without potential effects (blue line+circles).

where Γ_a is the width of particles of type $a = q, \bar{q}, g$, which defined by (4.4, 4.5). In our numerical simulation the volume averaged shear and bulk viscosities assume the following expressions:

$$\eta = \frac{1}{15TV} \sum_{i=1}^N \frac{|\mathbf{p}_i|^4}{E_i^2} \Gamma_i^{-1}, \quad (4.31)$$

$$\zeta = \frac{1}{9TV} \sum_{i=1}^N \frac{\Gamma_i^{-1}}{E_i^2} [(1 - 3v_s^2)E_i^2 - M_i^2]^2, \quad (4.32)$$

where the speed of sound $v_s = v_s(T)$ is taken from the DQPM using

$$v_s^2 = \frac{\partial P}{\partial \epsilon}. \quad (4.33)$$

In Fig. 4.6 we present the shear viscosity to entropy density ratio η/s as a function of the temperature of the system extracted from the PHSD simulations in the box employing different methods: the relaxation time approximation (red line+diamonds) and the Kubo formalism (blue line+dots). For comparison, the results from the virial expansion approach (green line) and lattice QCD data for pure $SU_c(3)$ gauge theory are shown as a function of temperature, too.

Mean-field or potential effects

In the absence of the chemical potential there should be no consideration of vector or tensor fields, only scalar fields. This affects the bulk viscosity, but not the shear viscosity. The

expression for bulk viscosity with potential effects is

$$\begin{aligned} \zeta &= \frac{1}{T} \sum_a \int \frac{d^3p}{(2\pi)^3} \frac{\tau_a(E_a)}{E_a^2} f_a^{eq}(E_a/T) \\ &\times \left[\left(\frac{1}{3} - v_s^2 \right) |\mathbf{p}|^2 - v_s^2 \left(M_a^2 - T^2 \frac{d(M_a^2)}{d(T^2)} \right) \right]^2. \end{aligned} \quad (4.34)$$

In the numerical simulation the volume averaged bulk viscosity with mean-field effects is used

$$\zeta = \frac{1}{TV} \sum_{i=1}^N \frac{\Gamma_i^{-1}}{E_i^2} \left[\left(\frac{1}{3} - v_s^2 \right) |\mathbf{p}|^2 - v_s^2 \left(M_i^2 - T^2 \frac{d(M_i^2)}{d(T^2)} \right) \right]^2. \quad (4.35)$$

Using the DQPM expressions for masses of quarks and gluons (for $\mu_q = 0$)

$$M_q^2 = \frac{1}{3} g^2 T^2, \quad M_g^2 = \frac{3}{4} g^2 T^2$$

we can calculate the derivative $d(M^2)/d(T^2)$ as well as v_s^2 (4.33).

In Fig. 4.7 (l.h.s.) we show the bulk viscosity to entropy density ratio as a function of temperature of the system obtained by the PHSD simulations in the box employing the relaxation time approximation including mean-field (or potential) effects (red line+diamonds) and without potential effects (blue line+open triangles) as well as the available lattice QCD data from different sources.

Finally, in Fig. 4.7 (r.h.s.), we show the bulk to shear viscosity ratio as a function of temperature of the system extracted from the PHSD simulations in the box using the relaxation time approximation including mean-field (or potential) effects (red line+diamonds) and without potential effects (blue line+circles).

4.2.3 Electric conductivity

Whereas shear and bulk viscosities of hot QCD matter at finite temperature T presently are roughly known, the electric conductivity σ_0 is a further macroscopic quantity of interest since it controls the electromagnetic emissivity of the plasma. First results from lattice calculations on the electromagnetic correlator have provided results that varied by more than an order of magnitude. Furthermore, the conductivity dependence on the temperature T (at $T > T_c$) is widely unknown, too. The electric conductivity σ_0 is also important for the creation of electromagnetic fields in ultra-relativistic nucleus-nucleus collisions from partonic degrees of freedom, since σ_0 specifies the imaginary part of the electromagnetic (retarded) propagator and leads to an exponential decay of the propagator in time $\sim \exp(-\sigma_0(t-t')/(\hbar c))$.

In order to include the effects from an external electric field \mathbf{E} or magnetic field \mathbf{B} , the propagation of each charged test-particle j is performed with the additional Lorentz force in the equation of motion:

$$\frac{d}{dt} \mathbf{p}^j = q_j e (\mathbf{E} + \frac{\mathbf{p}^j}{E^j} \times \mathbf{B}), \quad (4.36)$$

where q_j denotes the fractional charge of the test-particle ($\pm 1/3, \pm 2/3$) and E^j its energy. We recall that the external electric field will lead to an acceleration of positively and negatively

charged particles in opposite directions while the particle scatterings/interactions will damp this acceleration and eventually lead to an equilibrium current if the external field is of moderate strength. The electric current density $j_z(t)$ (for an external electric field in z -direction) is calculated by

$$j_z(t) = \frac{1}{VN} \sum_{k=1}^N \sum_{j=1}^{N_k(t)} e q_j \frac{p_z^j(t)}{M_j(t)}, \quad (4.37)$$

where $M_j(t)$ is the mass of the test-particle j at time t . The summation in (4.37) is carried out over N ensemble members $k = 1 \dots N$ while $N_k(t)$ denotes the time-dependent number of 'physical' (u, d, s) quarks and antiquarks that varies with time t due to the processes $q + \bar{q} \leftrightarrow g \leftrightarrow q' + \bar{q}'$ in a single member of the ensemble (run). The number of runs N is typically taken as a few hundred which gives a current $j_z(t)$ practically independent on the number of ensemble members N . We recall that (without external fields) each run of the ensemble is a micro-canonical simulation of the dynamics as inherent in the PHSD transport approach which strictly conserves the total four-momentum as well as all discrete conservation laws (e.g. net fermion number for each flavor etc.). A note of caution has to be given, since due to an external field we deal with an open system with increasing energy density (temperature) in time. Therefore we employ sufficiently small external fields eE_z , such that the energy increase during the computation time (in each run) stays below 2% and the increase in temperature below 1 MeV.

Constant electric fields

We find that for constant electric fields up to $eE_z = 50$ MeV/fm a stable electric current j_{eq} emerges that is $\sim E_z$ (cf. Fig. 4.8 (l.h.s.)). Accordingly, we obtain the conductivity $\sigma_0(T, \mu_q)$ from the ratio of the stationary current density j_{eq} and the electric field strength as

$$\frac{\sigma_0(T, \mu_q)}{T} = \frac{j_{eq}(T, \mu_q)}{E_z T}. \quad (4.38)$$

The results for the dimensionless ratio (4.38) at $\mu_q = 0$ are displayed in Fig. 4.8 (r.h.s.) as a function of the scaled temperature T/T_c in comparison to more recent lattice QCD results and suggest a minimum in the ratio $\sigma_0(T, \mu_q = 0)/T$ close to the critical temperature T_c followed by an approximate linear rise up to $2 T_c$. The most recent lQCD results are roughly compatible with the PHSD predictions.

We now focus on the explicit dependence of $\sigma_0(T, \mu_q)/T$ as a function of the chemical potential μ_q which is shown in Fig. 4.9 (l.h.s.) for a fixed temperature $T=200$ MeV. The numerical result can be fitted with a quadratic correction (solid line in Fig. 4.9)

$$\frac{\sigma_0(T, \mu_q)}{T} = \frac{\sigma_0(T, \mu_q = 0)}{T} (1 + a(T)\mu_q^2). \quad (4.39)$$

with $a(T) \approx 11.6 \text{ GeV}^{-2}$ for $T = 0.2 \text{ GeV}$. This result comes about as follows: We recall that the electric conductivity of gases, liquids and solid states is described in the relaxation time approach by the Drude formula

$$\sigma_0 = \frac{e^2 n_e \tau}{m_e^*}, \quad (4.40)$$

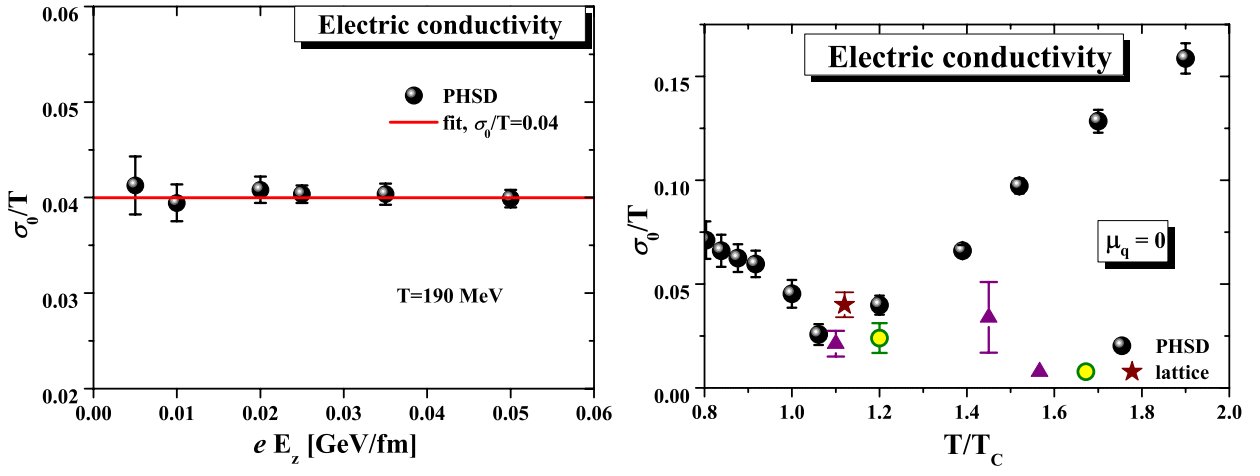


Figure 4.8: (l.h.s.) The electric conductivity over temperature at $T = 190$ MeV as a function of the external electric field eE_z . (r.h.s.) The dimensionless ratio of electric conductivity over temperature σ_0/T (4.38) as a function of the scaled temperature T/T_c for $\mu_q = 0$ in comparison to recent lattice QCD results. (r.h.s.)

where n_e denotes the density of non-localized charges, τ is the relaxation time of the charge carriers in the medium and m_e^* their effective mass. This expression can be directly computed for partonic degrees-of-freedom within the DQPM, which matches the quasiparticles properties to lattice QCD results in equilibrium. In the DQPM, the relaxation time for quarks/antiquarks is given by $\tau = 1/\Gamma_q(T, \mu_q)$, where $\Gamma_q(T, \mu_q)$ is the width of the quasiparticle spectral function (4.4), (4.5). Furthermore, the spectral distribution for the mass of the quasiparticle has a finite pole mass $M_q(T, \mu_q)$ that is also fixed in the DQPM (4.3) as well as the density of $(u, \bar{u}, d, \bar{d}, s, \bar{s})$ quarks/antiquarks as a function of temperature T and chemical potential μ_q . The latter is given by an expression similar to the scalar density ρ_s in (4.9) but $\sqrt{p^2}$ replaced by ω . Thus, we obtain for the dimensionless ratio (4.38) the expression

$$\frac{\sigma_0(T, \mu_q)}{T} \approx \frac{2}{9} \frac{e^2 n_{q+\bar{q}}(T, \mu_q)}{M_q(T, \mu_q) \Gamma_q(T, \mu_q) T}, \quad (4.41)$$

where $n_{q+\bar{q}}(T, \mu_q)$ denotes the total density of quarks and antiquarks and the prefactor $2/9$ reflects the flavor averaged fractional quark charge squared $(\sum_f q_f^2)/3$. The DQPM results match well with the explicit PHSD calculations in the box for $\mu_q=0$ since PHSD in equilibrium is a suitable transport realization of the DQPM.

In the DQPM we have $\Gamma_q(T, \mu_q) \approx \Gamma_q(T, \mu_q = 0)$ and $M_q(T, \mu_q) \approx M_q(T, \mu_q = 0)$ for $\mu_q \leq 100$ MeV, however,

$$n_{q+\bar{q}}(T, \mu_q) \approx n_{q+\bar{q}}(T, \mu_q = 0) (1 + a(T) \mu_q^2) \quad (4.42)$$

with the same coefficient $a(T)$ as in Eq. (4.39). This is demonstrated explicitly in Fig. 4.9 (r.h.s.) where the actual DQPM results for the quark+antiquark density (full dots) are compared to the fit (4.42) (solid line).

The temperature dependence of the expansion coefficient $a(T)$ is found to be $\sim 1/T^2$ such that

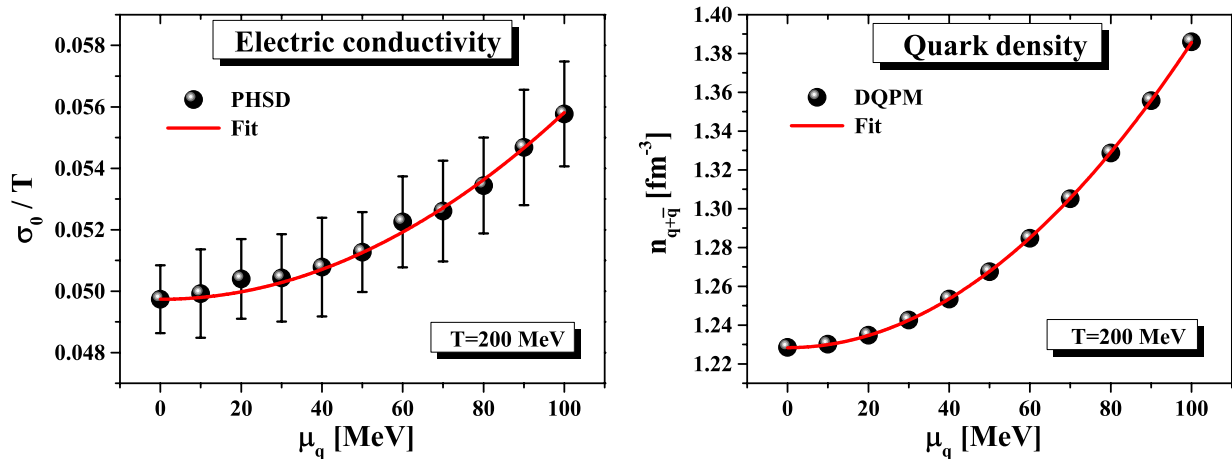


Figure 4.9: (l.h.s.) The electric conductivity over temperature σ_0/T as a function of the chemical potential μ_q for $T=200$ MeV from the PHSD calculations (full dots). The error bars indicate the statistical uncertainty for the ratio (4.38) when performing calculations for different external field strength eE_z up to 50 MeV/fm. (r.h.s.) Quark+antiquark density from the DQPM (full dots) as a function of the quark chemical potential μ_q for $T=200$ MeV. The solid (red) line displays the fit (4.42) to the DQPM results.

the ratio σ_0/T can be approximated by

$$\frac{\sigma_0(T, \mu_q)}{T} \approx \frac{\sigma_0(T, \mu_q = 0)}{T} \left(1 + c_{\sigma_0} \frac{\mu_q^2}{T^2} \right). \quad (4.43)$$

In Fig. 4.10 (l.h.s.) we display the coefficient c_{σ_0} in the temperature range $170 \text{ MeV} \leq T \leq 250 \text{ MeV}$ giving $c_{\sigma_0} \approx 0.46$ as a best fit. This completes our study on the stationary electric conductivity σ_0 which can be well understood in its variation with T and μ_q within the DQPM.

Periodic electric fields

We now extent our study to external periodic fields of frequency Ω ,

$$E_z(t) = E_z^0 \sin(\Omega t). \quad (4.44)$$

In this case the electric current density $j_z(t)$ for the charged particles in the box does not achieve a constant equilibrium value and also oscillates with the frequency Ω . Fig. 4.10 (r.h.s) shows the time-dependence of the current $j_z(t)$ from PHSD for different frequencies as a function of Ωt with their amplitudes normalized to one in comparison to the external electric field $E_z(t)$ (dotted red line). The current $j_z(t)$ is seen to be shifted in phase compared to the electric field; the phase shift δ increases with the frequency Ω up to $\pi/2$. The currents in Fig. 4.10 (r.h.s) can be well described by

$$j_z(t) = A(\Omega) j_{eq} \sin(\Omega t - \delta(\Omega)). \quad (4.45)$$

We find that the amplitude $A(\Omega)$ decreases with the frequency Ω since the current has less time to build up and to follow the external field. This behavior is in line with the complex

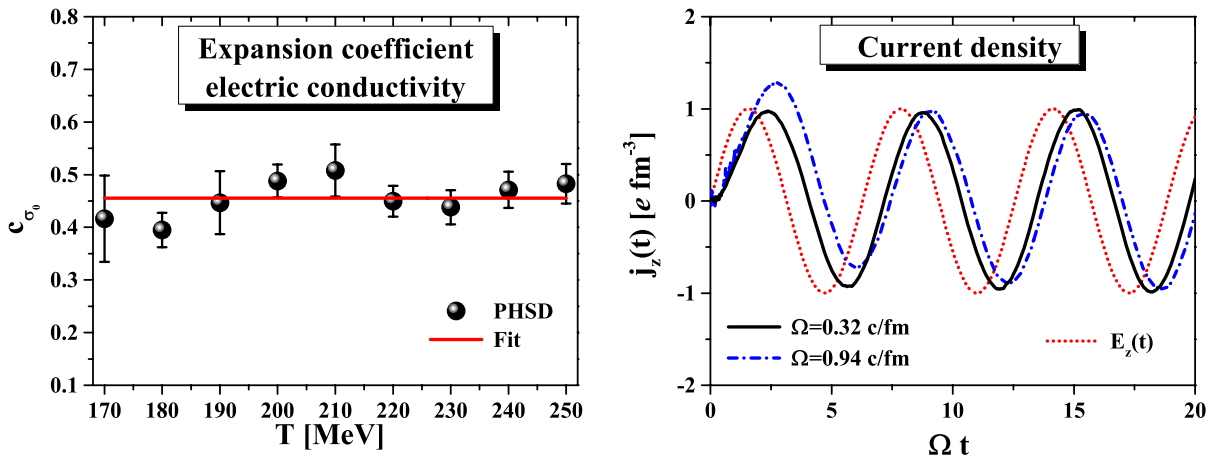


Figure 4.10: (l.h.s.) The expansion factor c_{σ_0} in (4.43) as a function of the temperature T for $\mu_q \leq 100$ MeV. The solid line shows the average value in the interval $170 \text{ MeV} < T < 250 \text{ MeV}$. (r.h.s.) The time-dependent electric current density $j_z(t)$ for $\Omega=0.32$ c/fm (solid black) and $\Omega=0.94$ c/fm (dash dotted blue) normalized to the equilibrium amplitude for temperature $T = 190$ MeV and $eE_z^0 = 0.005 \text{ GeV}^2 \approx 25 \text{ MeV/fm}$. The dotted red line shows the time-dependence of the external electric field $E_z(t)$.

conductivity $\sigma(\Omega)$ for oscillating fields,

$$\sigma(\Omega) = \frac{\sigma_0}{1 - i\Omega/\Gamma_q} = \frac{\sigma_0}{1 + \Omega^2/\Gamma_q^2} + i \frac{\sigma_0 \Omega/\Gamma_q}{1 + \Omega^2/\Gamma_q^2}, \quad (4.46)$$

where Γ_q is the quasi-particle width of the charged particles (quarks and antiquarks). We have computed the current $j_z(t)$ for $T = 190$ MeV and $eE_z^0 = 0.005 \text{ GeV}^2 \approx 25 \text{ MeV/fm}$ in the frequency range $0.02 \text{ c/fm} < \Omega < 25 \text{ c/fm}$. Fig. 4.11 shows the phase shift $\delta = \arctan(\Omega/\Gamma_q)$ (l.h.s.) and the amplitude $A(\Omega) = 1/\sqrt{1 + \Omega^2/\Gamma_q^2}$ (full dots; r.h.s.). The PHSD results can be easily followed up within the DQPM results (shown by the red lines) which provide again a good description of the microscopic calculations. Since the complex conductivity $\sigma(\Omega)$ depends only on the width Γ_q and the stationary conductivity σ_0 in (4.46) its actual values for different temperatures T and finite chemical potential μ_q follow directly from our previous results in this Section.

Note that for actual electric fields in peripheral Au+Au collisions at the top RHIC energy we have $\Omega \approx 22$ c/fm such that the electric conductivity $\sigma(\Omega)$ is suppressed relative to its equilibrium value by more than a factor of 100.

4.2.4 Magnetic response

In order to explore the magnetic response of the partonic system within PHSD we will assume the magnetic field to be sufficiently small such that terms $\sim B^2$ can be neglected (see below). Note that this limit does not hold for the strong fields $eB(\sim 0.1\text{-}1 \text{ GeV}^2 \approx 0.5\text{-}5 \text{ GeV/fm})$ in

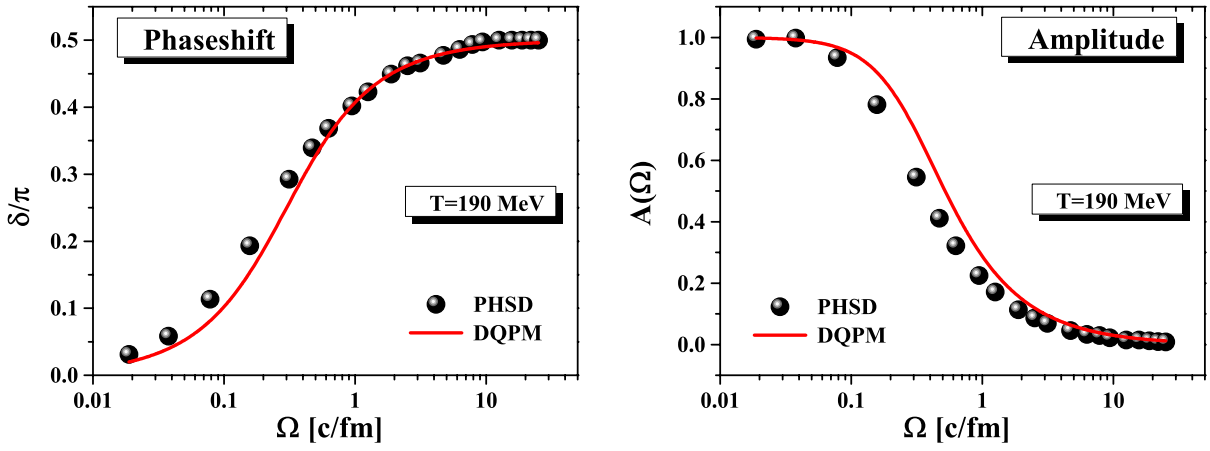


Figure 4.11: (l.h.s.) The phase shift δ over π as a function of the frequency Ω from the PHSD calculations (full dots) for $T = 190$ MeV. The red line shows the phase shift as expected from the DQPM using (4.46). (r.h.s.) The amplitude $A(\Omega)$ as a function of the frequency Ω from the PHSD calculations (full dots) for $T = 190$ MeV. The red line shows the expected amplitude within the DQPM.

actual lattice QCD studies. Using

$$(\vec{\sigma}\mathbf{D})^2 = \mathbf{D}^2 - qe\vec{\sigma} \cdot \mathbf{B}, \quad \mathbf{D}^2 = (\mathbf{p} - qe\mathbf{A})^2 = \mathbf{p}^2 - qe\mathbf{L} \cdot \mathbf{B} \quad (4.47)$$

with the Pauli matrices $\vec{\sigma}$, the kinetic momentum \mathbf{p} and the angular momentum \mathbf{L} the Dirac equation can be rewritten for 2-component quark and antiquark spinors leading to the Hamiltonian

$$\begin{aligned} H_{Dirac} &= \sqrt{\mathbf{p}^2 + m^2 - qe(\mathbf{L} + \vec{\sigma}) \cdot \mathbf{B}} \\ &\approx E - \frac{qe}{2E}(\mathbf{L} + \vec{\sigma}) \cdot \mathbf{B} = E - \frac{qe}{2E}(\mathbf{L} + 2\mathbf{S}) \cdot \mathbf{B} \end{aligned} \quad (4.48)$$

with $E = \sqrt{\mathbf{p}^2 + m^2}$. In case of small energies $E \rightarrow \mathbf{p}^2/2m + m$ this leads to the well known expression for the non-relativistic Pauli equation:

$$H_{Pauli} = \frac{\mathbf{p}^2}{2m} - \frac{qe}{2m}(\mathbf{L} + \vec{\sigma}) \cdot \mathbf{B}. \quad (4.49)$$

The change of the energy of the system in the presence of an external magnetic field \mathbf{B} is determined by the magnetic moment $\vec{\mu}$:

$$\vec{\mu} = \vec{\mu}_L + \vec{\mu}_S = \frac{qe}{2E}(\mathbf{L} + 2\mathbf{S}), \quad (4.50)$$

which has a contribution from the angular momentum \mathbf{L} of a particle and from the spin $\mathbf{S} = \vec{\sigma}/2$. In the following we will investigate both terms separately since they provide contributions to the magnetic moment of opposite sign. In analogy to the previous section we are dealing with an open system but the increase in the total energy stays below 1%.

4.2.5 Diamagnetic contribution

The induced angular momentum \mathbf{L} emerges from the Lorentz force (4.36) on a charged particle due to an external field \mathbf{B} ,

$$\mathbf{F}_L = \frac{qe}{E}(\mathbf{p} \times \mathbf{B}), \quad (4.51)$$

and induces a magnetic moment opposite to the direction of the \mathbf{B} -field since the charged particle spirals around the magnetic field with frequency

$$\omega = \frac{qeB}{E} = \frac{p_\perp}{ER}$$

, where p_\perp is the momentum component of the particle perpendicular to the direction of the magnetic field and R is the radius of the spiral². We obtain alternatively for the angular momentum

$$\mathbf{L} = \frac{Rqe}{|\mathbf{F}_L|E}(\mathbf{p}(\mathbf{p} \cdot \mathbf{B}) - \mathbf{B}p^2), \quad (4.52)$$

where $\mathbf{p}(\mathbf{p} \cdot \mathbf{B})$ is the projection of the momentum on the direction of the magnetic field \mathbf{e}_B . Inserting the expression for the radius R we get

$$\mathbf{L} = \frac{-p_\perp^3}{|\mathbf{F}_L|E} \text{sign}(q) \mathbf{e}_B. \quad (4.53)$$

Assuming the magnetic field to be oriented in y -direction and employing the Lorentz force $|\mathbf{F}_L| = \frac{|qeB|}{E} p_\perp$ we end up with

$$L_y = \frac{-p_\perp^2}{qeB}. \quad (4.54)$$

This gives the induced magnetic moment

$$\mu_L = \frac{-p_\perp^2}{2BE}. \quad (4.55)$$

Since the Lorentz force changes only the direction of \mathbf{p} and not its magnitude $|\mathbf{p}|$ the particle energy E is conserved, too. As a consequence the energy contribution in the Hamiltonian (4.48) is independent from the magnetic field strength in the limit of low B :

$$\Delta E_{mag,L} = -\mu_L B = -\frac{-p_\perp^2}{2BE} B = \frac{p_\perp^2}{2E}. \quad (4.56)$$

We note that the diamagnetic contribution can not be seen in approaches that calculate the magnetization by differentiation of the thermodynamic potential (e.g. free energy F) with respect to the magnetic field B . In principle, the angular momentum \mathbf{L} has to be quantized. However, the actual values for \mathbf{L} (in units of \hbar) are $\gg 1$ for 'small' field strength since $|\mathbf{L}| \sim 1/(eB)$ such that quantum corrections are subleading in our case.

In order to explore the range of external magnetic fields eB we can handle reliably within the PHSD calculations for partonic systems we show in Fig. 4.12 the energy contribution to the magnetic field (4.56) as a function of eB for a temperature $T=190$ MeV. In fact, the calculations

²Note that in case of charged but spinless particles this diamagnetic response is the only response.

for the energy shift due to the magnetic field eB give constant results for $eB < 50$ MeV/fm while for stronger fields more significant deviations emerge up to $\sim 10\%$ for eB 200 MeV/fm. Accordingly, we will restrict to $eB \leq 50$ MeV/fm (≈ 0.01 GeV²) in the following.

The temperature dependence of $\Delta E_{mag,L}$ from the PHSD calculation is shown in Fig. 4.12 (r.h.s.) by full dots and can be well fitted in the interval $170 \text{ MeV} \leq T \leq 250 \text{ MeV}$ by

$$\Delta E_{mag,L}(T) = 0.3 \cdot (T - 96)^{2.82} [\text{MeV}] \quad (4.57)$$

where the temperature T is given in units of MeV. The diamagnetic contribution to the magnetization from the Lorentz force on the quarks and antiquarks then can be readily extracted by dividing $\Delta E_{mag,L}(T)$ by the strength of the magnetic field.

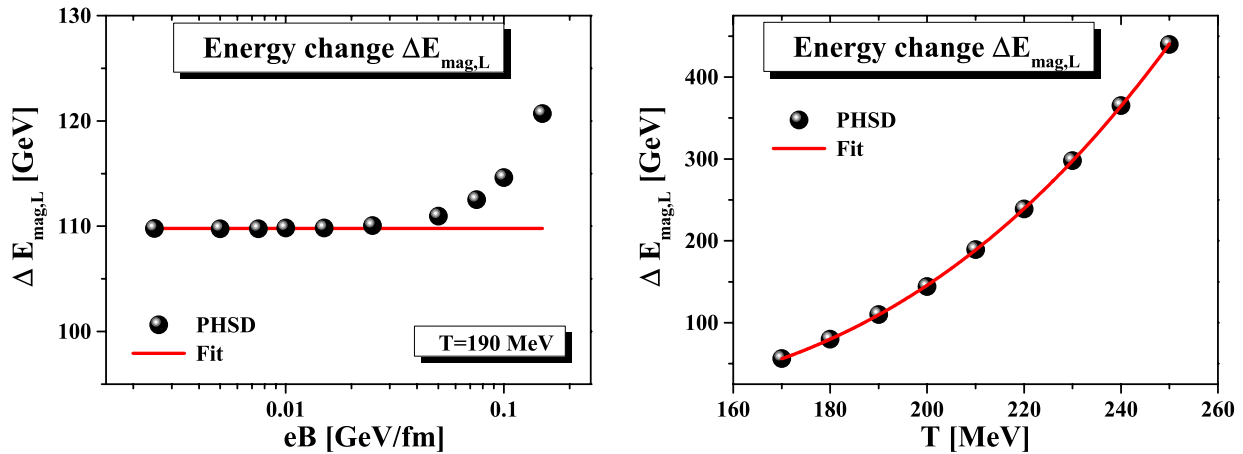


Figure 4.12: (l.h.s.) The energy shift due to the magnetic field $\Delta E_{mag,L} = -\mu_L B$ in the PHSD calculation (full dots) as a function of the field strength eB for a temperature of $T = 190$ MeV at $\mu_q=0$. The solid line reflects a constant for small/moderate field strength. (r.h.s.) The energy shift due to be magnetic field $\Delta E_{mag,L} = -\mu_L B$ in the PHSD calculation as a function of the temperature T for $\mu_q = 0$. The numerical uncertainties are smaller than the size of the dots. The solid line shows the fit (4.57).

4.2.6 Paramagnetic contribution

In QCD the quark and antiquark spins provide a paramagnetic contribution since the spin precession around the direction of the magnetic field \mathbf{B} in thermal equilibrium gives a positive magnetic moment μ_S since the energy becomes reduced according to Eq. (4.48). The spin degree-of-freedom is introduced in PHSD in line with the generalized test-particle ansatz (3.31) for the Wightman function

$$iG^<(X, P, S) = \frac{1}{N} \sum_{k=1}^N \sum_{i=1}^{N_k(t)} \delta^{(3)}(\mathbf{X} - \mathbf{X}_i(t)) \quad (4.58)$$

$$\times \delta^{(3)}(\mathbf{P} - \mathbf{P}_i(t)) \delta(P_0 - \epsilon_i(t)) \delta^{(2)}(\mathbf{S} - \mathbf{S}_i(t))$$

where X and P stand for space-time and four-momentum coordinates, respectively, while \mathbf{S} denotes the spin degree-of-freedom. In (4.58) the number of ensemble members (runs) is denoted by N whereas N_k is the number of partons in the run $k = 1 \dots N$ that describe the 'physical' particles in each micro-canonical simulation. The spin degree-of-freedom has to be treated in line with quantum mechanics according to the interaction Hamiltonian (4.48), i.e.

$$\hat{H}_S = -\frac{qe}{2E}\vec{\sigma} \cdot \mathbf{B}. \quad (4.59)$$

The spin-wavefunction for a spin 1/2 fermion is taken as a 2-component spinor with spin-up and spin-down elementary basis states. The time evolution of the spin operator can be evaluated in a straight forward manner with the help of the time evolution operator $\exp(-i\hat{H}_s(t - t_0))$. The resulting equations of motion lead to a precession of the spin of a quark/antiquark with frequency $\omega = qeB/E$ which changes only if the energy of the particle E changes in a collision or in the inelastic reaction $q + \bar{q} \rightarrow g \rightarrow q' + \bar{q}'$.

In order to describe an equilibration of the spin degree-of-freedom we introduce a spin flip in 1/3 of the elastic collisions with the constraint (in equilibrium):

$$\begin{aligned} n_\uparrow P_{\uparrow,\downarrow} &= n_\downarrow P_{\downarrow,\uparrow} \iff \frac{P_{\uparrow,\downarrow}}{P_{\downarrow,\uparrow}} \\ &= \frac{n_\downarrow}{n_\uparrow} = \exp(-(E_\downarrow - E_\uparrow)/T) = \exp\left(-\frac{qeB}{ET}\right). \end{aligned} \quad (4.60)$$

In (4.60) P denotes the probability for a spin flip and n the occupation probability for given spin orientation. The probabilities P are taken as

$$P_{\downarrow,\uparrow} = 1, \quad P_{\uparrow,\downarrow} = \exp\left(-\frac{qeB}{ET}\right) \quad (4.61)$$

and lead to the proper equilibrium distribution when neglecting the $q + \bar{q} \leftrightarrow g$ channels.

The magnetization M is defined by the spin density of the system as

$$M = \frac{\langle \mu_S \rangle}{V} \approx \chi_S e^2 B, \quad (4.62)$$

which in case of small magnetic fields eB - as in our present study - is proportional to the strength of the B -field thus defining a magnetic susceptibility χ_S by

$$\chi_S = \frac{\langle \mu_S \rangle}{e^2 B V}. \quad (4.63)$$

As a next step we compute the magnetic susceptibility χ_S in the PHSD calculations according to Eq. (4.63) for different field strength eB at $\mu_q = 0$. The results for the susceptibility χ_S are displayed in Fig. 4.13 (l.h.s.) for $T = 190$ MeV and (within numerical accuracy) show a constant value even up to $eB = 200$ MeV/fm. In this case the numerical accuracy increases with the field strength since the spin-flip probabilities in Eq. (4.61) differ more significantly for larger magnetic fields. Nevertheless, we have a stable numerical 'window' eB from 25-50 MeV/fm where the diamagnetic and parametric contributions to the magnetic moment can be calculated

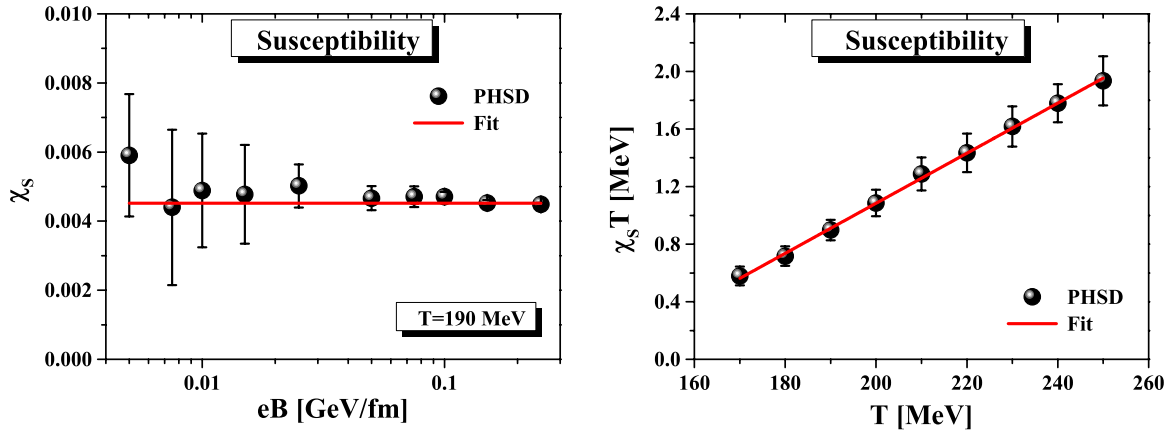


Figure 4.13: (l.h.s.) Magnetic susceptibility χ_S (4.63) from PHSD as a function of the external magnetic field eB for a temperature $T=190$ MeV at vanishing quark chemical potential $\mu_q=0$. (r.h.s.) Temperature dependence of the magnetic susceptibility $\chi_S(T)T$ from PHSD (full dots) in comparison to the fit (4.65) for $\mu_q=0$. The numerical uncertainties are indicated by the errorbars.

with sufficient accuracy. Note that the energy shift due to the paramagnetic contribution is given by

$$\Delta E_{mag,S} = -\chi_S V (eB)^2 \quad (4.64)$$

and decreases quadratically with the field strength.

The temperature dependence of the magnetic susceptibility $\chi_S(T)$ from PHSD is displayed in Fig. 4.13 (r.h.s.) by the full dots and can be fitted as

$$\chi_S(T) = 0.017 - \frac{2.39}{T} \quad (4.65)$$

with T given in MeV (in the interval $170 \text{ MeV} \leq T \leq 250 \text{ MeV}$).

The total energy shift due to the both interactions with the magnetic field is given by

$$\Delta E(T, B) = \Delta E_{mag,L}(T) - \chi_S(T) V (eB)^2 \quad (4.66)$$

and decreases with B^2 at constant temperature T . At a 'critical' field $B_c(T)$ the energy shift changes sign, i.e. for

$$B_c(T) = \sqrt{\frac{\Delta E_{mag,L}}{e^2 \chi_S V}} \quad (4.67)$$

the magnetization changes from diamagnetic to paramagnetic with increasing magnitude of the field \mathbf{B} .

This quantity has a minimum (within PHSD) close to the critical temperature $T_c \approx 158$ MeV (cf. Fig. 4.14) with a minimum $eB_{c,min} \approx 0.4 \text{ GeV}^2$ (thick solid black line - extrapolated by the dashed line according to the fits performed). For comparison we also show the limiting results when assuming all quark/antiquark spins to be oriented in \mathbf{B} direction. In the QGP phase the 'critical' field B_c rises with temperature and separates the diamagnetic (below) from the paramagnetic response (above) of the QGP. Note that the maximal field strength in peripheral

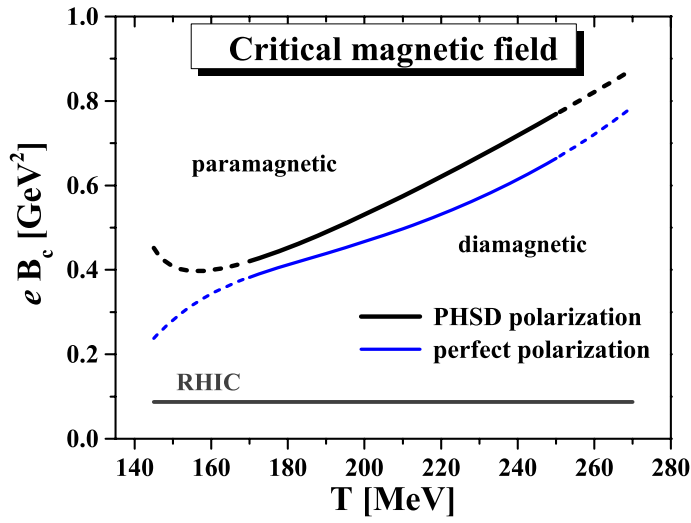


Figure 4.14: The 'critical' magnetic field (4.67) as a function of the temperature T for $\mu_q = 0$ from the PHSD calculations (thick solid black line). The dashed extensions are based on the extrapolated fits and not explicitly controlled by PHSD calculations. The (lower) thin solid blue line results when assuming all quark/antiquark spins to be oriented in \mathbf{B} direction. The constant lower line displays the maximum value for the magnetic field strength at the top RHIC energy of $\sqrt{s_{NN}} = 200$ GeV.

Au + Au collisions at the top RHIC energy $\sqrt{s_{NN}} = 200$ GeV was found to be ~ 0.09 GeV² (constant solid line) - during the passage time of the nuclei - which is significantly lower than the 'critical' field in Fig. 4.14. Accordingly, the response of the QGP in actual heavy-ion experiments should be diamagnetic. However, for the much higher field strength explored in lattice QCD calculations for temperatures close to T_c the response should be paramagnetic.

4.2.7 Finite quark chemical potential

As in case of the electric conductivity $\sigma_0(T, \mu_q)$ we can also compute the magnetic response at finite quark chemical potential μ_q in PHSD. In analogy to Fig. ?? we find essentially a quadratic dependence on μ_q for $\Delta E_{mag,L}(\mu_q)$ at $T = 200$ MeV. This dependence is also obtained for the magnetic susceptibility $\chi_S(T, \mu_q)$ although with larger numerical errorbars. Again we find the temperature dependence of the coefficient to be $\sim 1/T^2$ such that we get the approximations

$$\Delta E_{mag,L}(T, \mu_q) \approx \Delta E_{mag,L}(T, \mu_q = 0) \left(1 + c_L \frac{\mu_q^2}{T^2}\right), \quad (4.68)$$

$$\chi_S(T, \mu_q) \approx \chi_S(T, \mu_q = 0) \left(1 + c_S \frac{\mu_q^2}{T^2}\right).$$

The scaling (4.68) can be traced back again to the scaling of the quark+antiquark density $n_{q+\bar{q}}(T, \mu_q)$ in the DQPM.

Chapter 5

Appendix

5.1 Kramers-Kronig relation

The Kramers–Kronig relations are bidirectional mathematical relations, connecting the real and imaginary parts of any complex function that is analytic in the upper half-plane. These relations are often used to calculate the real part from the imaginary part (or vice versa) of response functions or retarded propagators in physical systems, because for stable systems causality implies the analyticity condition, and conversely, analyticity implies causality of the corresponding stable physical system. The relation is named according to Ralph Kronig and Hendrik Anthony Kramers.

Let $\chi(\omega) = \chi_1(\omega) + i\chi_2(\omega)$ be a complex function of the complex variable ω , where $\chi_1(\omega)$ and $\chi_2(\omega)$ are real. Assume this function to be analytic in the closed upper half-plane of ω and to vanish like $1/|\omega|$ or faster as $|\omega| \rightarrow \infty$. Slightly weaker conditions are also possible. The Kramers-Kronig relations are given by

$$\chi_1(\omega) = \frac{1}{\pi} \mathcal{P} \int_{-\infty}^{\infty} \frac{\chi_2(\omega')}{\omega' - \omega} d\omega' \quad (5.1)$$

and

$$\chi_2(\omega) = -\frac{1}{\pi} \mathcal{P} \int_{-\infty}^{\infty} \frac{\chi_1(\omega')}{\omega' - \omega} d\omega', \quad (5.2)$$

where \mathcal{P} denotes the Cauchy principal value (see below). So the real and imaginary parts of such a function are not independent, and the full function can be reconstructed given just one of its parts.

The proof begins with an application of Cauchy’s residue theorem for complex integration. Given any analytic function χ in the closed upper half plane, the function $\omega' \rightarrow \chi(\omega')/(\omega' - \omega)$ where ω is real will also be analytic in the upper half of the plane. The residue theorem consequently states that

$$\oint \frac{\chi(\omega')}{\omega' - \omega} d\omega' = 0 \quad (5.3)$$

for any contour within this region. We choose the contour to trace the real axis, a hump over the pole at $\omega = \omega'$ in the upper half plane, and close with a large semicircle in the upper half plane (cf. Fig. 5.1). We then decompose the integral into its contributions along each of these three contour segments and pass them to limits. The length of the semicircular segment increases

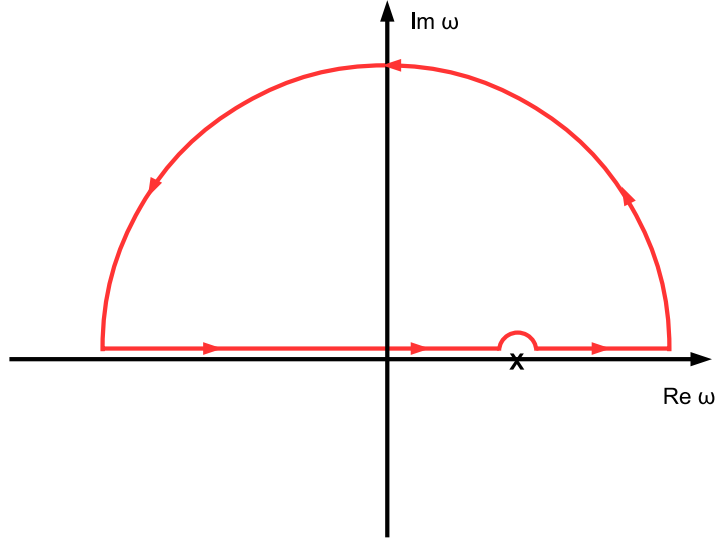


Figure 5.1: The contour in the complex ω -plane employed for the proof of (5.5).

proportionally to $|\omega|$, but the integral over it vanishes in the limit because $\chi(\omega)$ vanishes faster than $1/|\omega|$. We are left with the segments along the real axis and the half-circle around the pole. We pass the size of the half-circle to zero and obtain

$$0 = \oint \frac{\chi(\omega')}{\omega' - \omega} d\omega' = \mathcal{P} \int_{-\infty}^{\infty} \frac{\chi(\omega')}{\omega' - \omega} d\omega' - i\pi\chi(\omega). \quad (5.4)$$

The second term in the last expression is obtained using the theory of residues. Rearranging, we arrive at the compact form of the Kramers–Kronig relations,

$$\chi(\omega) = \frac{1}{i\pi} \mathcal{P} \int_{-\infty}^{\infty} \frac{\chi(\omega')}{\omega' - \omega} d\omega'. \quad (5.5)$$

The single i in the denominator will effectuate the connection between the real and imaginary components. Finally, split $\chi(\omega)$ and the equation into their real and imaginary parts to obtain the forms quoted above in Eqs. (5.1) and (5.2).

Applications: We can apply the Kramers–Kronig formalism to response functions. The imaginary part of a response function describes how a system dissipates energy, since it is out of phase with the driving force. The Kramers–Kronig relations imply that observing the dissipative response of a system is sufficient to determine its in-phase (reactive) response, and vice versa.

The integrals run from $-\infty$ to ∞ , implying we know the response at negative frequencies. Fortunately, in most systems, the positive frequency-response determines the negative-frequency response because $\chi(\omega)$ is the Fourier transform of a real quantity $\chi(t - t')$, so $\chi(-\omega) = \chi^*(\omega)$. This means $\chi_1(\omega)$ is an even function of frequency and $\chi_2(\omega)$ is odd.

Using these properties, we can collapse the integration ranges to $[0, \infty)$. Consider the first relation, which gives the real part $\chi_1(\omega)$. We transform the integral into one of definite parity

by multiplying the numerator and denominator of the integrand by $\omega' + \omega$ and separating:

$$\chi_1(\omega) = \frac{1}{\pi} \mathcal{P} \int_{-\infty}^{\infty} \frac{\omega' \chi_2(\omega')}{\omega'^2 - \omega^2} d\omega' + \frac{\omega}{\pi} \mathcal{P} \int_{-\infty}^{\infty} \frac{\chi_2(\omega')}{\omega'^2 - \omega^2} d\omega'. \quad (5.6)$$

Since $\chi_2(\omega)$ is odd, the second integral vanishes, and we are left with

$$\chi_1(\omega) = \frac{2}{\pi} \mathcal{P} \int_0^{\infty} \frac{\omega' \chi_2(\omega')}{\omega'^2 - \omega^2} d\omega'. \quad (5.7)$$

The same derivation for the imaginary part gives

$$\chi_2(\omega) = -\frac{2}{\pi} \mathcal{P} \int_0^{\infty} \frac{\omega \chi_1(\omega')}{\omega'^2 - \omega^2} d\omega' = -\frac{2\omega}{\pi} \mathcal{P} \int_0^{\infty} \frac{\chi_1(\omega')}{\omega'^2 - \omega^2} d\omega'. \quad (5.8)$$

These are the Kramers–Kronig relations in a form that is useful for physically realistic response functions and also retarded propagators or selfenergies.

5.2 Cauchy's principal value

Depending on the type of singularity in the integrand $f(x)$, the Cauchy principal value is defined as one of the following: the finite number

$$\lim_{\varepsilon \rightarrow 0^+} \left[\int_a^{b-\varepsilon} f(x) dx + \int_{b+\varepsilon}^c f(x) dx \right] \quad (5.9)$$

where b is a point at which the behavior of the function f is such that

$$\int_a^b f(x) dx = \pm\infty \quad (5.10)$$

for any $a < b$ and

$$\int_b^c f(x) dx = \mp\infty \quad (5.11)$$

for any $c > b$ (one sign is "+" and the other is "-"; see plus or minus for precise usage of notations \pm); or the finite number

$$\lim_{a \rightarrow \infty} \int_{-a}^a f(x) dx \quad (5.12)$$

where

$$\int_{-\infty}^0 f(x) dx = \pm\infty \quad (5.13)$$

and

$$\int_0^{\infty} f(x) dx = \mp\infty \quad (5.14)$$

In some cases it is necessary to deal simultaneously with singularities both at a finite number b and at infinity. This is usually done by a limit of the form

$$\lim_{\varepsilon \rightarrow 0^+} \left[\int_{b-\frac{1}{\varepsilon}}^{b-\varepsilon} f(x) dx + \int_{b+\varepsilon}^{b+\frac{1}{\varepsilon}} f(x) dx \right]. \quad (5.15)$$

or in terms of contour integrals of a complex-valued function $f(z)$; $z = x + iy$, with a pole on the contour. The pole is enclosed with a circle of radius ε and the portion of the path outside this circle is denoted $L(\varepsilon)$. Provided the function $f(z)$ is integrable over $L(\varepsilon)$ no matter how small ε becomes, then the Cauchy principal value is the limit:

$$\mathcal{P} \int_L f(z) dz = \int_L^* f(z) dz = \lim_{\varepsilon \rightarrow 0} \int_{L(\varepsilon)} f(z) dz, \quad (5.16)$$

where two of the common notations for the Cauchy principal value appear on the left of this equation. In the case of Lebesgue-integrable functions, that is, functions which are integrable in absolute value, these definitions coincide with the standard definition of the integral.

Examples the Cauchy principal value:

Consider the difference in values of two limits:

$$\lim_{a \rightarrow 0^+} \left(\int_{-1}^{-a} \frac{dx}{x} + \int_a^1 \frac{dx}{x} \right) = 0, \quad (5.17)$$

$$\lim_{a \rightarrow 0^+} \left(\int_{-1}^{-2a} \frac{dx}{x} + \int_a^1 \frac{dx}{x} \right) = \ln 2. \quad (5.18)$$

The former is the Cauchy principal value of the otherwise ill-defined expression

$$\int_{-1}^1 \frac{dx}{x} \quad (\text{which gives } -\infty + \infty). \quad (5.19)$$

Similarly, we have

$$\lim_{a \rightarrow \infty} \int_{-a}^a \frac{2x dx}{x^2 + 1} = 0, \quad (5.20)$$

but

$$\lim_{a \rightarrow \infty} \int_{-2a}^a \frac{2x dx}{x^2 + 1} = -\ln 4. \quad (5.21)$$

The former is the principal value of the otherwise ill-defined expression

$$\int_{-\infty}^{\infty} \frac{2x dx}{x^2 + 1} \quad (\text{which gives } -\infty + \infty). \quad (5.22)$$

Bibliography

- [1] M. Bonitz, *Quantum kinetic theory*, B.G. Teubner Stuttgart, 1998.
- [2] S. Juchem, W. Cassing, and C. Greiner, Phys. Rev. D 69 (2004) 025006.
- [3] L. P. Kadanoff, G. Baym, *Quantum Statistical Mechanics*, Benjamin, 1962.
- [4] S. Juchem, W. Cassing and C. Greiner, Nucl. Phys. A 743 (2004) 92.
- [5] W. Botermans and R. Malfliet, Phys. Rep. 198 (1990) 115.